WHITE-EMITTING CONJUGATED POLYMER NANOPARTICLES: TUNING EMISSION VIA FÖRSTER RESONANCE ENERGY TRANSFER IN NANOSTRUCTURES ASSEMBLED THROUGH CLICK REACTIONS

A THESIS
SUBMITTED TO THE DEPARTMENT OF CHEMISTRY
AND THE GRADUATE SCHOOL OF ENGINEERING AND SCIENCE
OF BİLKENT UNIVERSITY
IN PARTIAL FULFILLMENT OF THE REQUIREMENTS
FOR THE DEGREE OF
MASTER OF SCIENCE

By
HAMIDOU KEITA
JUNE 2014

I certify that I have read this thesis and in my opinion it is fully adequate, in scope and in quality, as a thesis for the degree of Master of Science.

_____

Assoc. Prof. Dr. Dönüş Tuncel
Supervisor

I certify that I have read this thesis and in my opinion it is fully adequate, in scope and in quality, as a thesis for the degree of Master of Science.

_____

Prof. Dr. Tuncer Çaykara
Examining Committee Member

I certify that I have read this thesis and in my opinion it is fully adequate, in scope and in quality, as a thesis for the degree of Master of Science.

_____

Assist. Prof. Dr. Ferdi Karadaş
Examining Committee Member

Approval of the Graduate School of Engineering and Sciences

_____

Prof. Dr. Levent Onural
Director of Graduate School of Engineering and Sciences

ABSTRACT

WHITE-EMITTING CONJUGATED POLYMER NANOPARTICLES: TUNING EMISSION VIA FÖRSTER RESONANCE ENERGY TRANSFER IN NANOSTRUCTURES ASSEMBLED THROUGH CLICK REACTIONS

HAMIDOU KEITA

M.S. in Chemistry

Supervisor: Assoc. Prof. Dr. Dönüş Tuncel

June 2014

In this work, we present the design, synthesis and characterization of water-dispersible conjugated polymer nanoparticles with tunable emission wavelengths for their potential applications in the areas of white organic light emitting diodes and cellular imaging. Blue, green and red emitting polymers carrying azide or alkyne groups are utilized and assembled together through 1,3-dipolar cycloaddition (click reaction) to obtain stable, shape-persistent white-emitting nanoparticles. The emission properties can both be tuned by varying polymer concentration and nanostructure design as a result of intimate interactions between the polymers within the nanostructure, which facilitate a highly efficient Förster Resonance Energy Transfer (FRET).

For this purpose, four different nanostructured architectures were designed and investigated. In the first method, NPs of donor and acceptor are prepared separately and then mixed physically at certain ratios. The second method involves the formation of homogenous solution of both donor and acceptor polymers in THF followed by formation of NPs from the resulting solution. And in the third and fourth methods, sequentially formed NPs were designed. In the former, donor NPs were core and coated with solution of the acceptor polymer as the outer shell, while the latter is quite the reverse where acceptor NPs form the core surrounded by the donor as the outer shell.

Polymers used in this study are namely, poly[(9,9-bis{3-azidopropyl}fluorenyl-2,7-diyl)-*co*-benzene] (**PFBN3**) which is a blue emitter that serves as a donor, while poly[(9,9-bis(3-(prop-2 ynyloxy)propyl)fluorenyl-2,7-diyl)-*co*-(1,4-benzo-{2,1,3}-thiadiazole)] (**PFBT-Pgy**) is a green emitting polymer whose absorbance strongly overlaps with the emission of the donor serves as the acceptor. Moreover, red emitting polymers such as poly[(2-azidoethyl)-2-(5-(thiophen-2-yl)thiophen-2-yl)thiophene (**PTN3**) and Poly[(4-(2-(prop-2-ynyloxy)ethyl)thiophen-2-yl)-co-(1.4-benzo{1,2,5}thiadiazole)] (**PBTTH-Pgy**) were incorporated into multi-shell nanoparticle design to form white emitting tandem nanoparticles.

The morphology and photophysical properties were investigated by DLS, SEM, TEM and UV-VIS, Steady-State Fluorescence, Time-resolved Fluorescence Spectroscopy respectively.

Keywords: Conjugated polymers, White-emitting nanoparticles, White organic light emitting diodes, click reaction, Förster Resonance Energy Transfer (FRET).

ÖZET

BEYAZ IŞIMA YAPAN KONJUGE POLİMER NANOPARÇACIKLARI: ÇITÇIT TEPKİMELERİYLE OLUŞTURULAN NANOYAPILARIN IŞIMALARININ FÖRSTER REZONANS ENERJİ TRANSFERİ İLE AYARLANMASI

HAMİDOU KEİTA

Kimya Bölümü Yüksek Lisans Tezi

Tez Yöneticisi: Doç. Dr. Dönüş Tuncel

Haziran 2014

Bu çalışmada, suda dağılan, ışıma dalgaboyu ayarlanabilen konjuge polimer nanoparçacıklarının, beyaz ışıyan organik diyot ve hücre görüntüleme uygulamalarına yönelik tasarım, sentez ve karakterizasyonunu sunmaktayız. Azit ve alkin grupları taşıyan mavi, yeşil ve kırmızı ışıyan polimerler kullanılarak 1,3-dipolar siklo katılma (çıtçıt reaksiyonu) ile dayanıklı, şekli korunan, beyaz ışıyan nanoparçacıklar elde edilmiştir. Işıma özellikleri polimerler arası yakın etkileşimle sağlanan yüksek verimli Förster Rezonans Enerji Transferi (FRET) yoluyla hem polimer konsantrasyonu hem nanoyapı tasarımı değiştirilerek ayarlanabilmektedir.

Bu amaçla, dört farklı nanoyapı tasarlandı ve incelendi. İlk yöntemde, verici ve alıcı nanoparçacıklar ayrı ayrı hazırlandı ve fiziksel olarak karıştırıldı. İkinci yöntem hem verici hem alıcı içeren homojen bir THF çözeltisi oluşturulup, akabinde bu çözeltiden nanoparçacık oluşturmayı içeriyor. Üçüncü ve dördüncü yöntemde ise ardarda oluşturulan nanoparçacıklar tasarlandı. Öncekinde, verici nanoparçacık çekirdeği, dış kabuk olarak alıcı polimer çözeltisiyle kaplandı. Sonrakinde ise tersi şekilde alıcı nanoparçacık çekirdeği verici dış kabuk ile çevrelenmiştir.

Bu çalışmada kullanılan polimerler, mavi ışıyan alıcı olarak kullanılan poli[(9,9-bis{3-azidopropil}fulorenil-2,7-diyil)-*co*-benzen] (**PFBN3**) , ve absorbansı vericinin ışımasıyla güçlü bir şekilde örtüşen, yeşil ışıma yapan poli[(9,9-bis(3-(prop-2 iniloksi)propil)fulorenil-2,7-diyil)-*co*-(1,4-benzo-{2,1,3}-tiyadiyazol)] (**PFBT-Pgy**) polimerleridir. Dahası, kırmızı ışıma yapan, poli[(2-azidoetil)-2-(5-(tiyofen-2-il)tiyofen-2-il)tiyofen (**PTN3**) ve poli[(4-(2-

(prop-2-iniloksi)etil)tiyofen-2-il)-co-(1.4-benzo{1,2,5}tiyadiyazol)] (**PBTTH-Pgy**) polimerleri de ayrıca çoklu-kabuklu nanoparçacık içine dahil edilerek beyaz ışıma yapan çift öğeli nanoparçacıklar tasarlanmıştır.

Morfolojik ve foto-fiziksel özellikler sırasıyla Dinamik Işık Saçılımı (DLS) ölçümleri, Taramalı Elektron Mikroskopu (SEM), Geçirimli Elektron Mikroskopu (TEM), ve de UV-vis, Durağan-Hal Flüoresans, Zaman-Çözünümlü Flüoresans Spektroskopi yöntemleriyle incelenmiştir.

Anahtar kelimeler: Konjuge polimerler, Beyaz ışıyan nanoparçacıklar, Beyaz ışıyan organic diyotlar, Çıtçıt tepkimesi, Förster rezonans enerji transferi (FRET).

ACKNOWLEDGEMENTS

This thesis was made possible due to the mastery guidance of Assoc. Prof. Dr. Dönüş Tuncel who in many ways has been instrumental in expanding our academic and research experience. I am extremely grateful for her trust, advice, direction and determination to see us succeed not only in the lab but also in the outside world as professional and competent graduates.

I would like to thank my other examining committee members: Prof. Dr. Tuncer Çaykara and Assist. Prof. Dr. Ferdi Karadaş for their helpful comments and suggestions.

I would never forget the help I got from Burak Güzeltürk for the time-resolved fluorescence measurements.

I owe my deepest gratitude to Ebrima Tunkara and our entire research team: Dr. Jousheed Pennakalathil, Dr. Rehan Khan, Muazzam Idris, Alp Özgün, Esra Deniz Soner, Sinem Gürbüz and Ahmet Koç for their support, encouragement and sense of camaraderie throughout my research.

I am also grateful to my uncle, Mr. Sainey Jatta and his family, for their monumental support and trust in me. I have also enjoyed unabating encouragement and wisdom from my brother, Dr. Namaka Keita, without whom my quest for higher education would not have been realized.

Finally, I would like to thank my family, especially my Mom and Dad, whose constant encouragement and support was crucial for the completion of this thesis.

TABLE OF CONTENT

LIST OF FIGURES

LIST OF SCHEMES

LIST OF TABLES

ABBREVIATIONS

^{1}H-NMR	Proton-Nuclear Magnetic Resonance spectroscopy
FTIR	Fourier Transform Infrared spectroscopy
UV-Vis	Ultraviolet-Visible spectroscopy
PL	Fluorescence spectroscopy
DLS	Dynamic Light Scattering
SEM	Scanning Electron Microscope
TEM	Transmission Electron Microscope
TCSPC	Time Correlated Single Photon Counting
TRF	Time Resolved Fluorescence

THF	Tetrahydrofuran
CDCl3	Deuterated chloroform
DMSO	Dimethyl sulfoxide
TBAB	Tetra-*n*-butylammonium bromide
D	Donor
A	Acceptor
D-A	Donor –Acceptor pair
FRET	Förster Resonance Energy Transfer
CP	Conjugated polymer
CPN	Conjugated polymer nanoparticle
NPs	Nanoparticles
PFBN3	poly[(9,9-bis{3-azidopropyl}fluorenyl-2,7-diyl)-*co*-benzene]
PFB-Pgy	poly[(9,9-bis(3-(prop-2-ynyloxy)propyl)fluorenyl-2,7-diyl)-*co*-benzene
PFBTN3	poly[(9,9-bis(3-azidopropyl)fluorenyl-2,7-diyl)-co-1,4-benzo[2,1,3]thiadiazole
PFBT-Pgy	poly[(9,9-bis(3-(prop-2 ynyloxy)propyl)fluorenyl-2,7-diyl)-*co*-(1,4-benzo-{2,1,3}-thiadiazole)]
PTN3	poly[(2-azidoethyl)-2-(5-(thiophen-2-yl)thiophen-2-yl)thiophene
PBTTH-Pgy	poly[(4-(2-(prop-2-ynyloxy)ethyl)thiophen-2-yl)-co-(1.4-benzo{1,2,5}thiadiazole)
PFBN3 NP	poly[(9,9-bis{3-azidopropyl}fluorenyl-2,7-diyl)-*co*-benzene] nanoparticles
PFB-Pgy NP	poly[(9,9-bis(3-(prop-2-ynyloxy)propyl)fluorenyl-2,7-diyl)-*co*-benzene nanoparticles
PFBTN3 NP	poly[(9,9-bis(3-azidopropyl)fluorenyl-2,7-diyl)-co-1,4-benzo[2,1,3]thiadiazole nanoparticles
PFBT-Pgy NP	poly[(9,9-bis(3-(prop-2 ynyloxy)propyl)fluorenyl-2,7-diyl)-*co*-(1,4-benzo-{2,1,3}-thiadiazole)] nanoparticles
PTN3 NP	poly[(2-azidoethyl)-2-(5-(thiophen-2-yl)thiophen-2-yl)thiophene nanoparticles

PBTTH-Pgy NP	poly[(4-(2-(prop-2-ynyloxy)ethyl)thiophen-2-yl)-co-(1.4-benzo{1,2,5}thiadiazole) nanoparticles
NP mixed	Physical mixture of different polymers nanoparticles
DA	Bipolymer NPs; donor core and acceptor shell
cDA	DA prepared in the absence of catalyst
AD	Bipolymer NP; acceptor core and donor shell
cAD	AD prepared in the absence of catalyst
Soln NP	Bi polymer nanoparticles prepared initially from solution containing different polymers
DAR	Sequentially formed tandem nanoparticles; donor core, coated with acceptor (green polymer) and red polymer as the outer shell
RAD	Sequentially formed tandem nanoparticles; red core, coated with acceptor (green polymer) and donor (blue polymer) as the outer shell.
T.Soln NP	Tandem nanoparticles prepared initially from solution containing three polymers.
AE	Antenna effect

Chapter 1

INTRODUCTION

1.1. Conjugated polymers

Conjugated, conductive or electroactive polymers (CPs) are unique materials that exhibit semiconducting properties of metals while maintaining its desired mechanical properties as a polymer. [1- 3] Moreover, unlike inorganic materials, conjugated polymers can be tailored by varying functional group and design for a specific function, in this regard CPs have found wide varieties of applications in various areas of electronics, optoelectronics, sensors and biomedical Sciences. In 1977, Alan J. Heeger, Alan MacDiarmid and Hideki Shirakawa discovered a highly conductive polyacetylene by oxidizing with iodine vapour through a process known as doping.[4] Because of this groundbreaking finding they were awarded the 2000 Nobel Prize in Chemistry.[5] Basically, CPs are organic macromolecules with alternating double and single bonds. Their superior electrical properties are as a result of an extended π-electron system that spans across the polymer backbone due to overlapping π-orbital that enables delocalization of π-electrons. These conjugated π-electron system increase the overlap of π-electron, enhance the movement of electron along the polymer backbone by reducing the band gap of the material. Technically, band gap refers to the energy difference between the valence band and conduction band. It is the energy required to excite an electron from the Highest Occupied Molecular Orbital (HOMO) or valence band to the Lowest Unoccupied Molecular Orbital or the conduction band. In other words, the energy difference or band gap is a measure of conductivity of a material (Figure 1). For Insulators, they have wide band gap making it difficult to promote electrons from the valence band to the conduction band. Semiconductors have much smaller band gap and hence requires their electrons to be excited in other to be conductive. Conductors are intrinsically conductive material because they have no band gap and their electrons are free to move across the orbitals. Although conjugated polymers are generally regarded as semiconducting materials, their conductivity depends on a number of factors including the nature of repeating units.

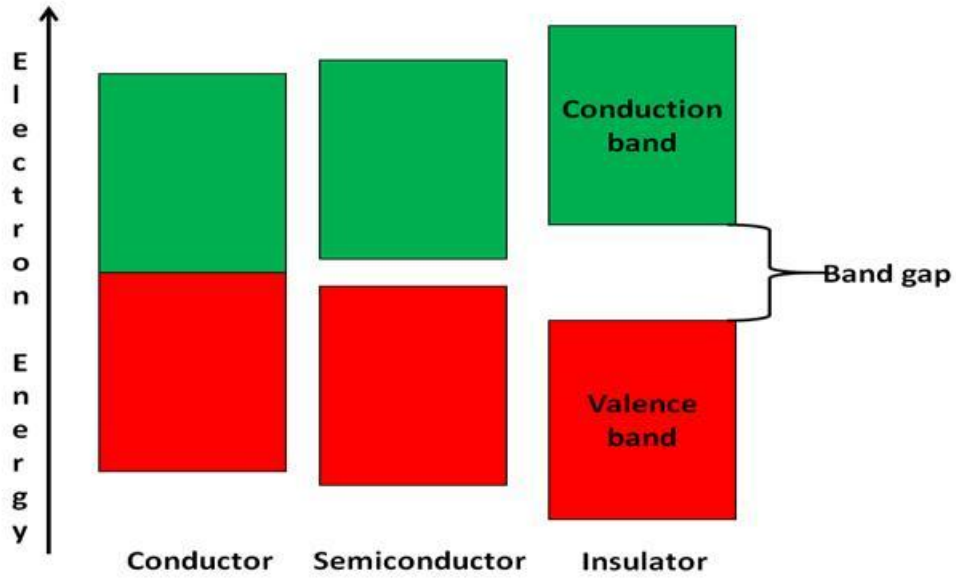

Figure 1: The band gap of a material as the energy require to excite an electron from valence band (red) to conduction band (green)

There are many CPs investigated for their potential optoelectronic and biomedical applications, among them are polyacetylene, polythiophene and polyfluorene (Scheme 1). Polyacetylene are one of the most widely investigated polymers and are known to have high conductivity. [5] Despite the high conductivity, polyacetylene was not the first polymer to be commercialized because of its sensitivity to oxygen in the air and humidity. Polyacetylene per se, does not find many practical applications but its discovery sparked numerous researches in other conjugated polymers both in the academia and industries.

Polythiophene and its derivatives are particularly suitable materials for organic transistors and solar cells .[6]This is due to, in addition to its superior electrical properties, the excellent stability of polythiophene in both doped and undoped states, solubility of substituted derivatives and ease of modifying the polymer backbone.[7]

Another polymer that is of a particular interest to researchers and industries is polyfluorene owing to their optical and electrical properties. They have high photoluminescence efficiencies, remarkably high thermal and mechanical stabilities[8] and ease of functionalization at the 9th –position. Introducing steric hindered substituent in C-9 position of polyfuorene in a way helps to prevent eximer and aggregate formation and hence improve the fluorescence efficiencies.[9,10] Polyfluorene have marked difference with other known conjugated polymers in that it can be tuned to emit light across the visible region of the electromagnetic spectrum. These properties are of special interest for application in many

devices such as in organic light emitting diodes, [11-14] solar cells, [15] field effect transistors, [16] chemo- and biosensors. [17-19]

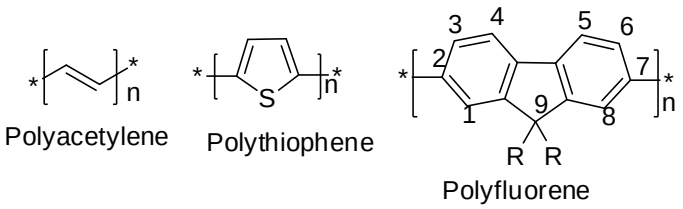

Scheme 1: Structure of conjugated polymers

In the case of using conjugated polymers in full color display, polyfluorene is more preferable choice among other polymers for their facile color tunability and high quantum yield. However, polyfluorene face major setbacks in terms of purity of blue emission in devices. Color instability is partly due to eximer/ aggregate formation or keto defects which tend to shift the emission to a longer wavelength. For this reason, various attempts have been made to obtain blue emission for full color display. Lui et al developed an efficient and pure blue light emitting polymers based on polyfluorene doped with 4-dimethylamino-1,8-naphthalimide (DMAN)[20] which also has high efficient blue emission. The energy transfer and charge trapping from polyfluorene to DMAN make the emission come from DMAN leading to high efficiency and color stable blue electroluminescence. Here polyflorene acts mainly as the host rather the emitter and hence color instability is averted. Lui's work represents one of the many strategies employed to tuned emission throughout the visible region. Similar strategy of blending different polymers has attracted great attention in synthesizing polymeric materials and designing organic light emitting diodes. Polymer blend with different emitter engineered through co-polymerization or layer-by-layer deposition are extensively studied for optoelectronic applications such as in solid state white lighting. Polyfluorene and their derivatives have been used with various polymer blends as a donor moiety to other lower band gap polymers in D-A fashion, where energy transfer is principally through Forster Resonance Energy Transfer (FRET). Examples of fluorene with different co-monomers and emissions are presented in Scheme 2.

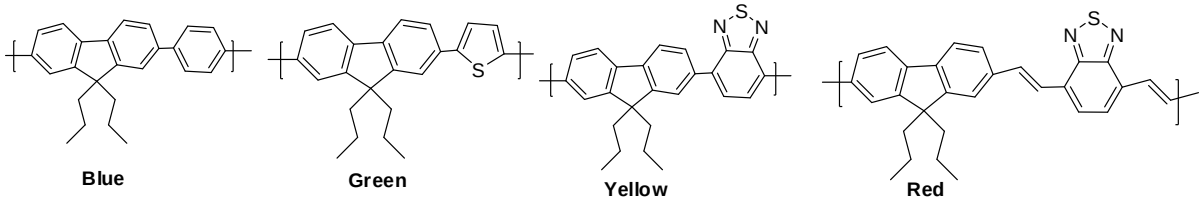

Scheme 2: Structure of some Fluorene-based polymers

Apart from the conducting properties of CPs, low cost and processing advantages are some of the most important features of CPs that draw greater impetus into their research and eventual commercialization. CPs are constantly improving in terms of synthesis, scope of application, manufacturability and cost.

1.2. Synthesis of conjugated polymers

With growing interest in conjugated polymer for their many applications, the synthesis of CPs have continued to improved thanks to the immense research effort. And for CPs to replace inorganic materials as an alternative, their synthesis and resulting materials should exhibit superior properties such as high efficiency, stability, processability and low cost. There are two main methods of CPs synthesis: Electrochemical and chemical polymerization. A number of applications towards various technologies of materials synthesized through these methods have been proposed and demonstrated.[21]

1.2.1. Electrochemical Polymerization

Electrochemical polymerization is one of the earliest mean of synthesizing conjugated polymers using a single compartment electrochemical cell with standard three electrodes configuration[22]. An electrochemical bath would typically consist of a low anodic oxidation monomer and a supporting electrolyte dissolved in a suitable aprotic solvent such as acetonitrile. The electrolytes used depend on their solubility in aprotic solvents. A good candidate is quaternary ammonium-based salts with general formula R4NX (R = Alkyl, aryl and X= Halogens, BF_4, CF_3SO_3, PF_6, ClO_4).[21] Hence such salts with good solubility are often used as supporting electrolytes during electrochemical polymerization of conjugated polymers. The polymerization procedure is simple and the polymeric films are deposited on the electrodes by oxidative process. The important features of electropolymerization is that, polymerization, doping and processing takes place simultaneously and the polymer formed does not need to be isolated and purified. However, electrochemical polymerization is limited to monomers with low anodic oxidation potential and the products usually suffer from solubility and processing issues.

1.2.2. Chemical Polymerization

Perhaps the most useful method of synthesizing conjugated polymers is chemical polymerization and virtually all the CPs can be synthesized by this technique. It has marked advantages over electrochemical polymerization in that there is wider selection of monomers, better solubility and the ability to obtained tailor-made polymers with respect to electrical, optical, mechanical and thermal properties. The most rewarding chemical polymerization

turns out to be cross-coupling reactions that evolved into a powerful strategy and a blueprint for the synthesis of conjugated polymers and beyond. In 2010, three scientists: Richard F. Heck, Ei-ichi Negishi and Akira Suzuki were jointly awarded the Nobel Prize in Chemistry "for palladium-catalyzed cross couplings in organic synthesis".[23]The basic mechanism of palladium–catalyzed cross coupling reaction is that two molecules are bonded to the metal center through metal-carbon bonds; an example of heterogeneous catalysis. The carbon atoms bounded to the Palladium are essentially brought to a very close proximity to the extent that they eventually form new C-C bond(s).

Suzuki and co-workers reported in 1979 that boronic acids or esters in the presence of base can be used in palladium-catalyzed cross coupling reactions with vinyl and aryl halides.[24, 25] The use of organoborane compounds makes Suzuki coupling simple and unique; they tolerate host of functional groups and are generally non-toxic and eco-friendly. Today it is applied extensively both in academia and industries in the production of fine chemicals including conjugated polymers, advance materials, pharmaceuticals, agricultural chemicals etc. In our study Suzuki coupling was preferable not only because of the advantages mentioned above but also:

1. The mild reaction conditions required
2. Cheaper and commercial availability of various organoborane derivatives that are more environmental friendly compare to other organometallic reagents.
3. In large scale synthesis, removal and handing of boron-containing by-products are lot easier as per other organometallic reagents.

In the reaction mechanism of Suzuki coupling (Scheme 3), there are three important steps: oxidative addition of palladium to the vinyl or aryl halide, trans-metallation and reductive elimination which are designated 1, 2, and 3 respectively in the reaction mechanism.

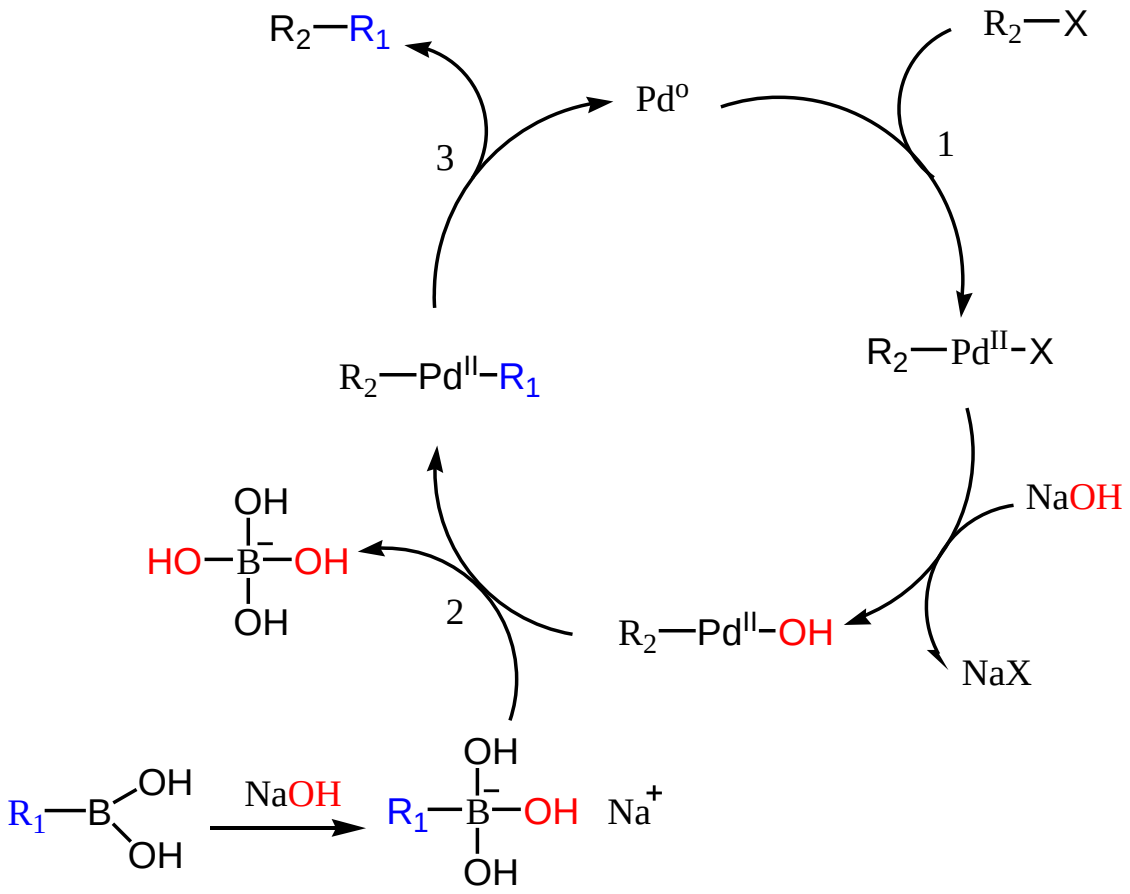

Scheme 3: Mechanism of Suzuki cross-coupling reaction, adapted from ref.24

Negishi reaction is quite similar to Suzuki cross-coupling reaction in that he used organozinc compounds instead of organoborane. organozinc compounds are tolerant to many functional groups, highly selective and mild and also they give good yield. [26, 27] In fact, Negishi noted in 1978 that organoboranes could be used to form C-C bond with organic halides in the presence of palladium catalyst.[28]However, he did not pursue further research in this particular area to provide deeper insight into cross-coupling reaction using organoborane derivatives.

[1]The C-C bond formation between aryl/vinyl halides with akenes in the presence of base and zerovalent palladium was reported by Richard F. Heck in 1972. [29] This coupling reaction was later known as the Heck-Mizoroki reaction. Heck reaction has been widely use in the synthesis of conjugated polymers, natural products and biological active compounds owing to its simplicity and the ability to substitute on planar sp^2 hybridized carbon center to obtain a trans product. The reaction mechanism of Heck reaction (Scheme 4) also starts with the so-called oxidative addition to form organopalladium bond.

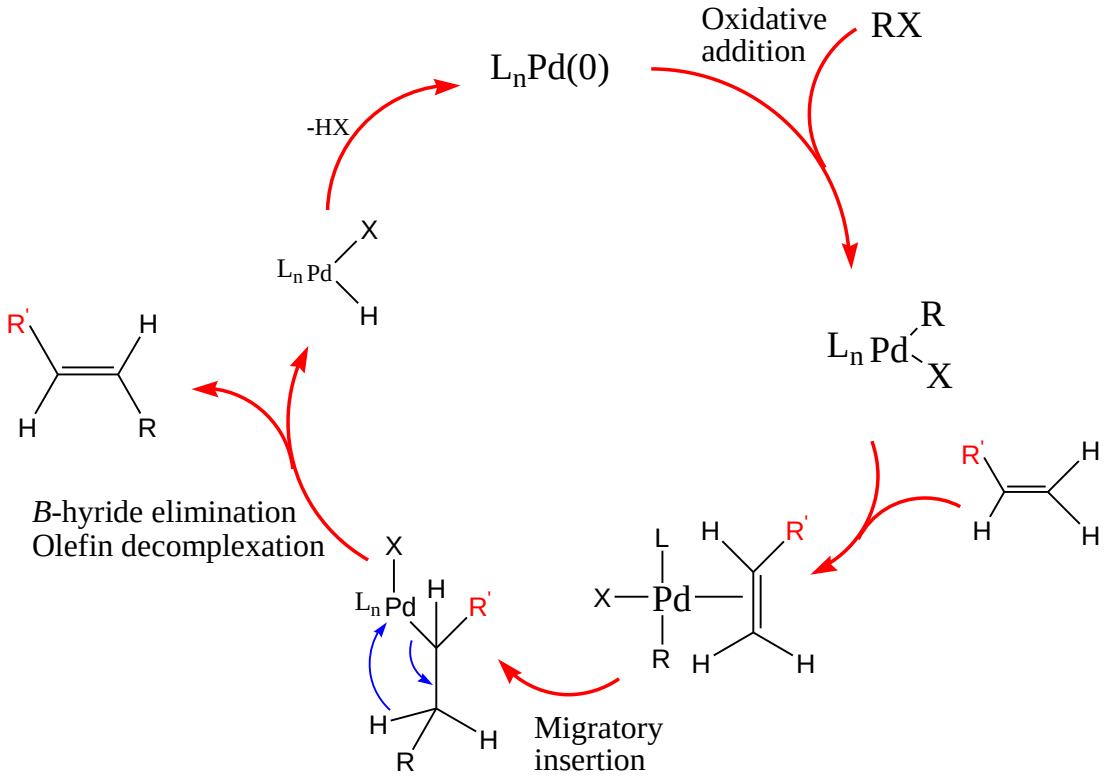

Scheme 4: Mechanism of the Heck reaction, adapted from ref. 29

The Stille coupling reactions are also another useful tool in the synthesis of conjugated polymers. The reaction involves organotin compounds that can form C-C bond with varieties of organic electrophiles (e.g. organic halides, triflates) through palladium catalyzed coupling reaction.[30] Stille coupling reaction gained prominence in organic synthesis due to the stability and ease of synthesis of organotin compounds. They are preferable in the synthesis of compounds with sensitive functional groups. However their large scale application is limited

[1] C-C means Carbon to Carbon bond formation.

due to the toxicity of organotin compounds. The mechanism of Stille coupling is presented in Scheme 5.

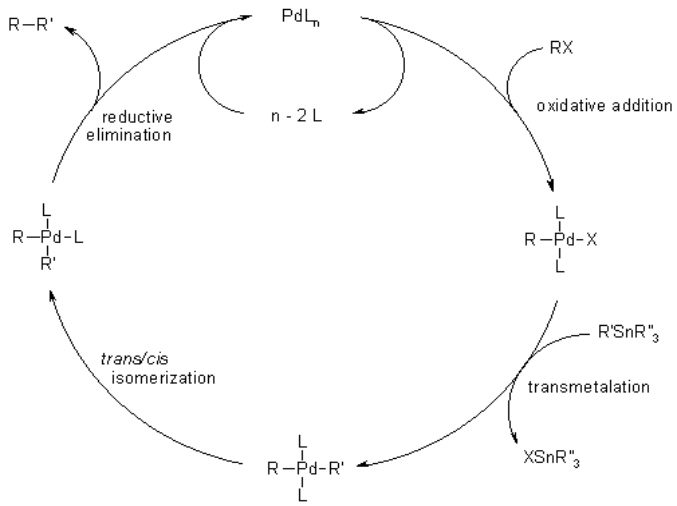

Scheme 5: Mechanism of the stille reaction[31]

Other contributors to the synthesis of conjugated polymers are A. Yamamoto[32] and M.Kumada[33] both of whom used Nickel catalyst to obtain new C-C bond.

Sonogashira reaction is one of the most useful and widely used in coupling terminal alkynes with aryl or vinyl halides to form new C-C bond in the presence of palladium catalyst and a base.[34]The early version of Sonogashira coupling involves the addition of copper as a co-catalyst. With continues advancement in Sonogashira coupling due to its wide applications, many copper-free Sonogashira coupling have now been reported.[35-37] These developments in copper-free coupling will pave way for large scale applications of Sonogashira coupling.

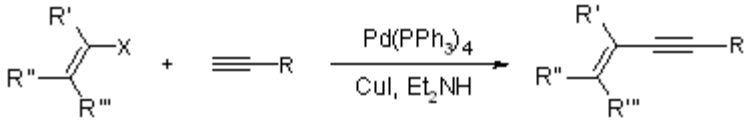

Scheme 6: Representation of Sonogashira coupling

1.2.3. Click Chemistry

The "click" concept was first coined by K. Sharpless and co-workers in 2001 with the goal of coupling two molecular units in a facile, highly selective, simple reaction conditions and provide high yield products which can be easily isolated by non-chromatographic means.[38] One of the most widely used reactions that fulfilled all these conditions is by far the Cu^{I}-

catalyzed azide-alkyne cycloaddition (CuAAC). Although other click reactions are known; such as Michael addition, thiol-ene , Diels-Alders and oximes,[39] Cu^{I}-catalyzed azide-alkyne cycloaddition (CuAAC) is considered as an epitome of click Chemistry . The CuAAC reaction is fast and completely selective; it forms only the 1, 4-disubstituted 1,2,3-triazole products. Non-catalyzed azide-alkyne reactions have been known many years ago and are generally called the Huisgen's reactions. The Huisgen's reaction does not fit within the definition of click reaction put forth by Sharpless, because they are not regioselective and yield a mixture of 1, 4- and 1, 5-disubstituted 1,2,3-triazoles and the reaction is rather slow (Scheme 7). In another development, Sharpless reported the regio-control synthesis of only the 1,5-disubstituted triazole isomers from organic azides and terminal alkynes using ruthenium cyclopentadienyl complexes as a catalyst (RuAAC).[40]

Huisgen's 1, 3-dipolar cycloaddition

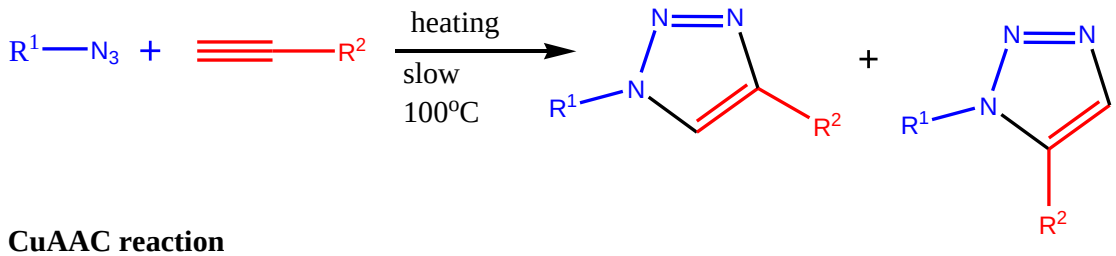

CuAAC reaction

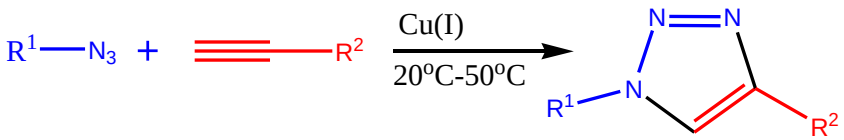

The 1,5-Isomer is not formed

1,4-Isomer only

Scheme 7: A comparison between Huisgen's reaction and CuAAC reaction

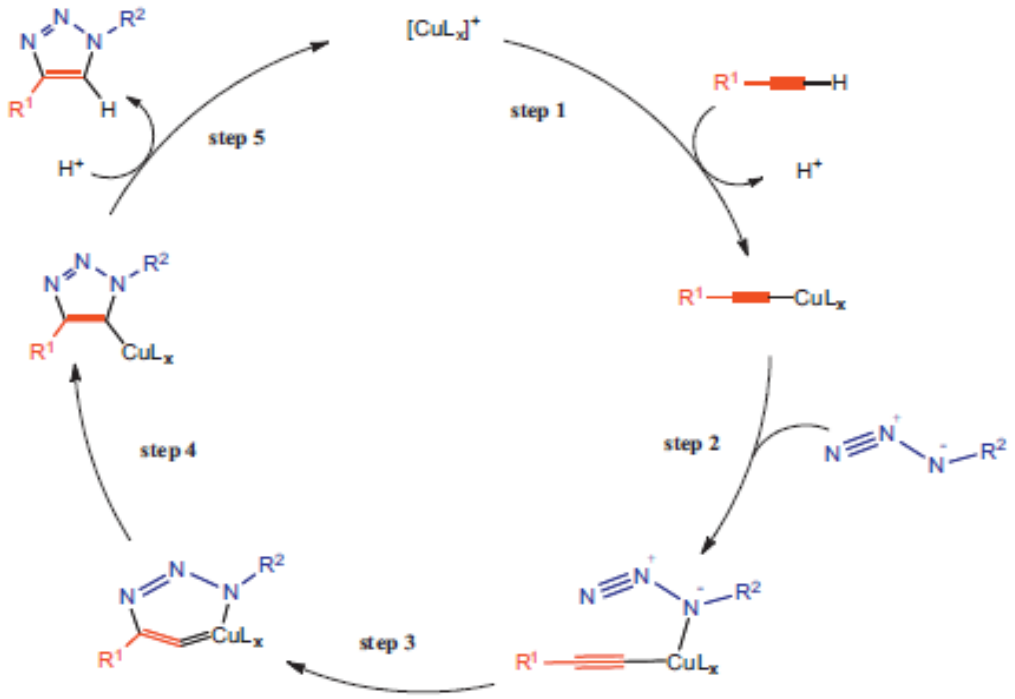

Scheme 8: Mechanism of CuAAC reactions, Adapted from ref 41.

The mechanism of CuAAC reaction (Scheme 8) involves the in situ generation of reactive Cu(I) species which coordinate with alkyne to give Cu(I) acetylide complex. The acetylide complex reacts with the azide group to form a six-member intermediate. The intermediate first produce a five-member ring pre-product in step 4, followed by protonation to yield 1,2,3-Triazole.[42]

The ease of coupling two molecular units with CuAAC reaction has opened increasing applications in organic synthesis, bioconjugation, chromophores and polymer science. These applications involve attaching monomers during polymerization or modifying polymers for a specific purpose such as conjugating with a fluorescent molecule. In 2005, Steenis et al demonstrated an efficient polymerization of fluorene using CuAAC reaction.[43]An average molecular weight of 40 x 10^3 corresponding to 73 repeating units of polyflourene was obtained at room temperature. This result showed that CuAAc click reaction is robust and hence could be used for the polymerization of conjugated polymers. In the biosciences, the two versatile features of click reaction that makes it appealing are that: they can be carried out in aqueous medium and at physiological conditions. And perhaps the other most significant feature of CuAAC reaction is their chemoselectivity. As such they can be used in the modification of highly functional biomolecules such as carbohydrates, polypeptides and nucleic acids. A facile reaction like CuAAC has been recently used in the modification of

biomaterials such as hydrogels, microgels, nanoparticle nanocarriers and polymer-based nanoparticles.[44,45] The ability to modify and cross-linked polymer nanoparticles using CuAAC reaction opens an entirely new avenues for designing tailored-made imaging agents, conjugated polymer-based biosensors and drug delivery systems. In this project, a whole different perspective of click reaction was designed and demonstrated for the generation of white emission from conjugated polymer nanoparticles.

1.3. Applications of conjugated polymers

Perhaps the distinct properties of conjugated polymers attracting tremendous attention for their potential wide range applications in optoelectronics devices such as organic light emitting diodes, organic solar cells, thin film transistors, chemical biosensors and memory devices, [46-53] are due to their ease of modification, structural flexibility, large area fabrication, solution processability and low cost. These unique advantages are recognized and efforts to improve and invent conjugated polymer-based devices are ongoing. Very recently, Wang *et al* reported the design and fabrication of a flexible memory device based on conjugated polymers with thermal/non-thermal recoverable memory behaviors [54]. Although the memory device is many steps away from conventional memories, the author demonstrated the structural flexibility of benzodithiophene (BDT)-based CPs by introducing various substituents to fine-tune the energy level and modulate the electronic structure which can usher in new generation of cheaper and robust polymer-based memory devices. Conjugated polymers have for the past few years been envisioned as a viable alternative to mainstream thin-film transistor (TFTs). Even though organic thin-film transistors have lower hole mobility and not suitable for applications requiring very high switching speeds, the processing advantages and demonstrated performance imply that they can be competitive for novel thin film transistors applications requiring structural flexibility, large area coverage and low cost.[55,56]

A major recent breakthrough in conjugated polymer is their application in organic light emitting diodes (OLEDs) and biosensors. These areas of research and development of conjugated polymer are much wider in scope and interest than any other applications. As a result, deeper analyses of OLEDs are considered exclusively in the next section.

1.3.1. Organic light emitting diodes

The discovery of electroluminescence, which is emission of light due to excitation with flow of electric current, in conjugated polymers at Cambridge University[57] served as a springboard for the development of polymer light emitting diodes (PLED) as a new technology for flat-

panel displays and future solid-state lighting applications. Generally speaking, organic light emitting diodes (OLEDs) consist of a thin-film organic material sandwiched between two electrodes; anode and cathode,that generates light with the application of electricity. When a voltage is applied across the OLED, electrons flow from the cathode to anode, the cathode injects electrons into the emissive layer of the polymer while the anode withdraws electrons from the conductive layer. In other words, the cathode injects electrons into the LUMO of organic material and removes from the HOMO at the anode. At the interface of emissive and conductive layer, electrons from the emissive layer find holes in the conductive layer. The recombination of electron and 'hole' pair results in a relaxation of the energy level of electron; this is followed by the emission of light whose frequency depends on the band gap of the organic material. In conjugated polymers, the emitted light appears in the visible region.

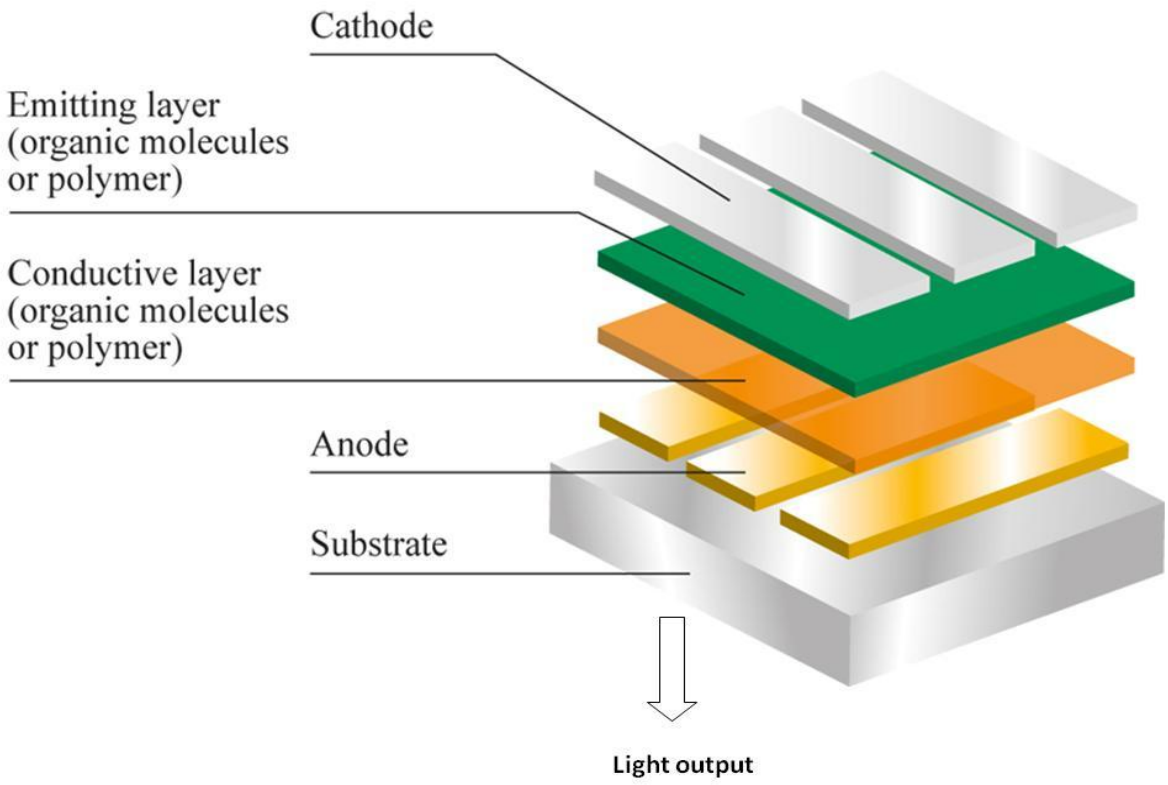

Figure 2: Schematic representation of OLED

With excellent properties of thin, light weight, high power efficiency, wide viewing angle and rapid response, OLED and PLED have the potential to outperform all other lighting sources like incandescent lamps and fluorescent tubes. The power efficiency of fluorescent tube is 60-70 lm/W which is the current benchmark for new lighting source. However, a record efficiency of 110lm/W for green light set a new benchmark for white light. The performance

targets of ongoing research and development activities focused on white emission indicate the potential of OLEDs to emerge as a solid state lighting source for a wide variety of potential applications. A breakthrough in white organic light emitting diodes came in 2009 when a power efficiency of 90lm/W was achieved by Reineke and co-workers.[58]They reported an improved OLED design which surpasses fluorescent tube efficiency by carefully choosing emitter layer with high-refractive- index substrates.[59]

Energy policies around the world encourage innovation that can offer maximum energy savings.[60] One of these innovations is OLED that offers many advantages over both LEDs and LCDs. Patronizing OLED has the following advantages in flexible-displays and solid state light applications:

- OLED have potential low cost because they can be printed easily onto any suitable surfaces.
- The fact that OLEDs can be printed onto any flexible substrates has ushered in several new applications like displays embedded in fabrics and roll-up displays.
- OLEDs pixels directly emit light and hence provides greater range of colors, brightness and viewing angle compare to LCDs.
- OLEDs have the ability of color tuning, that is, it can be tuned to emit light across the visible region.
- They have greater energy saving potentials.
- They are mercury-free
- New freedom in design
- High luminous efficacy

White organic light emitting diodes

The history of white organic light emitting diodes (WOLEDs) began when Kido and co-workers reported that they succeeded in fabricating a device generating light that contain wavelength across the visible region of the spectrum.[60] Since then, white organic light emitting diodes have become a hot research topic owing to their preference in next generation solid state lighting. In the early works of Kido *et al*, white emission was achieved by mixing three fluorescent dyes that is blue, green and orange into a single emissive layer which generated a broad white electroluminescence spectrum. Today different white light architectures for organic solid state lighting (SSL) are employed, including combination of

multiple emitters or using a blue /UV device that stimulate phosphorescence or fluorescence in other materials, which leads to white light emission (Figure 3).

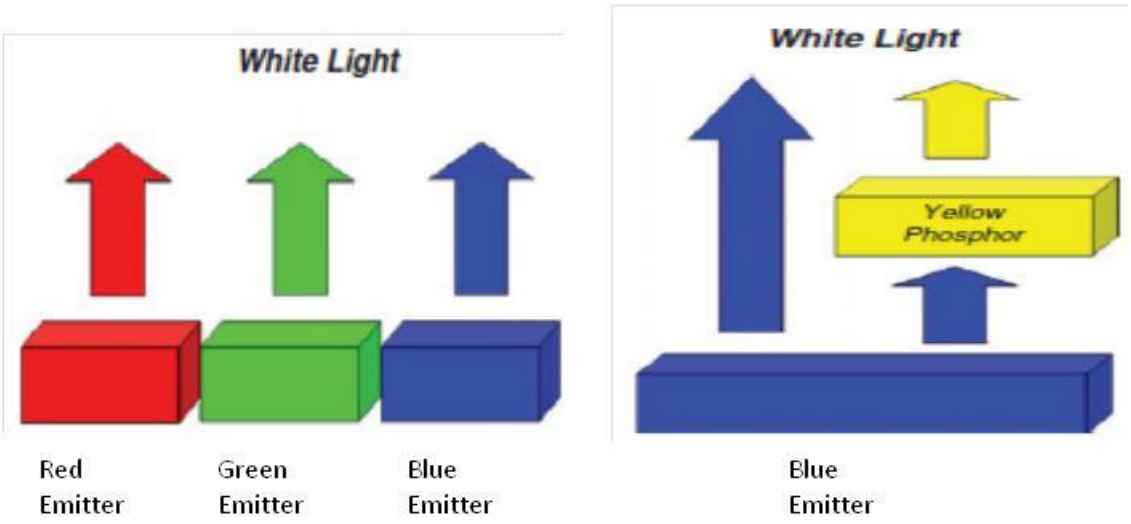

Figure 3: Two approaches to generate white light in OLEDs: direct combination of red, blue, and green light (left) using either lateral patterning or vertical stacking of the three emitters and partial down-conversion of blue light (right) using fluorescent or phosphorescent layers on the substrate. Adapted from ref. 61

OLEDs with stacked or laterally patterned multicolor emitter can have high efficiency while also allowing the user to control the lighting color. While it is possible to create white OLED from different dopants in a single layer, a careful control of dopant concentration is necessary to prevent the transfer of all the exciton energy to the longest-wavelength emitter.[61] Controlling the level of energy transfer is important in obtaining balance emission from chromophores to render white light. In any case, there is no such thing as "correct white" considering the main parameters used to determine the quality of white light. To this end, several standards and parameters to characterize the quality of white light source have been developed. White lights have three characteristics; the Commission Internationale d'Eclairage (CIE) chromaticity coordinates (x, y), the Color Rendering Index (CRI) and the Correlated Color Temperature (CCT)

The commission Internationale d'Eclairage (CIE) chromaticity diagram was established in 1931.[62]The coordinate (x,y) indicate the emission color in the chromaticity diagram in Figure

4(a). A perfect white light would have CIE coordinates (0.33, 0.33). Notwithstanding, there is broad region of the diagram around the white point that can be considered as white light. The color Rendering Index (CRI) is the measure of the ability of a light source to reveal the true color of an object with reference to an ideal or natural source. CRI values range from 0-100 and a value less than 70 is considered unacceptable for indoor lighting applications. WOLEDs have excellent CRI values due to their similarity to incandescent lamps (>90) and can be higher than most LCDs and fluorescent tubes.[61] Finally, the Correlated Color Temperature (CCT) which refers to the temperature of blackbody radiator that radiates light of the same color as the light source. A CCT values ranging from 2500-6500K are necessary for lighting applications; for instance, incandescent have a CCT of 2700K, and fluorescent lamps 3000-4000K, which is considered desirable for in-house lighting.[63]

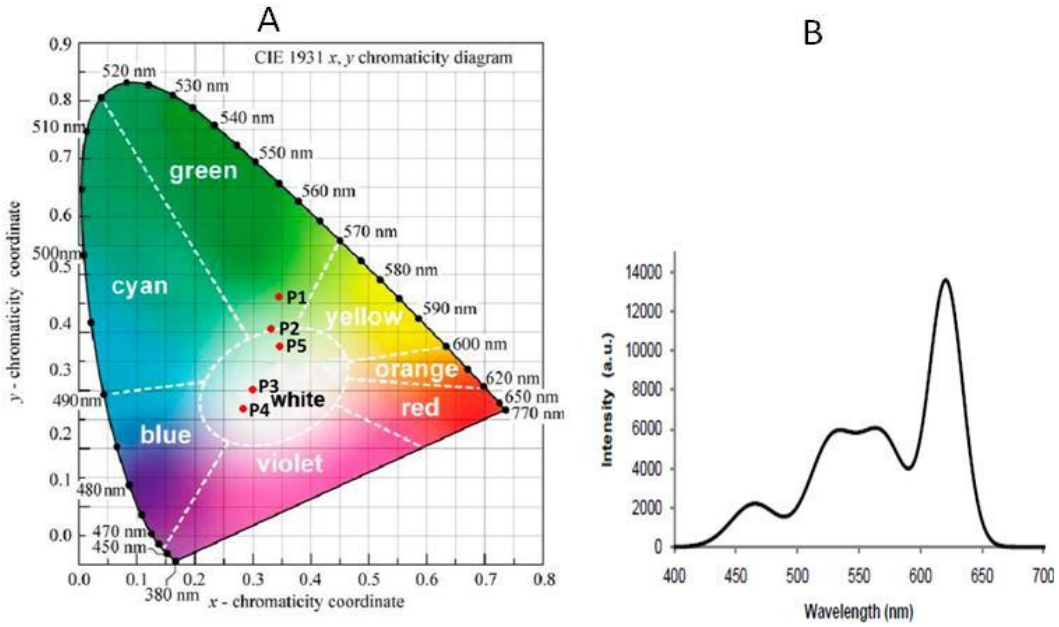

Figure 4: (a) CIE 1931 chromaticity diagram with the white region shown in a circle (b) Spectrum of an ideal white light. Reprinted with permission from ref. 64, Copyright © 2014, American Chemical Society.

Approaches toward white light generation in polymers

As oppose to monochromatic OLEDs, WOLEDs generates broad electroluminescence spectra that tends to mimic natural white light. Therefore, several emitters containing three primary colors (blue (B), green (G) and red (R)) or two complementary colors (blue and orange), are usually utilized to construct a WOLED. The common strategies used to produce white light in WPLEDs are as follow:

Polymer blend:

In this method, the emitters required to produce white light are mainly based on polymers especially the fluorescent ones.[65]The polymers emitting in different colors are dissolved in appropriate solvent with desired ratios, and used to prepare the emissive layer of WPLEDs. Similarly, a combination of small organic molecules can be doped into single polymer host (poly(N-vinylcarbazole) or polyfluorene etc) with specific ratio for each components.[66]Due to good compatibility among the polymers, the issue of phase separation is relieved. However, fluctuating energy transfer among the polymeric emitters is inevitable and WPEDs prepared with this approach show low electroluminescence efficiency.

Single white-emitting polymer:

In this approach, the emissive polymer bears R-G-B or B-O combinations, which can be incorporated into the polymer backbone. Calculated ratios of the different emitting moieties of the initial monomers are copolymerized to form a single white emitting polymer. This approach can be effective in terms of avoiding phase separation, but cascade of energy transfer among different emitting centers is still present in this system. The problem was successfully averted by Wang *et al* by precisely controlling the content of the long wavelength moieties at a low level in the white emitting polymer. As a result, energy transfer from the blue-emitting polymer backbone to the long wavelength moieties is incomplete. Moreover, energy transfer process among the long wavelength chromophores is negligible due to their low content in the emissive polymer. [67]

1.4. Synthesis and applications of conjugated polymer nanoparticles

Water dispersible conjugated polymers and oligomers nanoparticles (CPNs) have recently drawn considerable attention for their optoelectronic and biological applications owing to their small size, straight forward preparation method, and their tuneable and remarkable photoluminescence properties.[68-70] Conjugated polymers can be made water soluble by introducing ionic or hydrophilic functional groups. However, nanoparticle approach forming water dispersible conjugated polymer has opened up further opportunities. It is worth mentioning that the stability of CPNs is crucial in any potential applications. For this reason, any effort to obtain shape persistent and stable CPNs in water could find highly valuable applications. There are two main methods to prepare conjugated polymer nanoparticles: The miniemulsion and reprecipitation methods.

1.4.1. Miniemulsion method

The preparation of conjugated polymer nanoparticles by emulsification techniques require the generation of adequate small droplets that are stable enough to prevent coalescence and Ostwald ripening prior to solvent removal. First, polymer solution in water immiscible organic solvent is injected into aqueous solution of desired surfactant.[71] The resulting mixture is then ultrasonicated to generate miniemulsion of small droplets of polymer solution. When the organic solvent is removed, stable nanoparticle dispersion in water is formed (Figure 5). The formation of coalescence among the droplets is prevented by the surfactants adsorbed at the interface of polymer droplets and water. A hydrophobic agent may be added to prevent Ostwald ripening of the particles, but in most cases this role is presumably satisfied by the polymer itself. Nanoparticles size range from 13 nm to 500 nm depending on the content of surfactants and polymer concentration.[72]

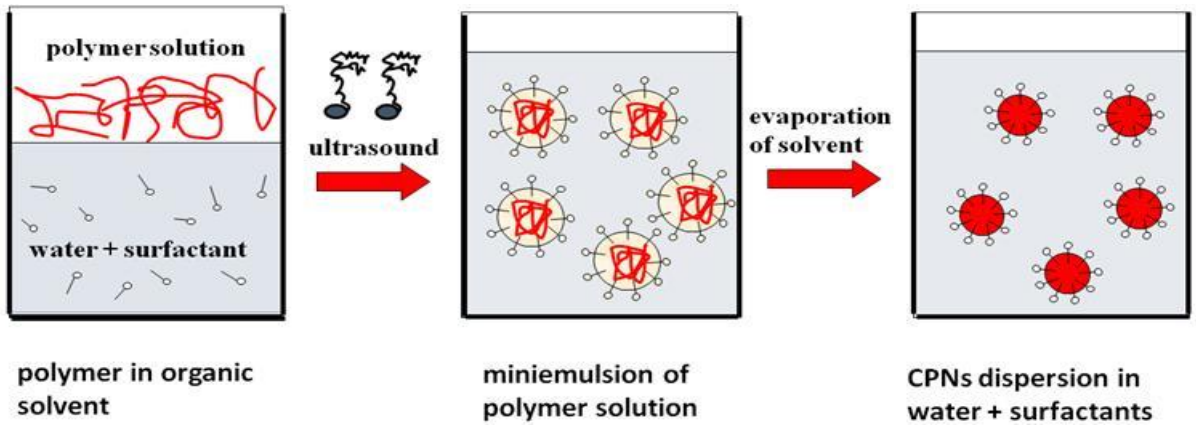

Figure 5: Preparation of polymer nanoparticles by miniemulsion technique

1.4.2. Reprecipitation method

The preparation of conjugated polymer nanoparticles by reprecipitation, also called nanoprecipitation or precipitation, requires the rapid addition of polymer dissolved in good organic solvent to excess volume of water. When the mixture is ultrasonicated, precipitation of the polymer is induced by hydrophobic effect. The polymers tend to avoid contact with water and coil into spherical nanoparticles. After the nanoparticles are formed, the organic solvent is removed to obtain stable water dispersible particles (Figure 6). Different from the aforementioned technique, no surfactant or hydrophobic agent is required to achieve shape persistent nanoparticles. The method is a versatile way of preparing conjugated polymer nanoparticles; just by varying the polymer concentration, the size of the nanoparticles can be tuned to the desired size.[73]

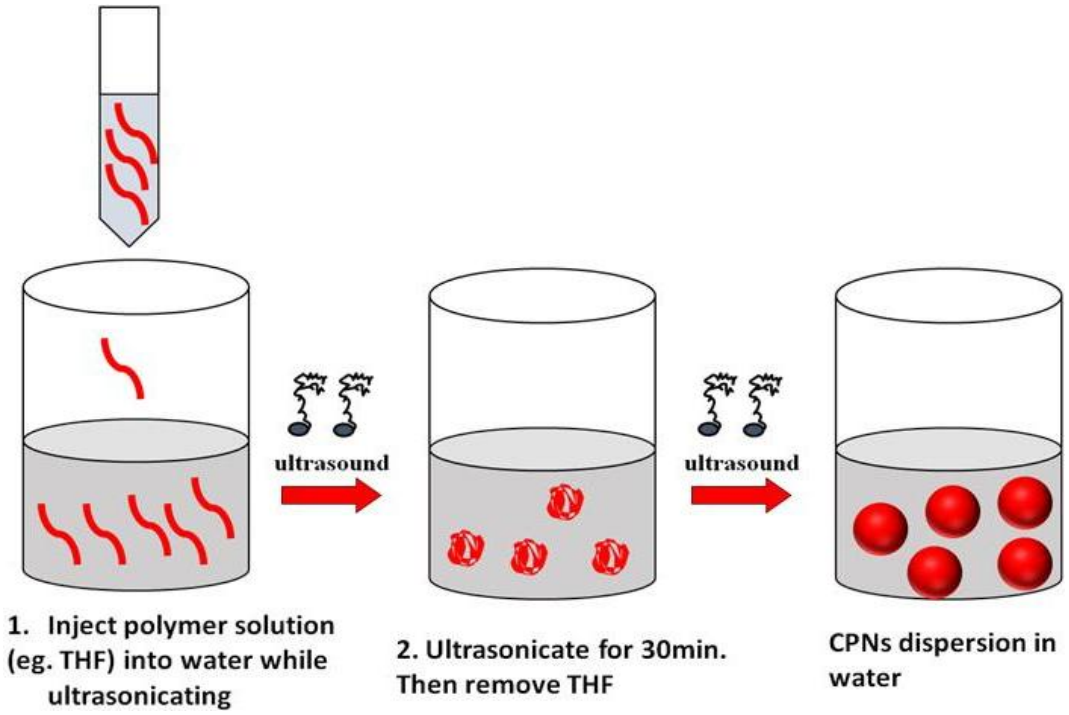

Figure 6: Preparation of polymer nanoparticles by reprecipitation technique

Recently, Wang *et al* demonstrated the preparation of carboxyl functionalized CPNs by co-precipitation of four conjugated polymer with poly(styrene-co-maleic anhydride (PSMA) (Scheme 9). The nanoparticles were then modified with antibody to form CPNs-antibody conjugates, which were found to have higher specificity for tumor cells detection.[74]With varying mixing ratio of the four polymers, an average particles size of 35 nm was obtained with muticolor emission at one excitation wavelength. The emissions of the polymers were regulated through FRET.

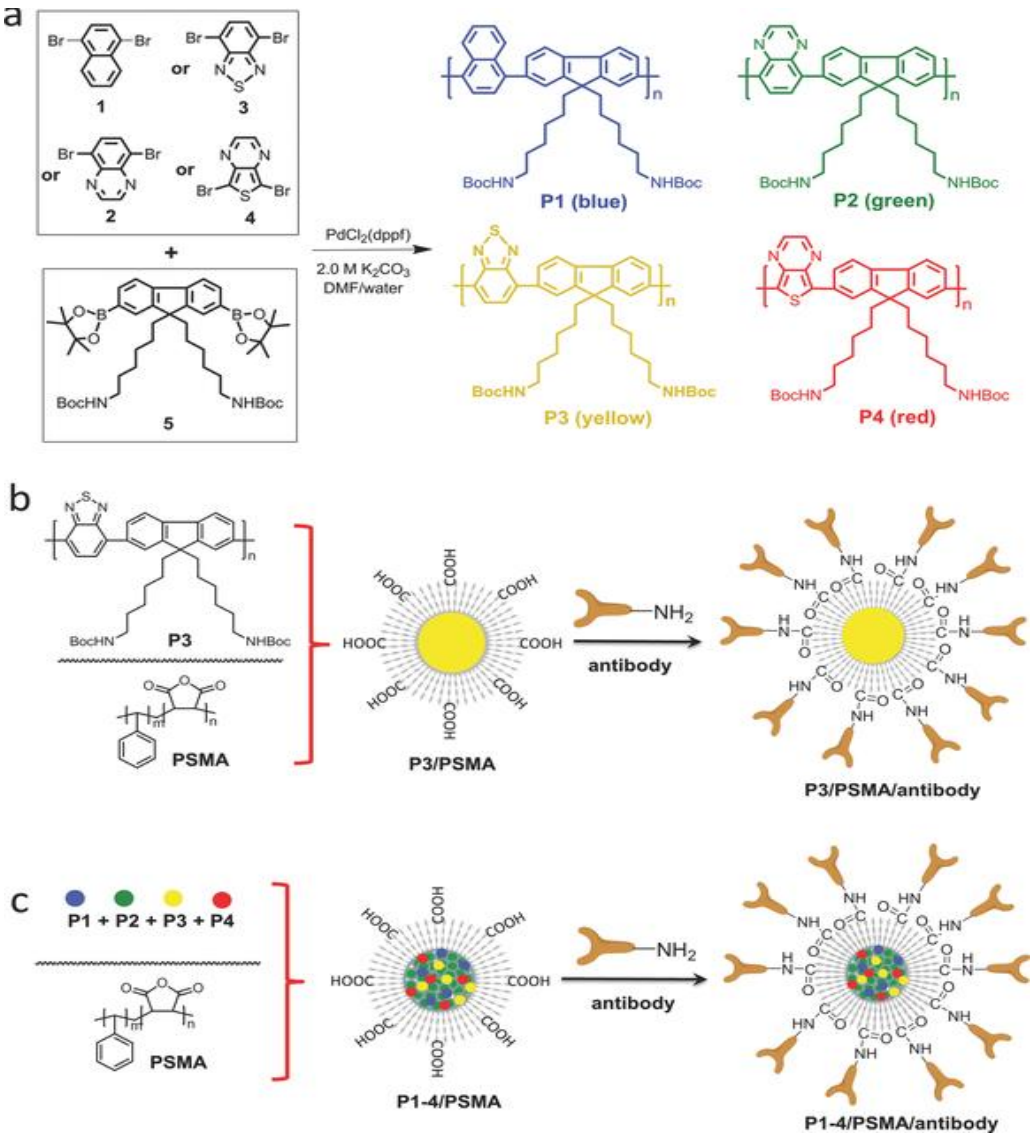

Scheme 9: (a) The synthetic route and chemical structures of conjugated polymers (P1∼ P4)

(b) The general preparation of conjugated polymer nanoparticles (P3/PSMA) and their modification with an antibody. (c) The preparation of multicolor conjugated polymer nanoparticles (P1–4/PSMA) and their modification with an antibody. Reproduced with permission from ref. 74, Copyright © 2014, WILEY-VCH Verlag GmbH & Co. KGaA, Weinheim.

1.4.3. Förster Resonance Energy Transfer

When chromophores are irradiated with photons of appropriate wavelength, electrons at the ground state are excited and promoted to excited state by absorbing photons. The excited state electron relaxes back to the ground state through a number of ways. Relaxation of the excited state electrons accompany by emission of photons is called fluorescence. However, in the case of FRET, excited state electron relaxes back to ground state through non-radiative

pathway without emitting photons. A typical Jablonski diagram describing FRET in donor and acceptor chromophores are presented in Figure 7. In FRET, donor chromophores at its excited state transfer energy to a nearby acceptor through dipole-dipole interactions.

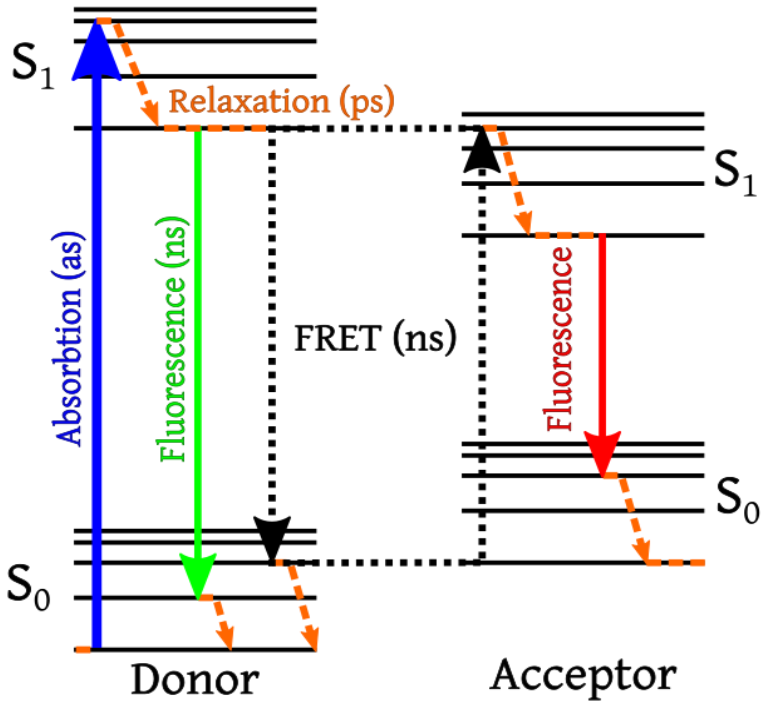

Figure 7: Jablonski diagram describing FRET in donor-acceptor pair[75]

Fluorescent energy transfer or Förster resonance energy transfer (FRET) in nanoparticles is an important phenomenon that can be exploited to tune the emission color of nanoparticles for optoelectronic (OLEDs), sensing and imaging applications.[76-79] FRET is a distance dependent non-radiative energy transfer from an excited donor chromophore to a suitable acceptor chromophore. This process is facilitated by the coupled dipole-dipole interactions between the donor and acceptor molecules. For energy transfer to occur there should be an overlap between the emission spectrum of the donor with the absorbance spectrum of the acceptor molecule. Moreover, the donor and acceptor pairs need to be in close distance, typically 1-10 nm.

In 2013, McNeill et al prepared blended poly[(9,9-dioctylfluorenyl-2,7-diyl)-co-(1,4-benzo-{2,1′,3}-hiadiazole)] (PFBT)/poly[2-methoxy-5-(2-ethylhexyloxy)-1,4-phenylenevinylene] (MEH-PPV) conjugated polymer nanoparticles and studied energy transfer from host polymer to dopant polymer.[80]The nanoparticles show red emission and improved quantum efficiency resulting from highly efficient energy transfer from donor PFBT to acceptor MEH-PPV as well as suppression of MEH-PPV aggregation (Figure 8). Apart from the efficient

energy transfer observed, the quantum efficiency was also due to the small molecule fraction of MEH-PPV which minimizes aggregation induced quenching typically observed in MEPV.[81,82] In addition, the blended nanoparticles exhibit better photostability than undoped MEH-PPV.

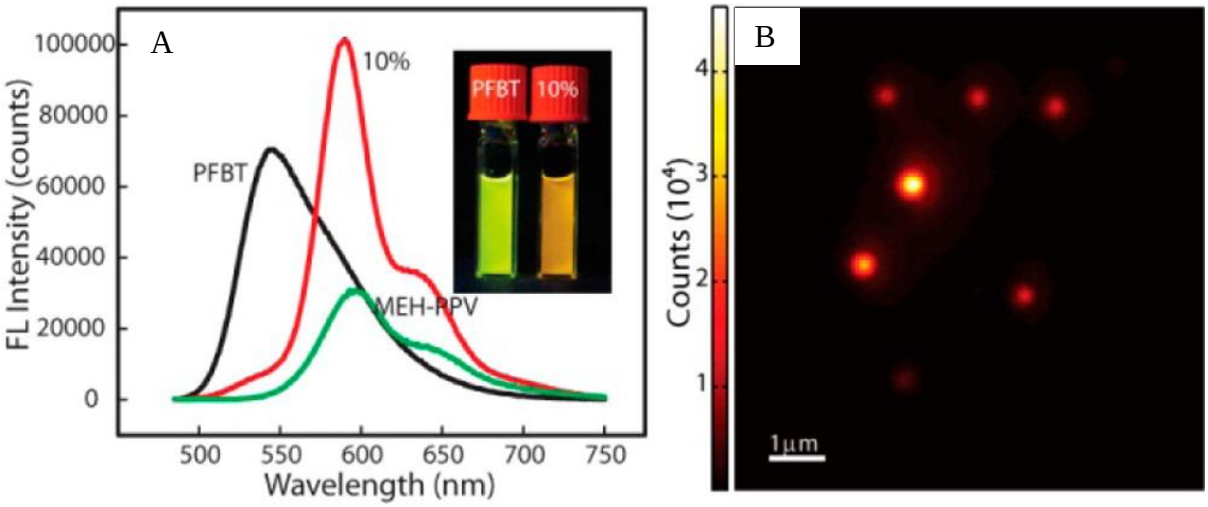

Figure 8: (a). Fluorescence spectra of polymer nanoparticles PFBT, 10% PFBT/MEH-PPV, and MEH-PPV under λex =473 nm.(b) Representative fluorescence image of single 10% PFBT/MEH-PPV nanoparticles immobilized on a coverslip. Reprinted with permission from ref. 80, Copyright © 2013, American Chemical Society

1.4.4. Optoelectronic applications

Conjugated polymer nanoparticles prepared through miniemulsion or reprecipitation methods have been investigated for their potential application in OLEDs, solar cells and imaging. Exploiting the tuneable emission in hybrid nanoparticles through energy transfer, Foulger and co-worker fabricated OLEDs from blue and green emitting polymer. They showed that the hybrid nanoparticles formed stable aggregate to construct OLED, but no information was given about the efficiency of this device.[83]

Mixed polymer nanoparticles can be obtained either as separate polymer particles or as a particle containing different polymers (Scheme 10). In a study to demonstrate energy transfer in bi-polymer nanoparticles for their optoelectronic applications, different bicomponent nanoparticles: separate, mixed and core-shell particles made of PF and MEH-PPV were prepared by reprecipition method.[84]The first case involves mixture of separate donor and acceptor nanoparticles, no energy transfer was observed due to the long distance in solution. Energy transfer was observed in the design were solution of donor and acceptor were mixed prior to nanoparticle formation. The energy transfer was attributed to the close distance

between donor and acceptor. Core-shell nanoparticles of PF and MEH-PPV were prepared by first injecting stock solution of one polymer into water and subsequently adding the second polymer. The highest energy transfer efficiency (up to 35%) was recorded for the core-shell in which PF forms the outer shell of the nanoparticles. This study showed that the emission of hybrid nanoparticles can be tuned by FRET and also by the morphology of the particles. This could be useful for preparing white emitting nanoparticles for OLED applications.

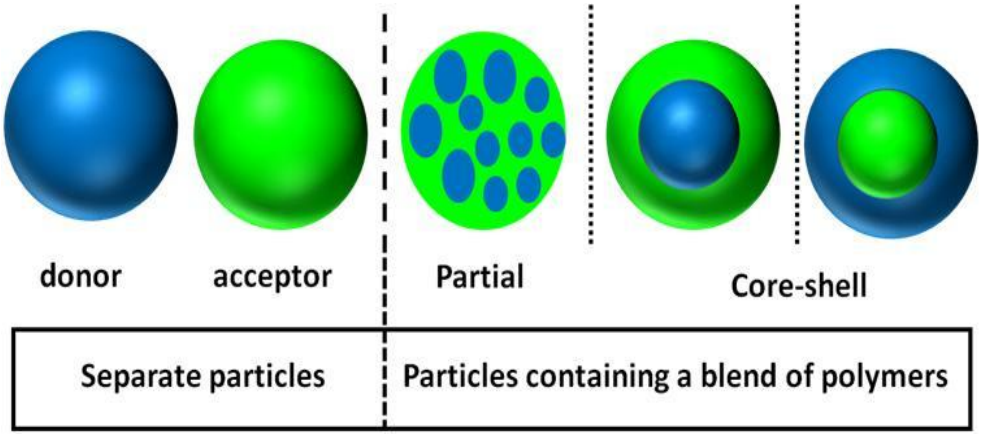

Scheme 10: Representation of bi-polymer nanoparticles

In 2013, Akagi *et al* investigated photo-switching of white fluorescence in nanosphere composing of three polymers (R-G-B) by introducing photo-isomeric moieties in the side chain. The nanospheres exhibit photo-switchable white fluorescence between emission and quenching by irradiating external lights in both the nanosphere solution and film state.[85]

1.4.5. Biological and Biomedical Applications

Water dispersible conjugated polymer nanoparticles hold great potential for biomedical applications owing to their organic nature and superior absorbing abilities. Many CPNs have been prepared recently and used as bright nanoprobes for biomedical imaging applications. Despite the high optical properties of conjugated polymers, their fluorescence quantum yield, particularly in the red or NIR region drops drastically when converted into nanoparticles. This quenching in fluorescence is common in most organic chromophores at high concentration or aggregated state.[86] The common approach to obtain brighter NPs for imaging is to use FRET to shift fluorescence emission to the NIR for improved tissue penetration depth and reduced autofluorescence background. This can be achieved by simply combining CP-based energy donors and various energy acceptors into nanoparticles.

However, Kim and co-workers successfully prepared a cyanosubstituted derivatives of poly(p-phenylenevinylene) (CN-PPVs) that exhibits efficient photoluminescence in the long

wavelength region in the aggregate film state with high quantum yield.[87] As a result they adopted CN-PPVs as the emissive core to produce water dispersible NPs with bright solid state fluorescence. It was also proved that NPs concentrated with dyes showing aggregation enhanced fluorescence can be used as bright probe for two-photon fluorescence microscopy.

Similar to using donor and acceptor to form FRET pair in NPs, Lui's group reported the formation of NPs from CPs with intramolecular energy transfer characteristics. They synthesized a highly emissive conjugated block copolymer, poly[(9,9-dihexylfluorene)-co-2,1,3-benzothiadiazole-co-4,7-di(thiophen-2-yl)-2,1,3-benzothiadiazole] (PFBTDBT10), which contain 90% of the donor units and 10% of the acceptor units in the polymer backbone. The small concentration of the acceptor was enough for complete energy transfer and also to minimized fluorescence quenching when the polymers collapse to form NPs.[88] The NPs have an impressive quantum yield of 27% in red/NIR region. They use murine hepatic tumor model and good tumor targeting and imaging efficiency was achieved (Figure 9). [89]

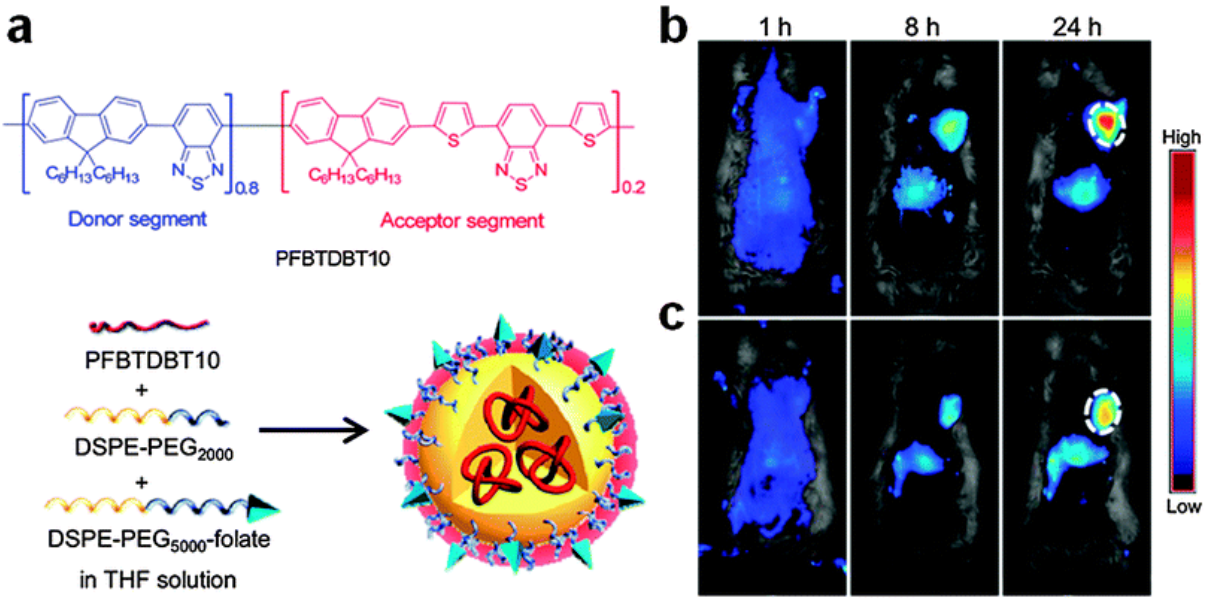

Figure 9: Nanoparticles loaded with PFBTDBT10 block copolymers for tumor molecular targeting and imaging.

(a) Chemical structures of PFBTDBT10 as well as the schematic illustration of PFBTDBT10-loaded folic acid-targeted nanoparticles. Two narrow-bandgap monomers, 2,1,3-benzothiadiazole (BT) and 4,7-di(thiophen-2-yl)-2,1,3-benzothiadiazole (DBT), are incorporated into the conjugated backbone of poly(9,9-dihexylfluorene) to yield PFBTDBT10. The concentration of DBT in the energy acceptor unit is set at 10 mol% of the total monomers to ensure complete energy transfer while avoiding self-quenching. (b) In vivo non-invasive fluorescence images of H22tumor-bearing mice at various time points post intravenous injection of the targeted nanoparticles and non-targeted nanoparticles. The white circles indicate the tumor sites. Reprinted with permission from ref. 89, Copyright © 2013, Royal Society of Chemistry.

1.5. Aim of the Thesis

The aim of this thesis was to synthesize conjugated polymers and convert them into shape-persistent and water dispersible multi-component nanoparticles for their applications in white polymer light emitting diodes and bioimaging

Polymers synthesized in this study are namely: poly[(9,9-bis{3-azidopropyl}fluorenyl-2,7-diyl)-*co*-benzene] (**PFBN3**), poly[(9,9-bis(3-(prop-2 ynyloxy)propyl)fluorenyl-2,7-diyl)-*co*-(1,4-benzo-{2,1,3}-thiadiazole)] (**PFBT-Pgy**), poly[(2-azidoethyl)-2-(5-(thiophen-2-yl)thiophen-2-yl)thiophene (**PTN3**) and poly[(4-(2-(prop-2-ynyloxy)ethyl)thiophen-2-yl)-co-(1.4-benzo{1,2,5}thiadiazole)] (**PBTTH-Pgy**), each of these polymers were incorporated into multi-shell nanoparticle design to form white emitting nanoparticles. Through energy transfer in these polymers we seek to control and investigate the emission of different bipolymer and tandem nanoparticles designs for the generation of white light.

Chapter 2

2. Results and Discussion

This chapter is divided into four sections. Section one deals with synthesis and characterization of conjugated polymers. In section two, preparation and characterization of conjugated polymer nanoparticles are discussed. Section three introduces a novel bipolymer nanoparticle design. The optical and photophysical properties as well as the morphological studies of these bipolymer nanoparticles are thoroughly explained. Finally, in the fourth section, preparation and characterization of tandem white emitting nanoparticles are discussed with special emphasis on the nanostructure design and mechanism of emission color tuning.

2.1. Synthesis and characterization of conjugated polymers

In order to design white emitting polymeric nanostructures, series of polymers based on fluorene, thiophene, benzene or benzothiadiazole were synthesized and characterized. For polymerization, Suzuki coupling reaction was utilized to form new C–C bond between the monomers. Suzuki coupling turns out to be ideal because of its simplicity and easy availability of starting materials such as boronic esters and boronic acids. It's environmental friendly and there is no known toxic by-product associated with the reaction. These polymers as shown in Scheme 11 carry functional groups such as azide or alkyne purposely for click reaction as strategy for obtaining stable and shape-persistent nanoparticles from polymer blends.

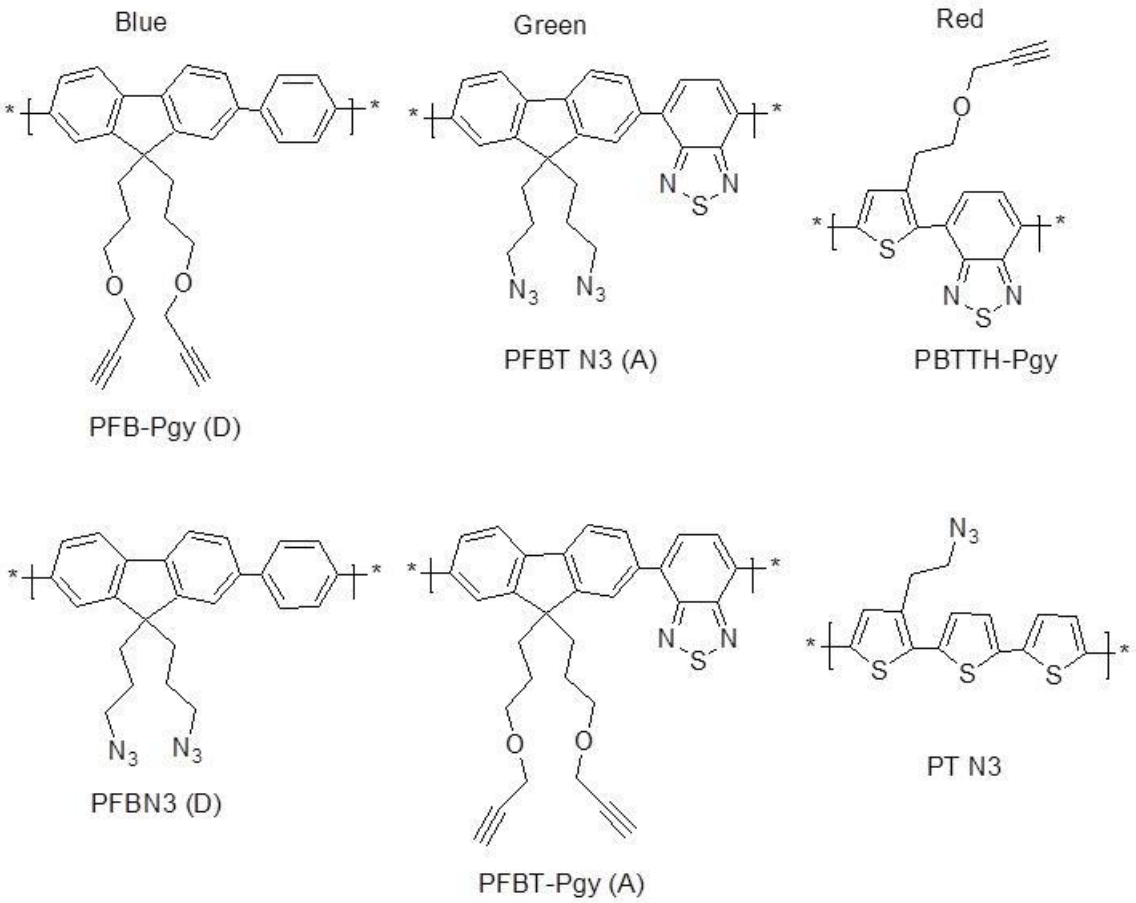

Scheme 11: Structure of polymers used in this study

The optical properties of the resulting polymers were tuned by using suitable monomers for polymerization. For example, the acceptor polymer was designed so that its UV-VIS absorbance overlaps with the emission of the donor polymer. The spectral overlap is an essential requirement for non-radiative energy transfer between polymers. The polymers were characterized by ^{1}H-NMR, FTIR, UV-Vis and fluorescence spectroscopy.

2.1.1. Synthesis and characterization of poly[(9,9-bis{3-azidopropyl}fluorenyl-2,7-diyl)-*co*-benzene] (PFBN3)

For the synthesis of PFBN3, M1 was first synthesized from 2,7-dibromofluorene and 1,3-dibromopropene according to Scheme 12 . The protons at 9th position of fluorene are acidic due to the electron withdrawing aromatic rings. Strong base was used to abstract these protons for nucleophilic substitution reaction with 1,3-dibromopropane.

The ^{1}H-NMR spectrum of M1 is shown in Figure 10. The protons near bromine show triplet at 3.17 ppm. Multiplets due to CH_2 protons appear at 2.16 ppm and 1.15 ppm. There are also characteristic aromatic peaks from 7.50-7.57 ppm.

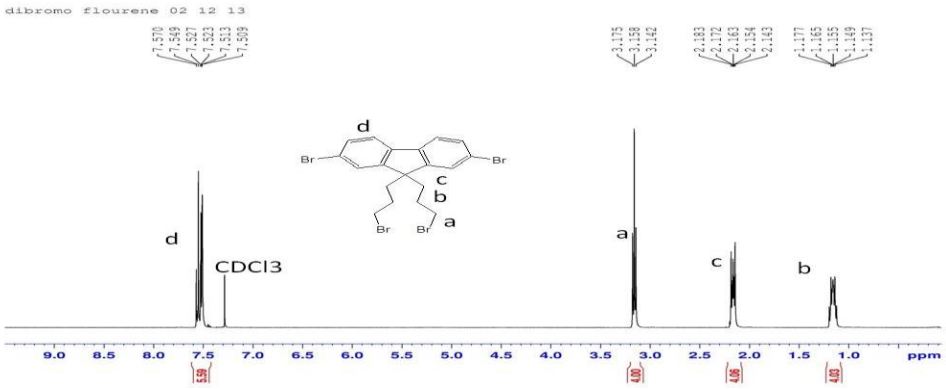

Figure 10: ^{1}H-NMR (400 MHz, $CDCl_3$, 25^{o}C) spectrum of M1

M1 and Benzene 1,4-boronic acid were polymerized through Suzuki cross coupling reaction in a mixture of toluene and THF to synthesized PFB as in Scheme 12.

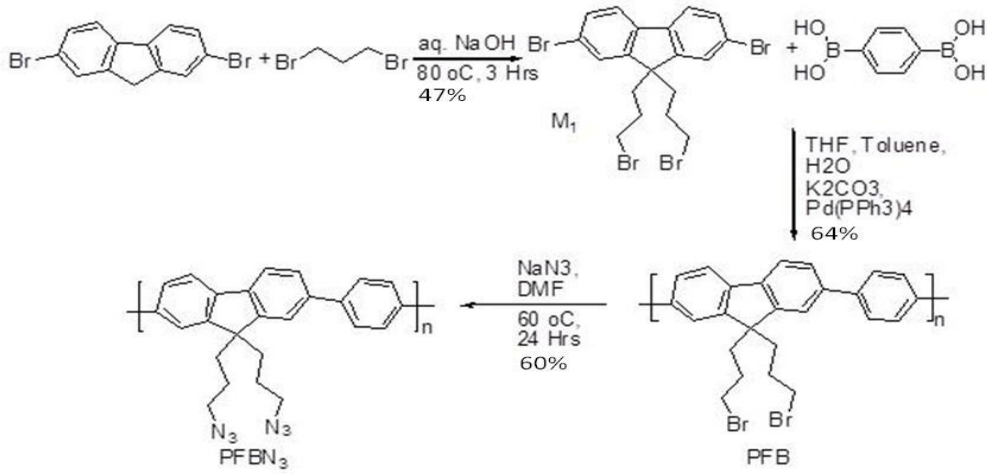

Scheme 12: Synthetic mechanism of poly[(9,9-bis{3-azidopropyl}fluorenyl-2,7-diyl)-co-benzene] (PFBN3)

After obtaining PFB, it was characterized with ^{1}H-NMR spectroscopy as shown in Figure 11.The ^{1}H-NMR spectrum indicate multiplet from 7.4-7.9 ppm due to protons on the aromatic ring, triplet at 3.2 ppm due to CH_2 protons which are near an electronegative bromine atom. Protons in CH_2 at position 'a' indicate triplet at 2.31 ppm and at 1.25 ppm multiplet observed for CH_2 closest to the aromatic ring.

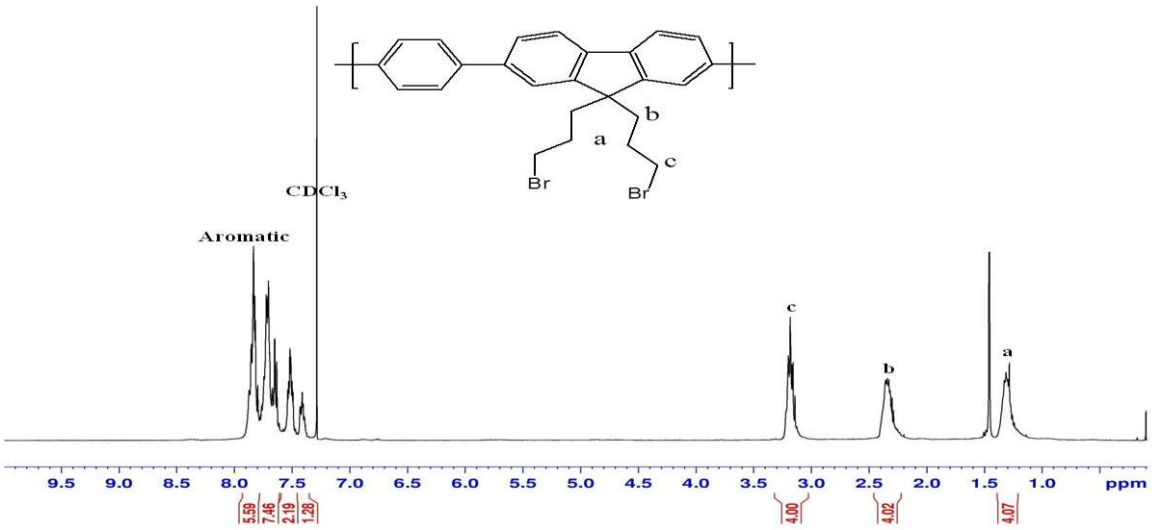

Figure 11: ^{1}H-NMR (400 MHz, $CDCl_3$, 25^{o}C) spectrum of Synthesis of poly[9,9-bis(3-bromopropyl)-9H-fluorene-co-benzene], PFB

To obtain PFBN3 as in Scheme 12, PFB was functionalized with azide using sodium azide in DMF. The ^{1}H-NMR spectrum in Figure 12 shows shift in methylene protons near azide from 3.20 ppm in PFB to 3.065 ppm in PFBN3. This strongly indicates the successful nucleophilic substitution of bromide with azide group. However, the methylene protons at position 'a' indicates triplet at 2.25 ppm, methylene protons closest to aromatic ring shows doublet at 1.063 ppm and multiplet from 7.42-7.832 ppm represent aromatic protons.

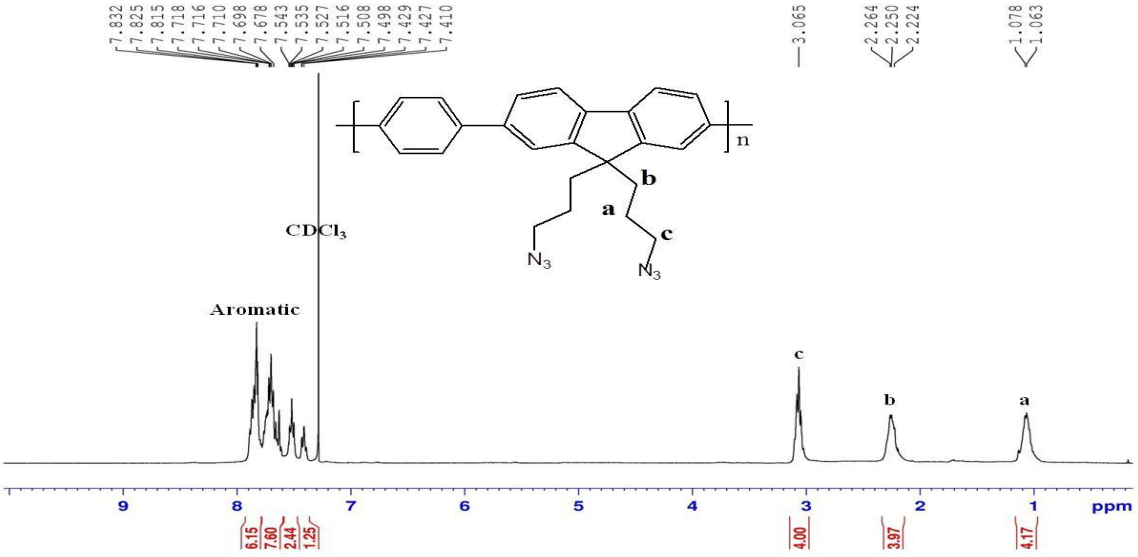

Figure 12: ^{1}H-NMR (400 MHz, $CDCl_3$, 25^{o}C) spectrum of azide functionalized poly[(9,9-bis{3-azidopropyl}fluorenyl-2,7-diyl)-co-benzene] (PFBN3)

FTIR spectra of PFB and PFBN3 polymers are shown in Figure 13. The spectrum shows aromatic Ar-H stretching band at 3030 cm^{-1} and aliphatic -C-H stretching band at 2928 cm^{-1}.

A strong peak at 2095 cm^{-1} is characteristic of azide stretching in PFBN3.This confirms the successful functionalization of PFB with sodium azide to yield PFBN3.

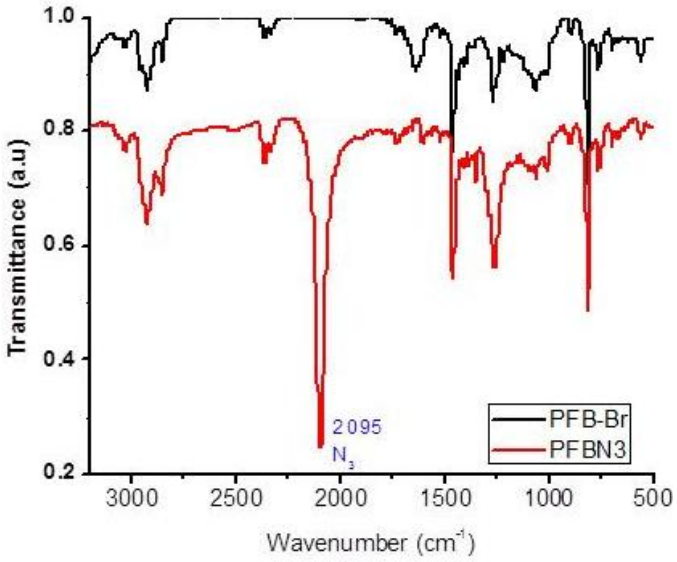

Figure 13: FTIR (Solid state, KBr pellet) spectra of poly[9,9-bis(3-bromopropyl)-9H-fluorene-co-benzene] (PFB-Br) and Azide functionalized poly[(9,9-bis{3-azidopropyl}fluorenyl-2,7-diyl)-co-benzene] (PFBN3)

For optical properties, PFBN3 was characterized by UV-Vis and fluorescence spectroscopy in THF. The absorption and emission spectra are shown in Figure 14. Absorption maximum band appears at 350 nm while emission maxima occur at 407 nm and 427 nm.

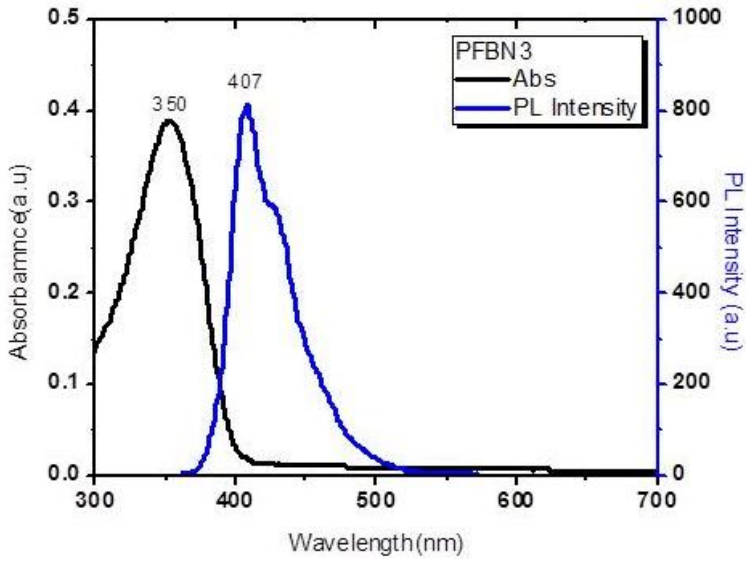

Figure 14: UV-VIS and Fluorescence Spectra of poly[(9,9-bis{3-azidopropyl}fluorenyl-2,7-diyl)-co-benzene] (PFBN3) in THF

2.1.2. Synthesis and characterization of poly[(9,9-bis(3-(prop-2-ynyloxy)propyl) fluorenyl-2,7-diyl)-*co*-benzene (PFB-Pgy)

The synthesis of PFB was described in Scheme 13. To synthesize polymer PFB-Pgy, PFB was dissolved in propargyl alcohol and solution of K_2CO_3 in DMF was added and stirred for 48h at room temperature. Here propargyl alcohol is acting as both solvent and reactant. After the reaction was over, excess solvent was removed and residue was dissolved in THF. Precipitation in water was done to remove any propargyl alcohol in the product and finally dried under vacuum.

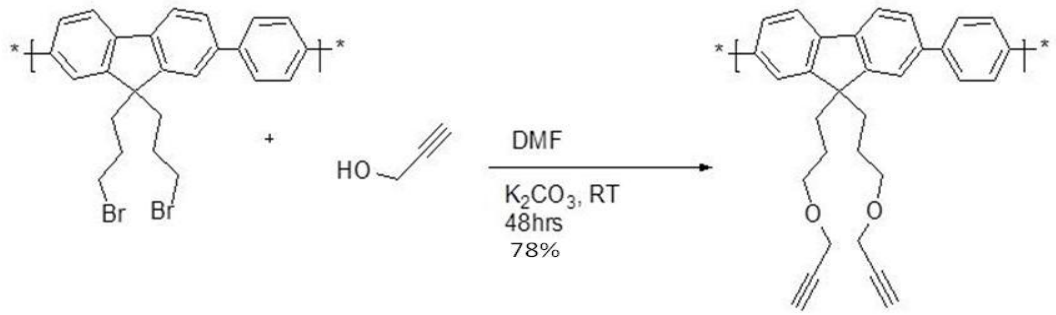

Scheme 13: Synthesis of poly[(9,9-bis(3-(prop-2-ynyloxy)propyl)fluorenyl-2,7-diyl)-co-benzene (PFB-Pgy)

Characterization of PFB-Pgy polymer was done by ^{1}H-NMR and FTIR spectroscopy. From the NMR spectrum in Figure 15, aromatic protons appear at 7.40-7.89 ppm, the proton designated as 'a' resonates at 2.38 ppm, which is characteristic of protons of terminal alkynes. Due to the presence of an electronegative oxygen atom, protons labelled 'b' and 'c' are deshielded and shifted downfield to 4.0 ppm and 3.30 ppm respectively.

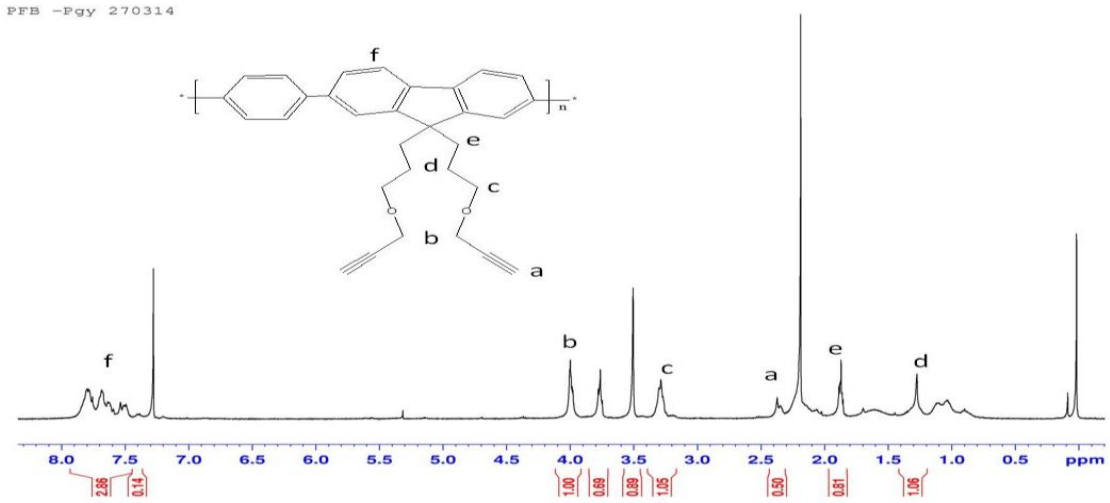

Figure 15: ^{1}H-NMR (400 MHz, $CDCl_3$, 25^{o}C) spectrum of poly[(9,9-bis(3-(prop-2-ynyloxy)propyl)fluorenyl-2,7-diyl)-co-benzene (PFB-Pgy)

The FTIR spectrum shown in Figure 16 clearly indicates two characteristic signals confirming polymer PFB-pgy. First, a sharp peak at 3300 cm^{-1} corresponds to C-H stretching in terminal alkynes. The second peak at 2119 cm^{-1} is weak and typical of -C≡C- stretching. In addition Ar-H stretching can be found at 3030 cm^{-1} and the peaks at 2928 cm^{-1} and 1450 cm^{-1} indicate C-H stretching and bending respectively in alkanes.

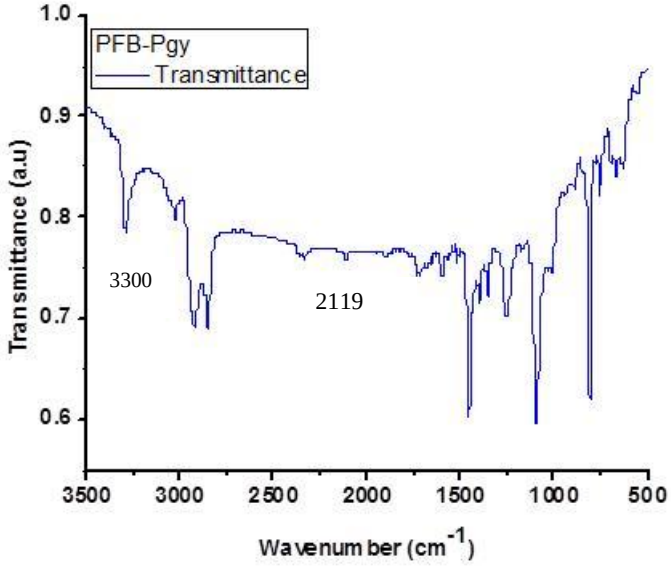

Figure 16: FTIR (Solid state, KBr pellet) spectrum of poly[(9,9-bis(3-(prop-2-ynyloxy)propyl)fluorenyl-2,7-diyl)-co-benzene (PFB-Pgy)

2.1.3. Synthesis and characterization of poly[(9,9-bis(3-(prop-2-ynyloxy)propyl) fluorenyl-2,7-diyl)-*co*-(1,4-benzo-{2,1,3}-thiadiazole)] (PFBT-Pgy)

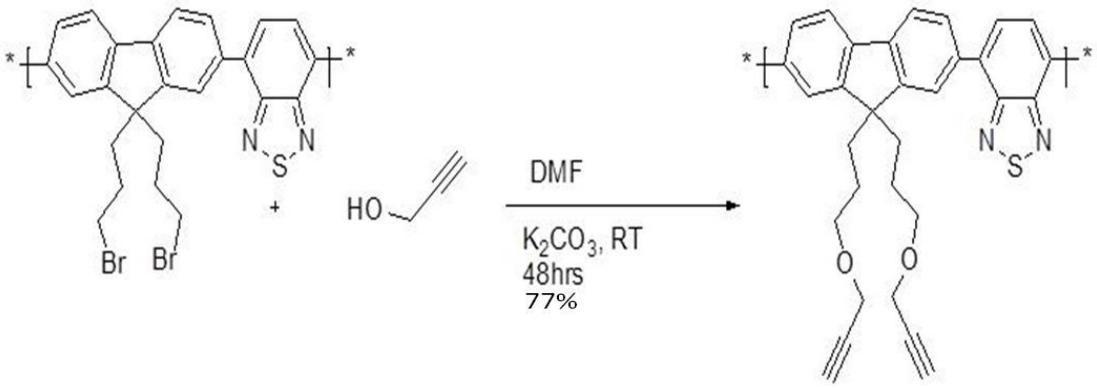

Scheme 14: Synthesis of poly[(9,9-bis(3-(prop-2-ynyloxy)propyl) fluorenyl-2,7-diyl)-co-(1,4-benzo-{2,1,3}-thiadiazole)] (PFBT-Pgy)

The synthesis and characterization of PFBT-pgy was done as in section 2.1.2. As can be seen from Figure 17, C-H proton of terminal alkyne was observed at 2.39 ppm. Meanwhile the protons labelled ‘b’ and ‘c’ resonates at 4.0 ppm and 3.30 ppm respectively. The peaks at 2.39 ppm and 4.0 ppm are particularly characteristic of terminal alkyne proton of propargyl group indicating the successful formation of polymer PFBT-Pgy.

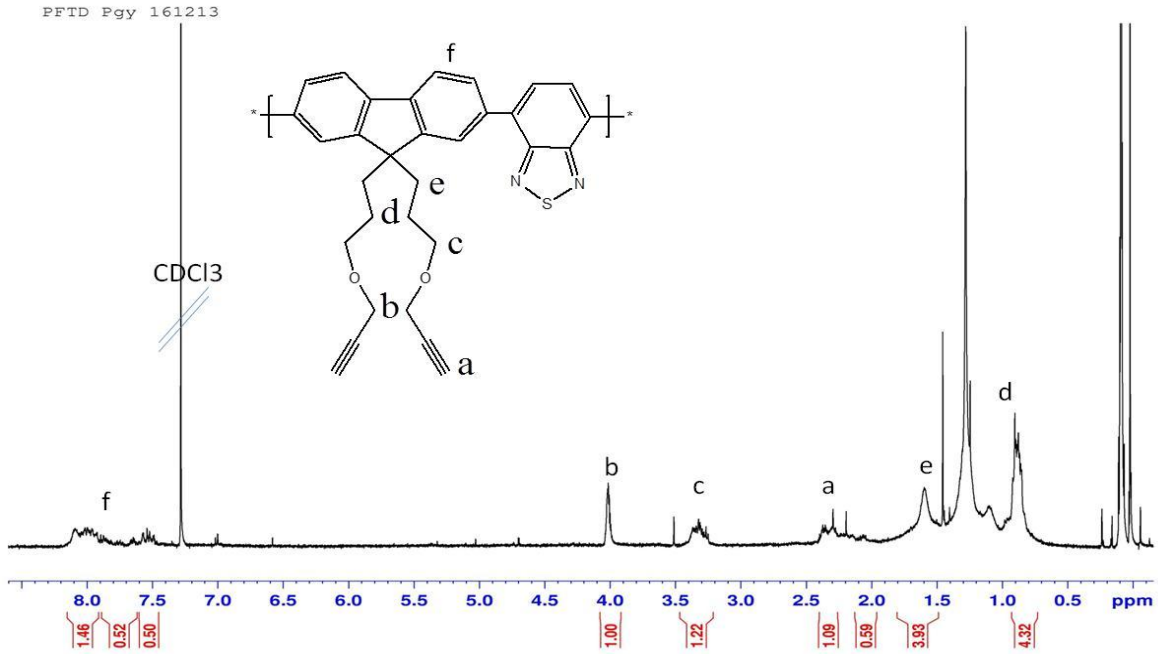

Figure 17: ^{1}H-NMR (400 MHz, $CDCl_3$, 25^{o}C) spectrum of poly[(9,9-bis(3-(prop-2 ynyloxy)propyl)fluorenyl-2,7-diyl)-co-(1,4-benzo-{2,1,3}-thiadiazole)] (PFBT-Pgy)

To further ascertain the structure of PFBT-Pgy, FITR spectroscopy was carried out. The spectrum in Figure 18 is a blueprint of the presence of alkyne. A characteristic signal at 3300 cm^{-1} due to C-H stretching in terminal alkyne and a weak and less conspicuous signal at 2119 cm^{-1} as result of -C≡C- stretching were observed.

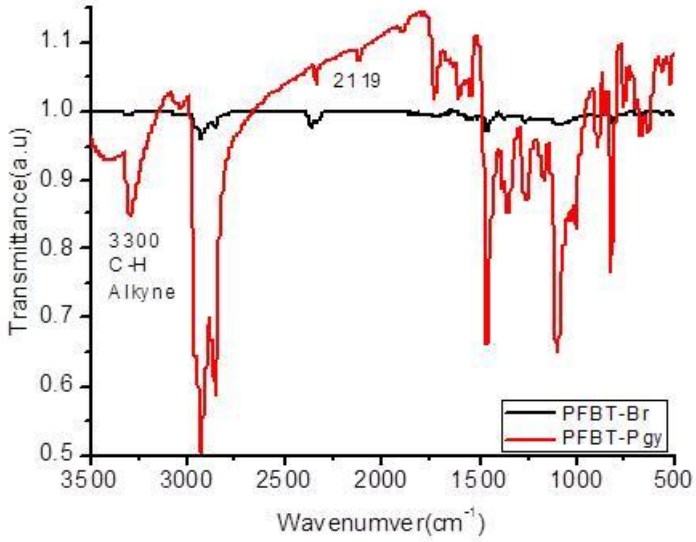

Figure 18:FTIR(Solid state, KBr pellet)spectra of poly[(9,9-bis(3-(prop-2 ynyloxy)propyl)fluorenyl-2,7-diyl)-*co*-(1,4-benzo-{2,1,3}-thiadiazole)] (PFBT-Pgy)

The optical properties of PFBT-pgy were investigated with UV-Vis and Fluorescence spectroscopy. As shown in Figure 19, PFBT-Pgy exhibits two absorbance maxima at 314 nm and 435 nm. It emits at 535 nm as typical green emitting polymer. The broad absorbance band at 435 nm accounts for significant overlap with emission of the donor polymer.

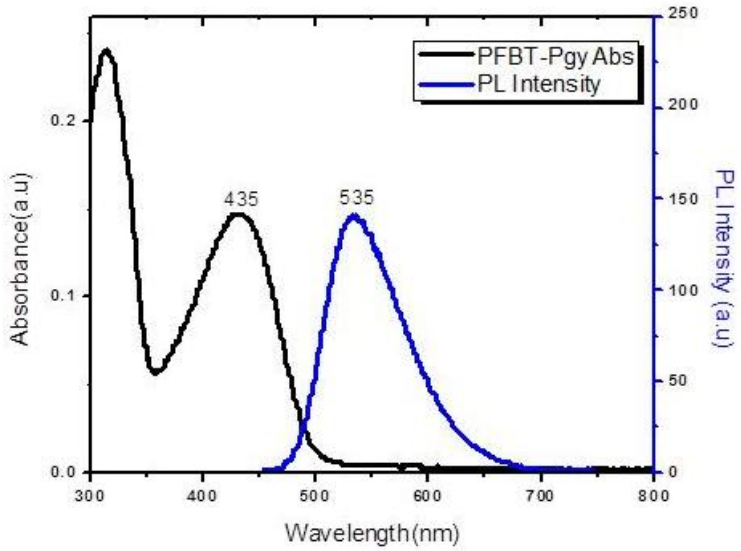

Figure 19: Absorbance and emission spectra of PFBT-Pgy in THF

2.1.4. Synthesis and characterization of poly[(9,9-bis(3-azidopropyl)fluorenyl-2,7-diyl)-co-1,4-benzo[2,1,3]thiadiazole (PFBTN3)

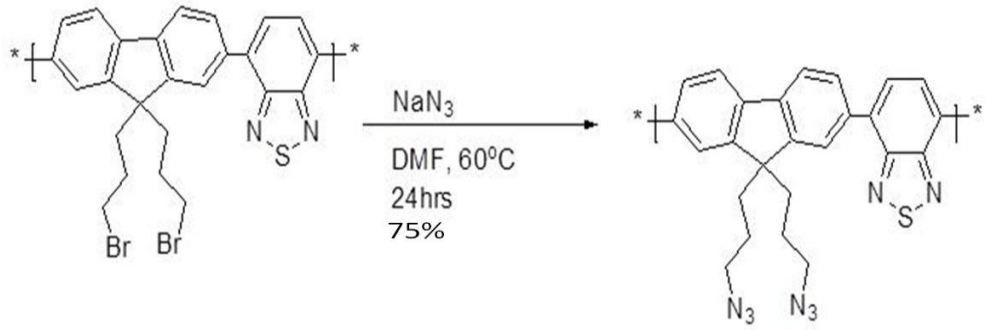

Scheme 15: Synthesis of poly[(9,9-bis(3-azidopropyl)fluorenyl-2,7-diyl)-co-1,4-benzo[2,1,3]thiadiazole (PFBTN3)

Polymer PFBN3 was synthesized according to Scheme 15. The precursor was treated with Sodium azide dissolved in small amount of DMF at 60^{o}C for 24h. After the reaction was over, solvent was removed under reduced pressure. The residue was then washed several times with water and dried under vacuum.

The characterization was done with ^{1}H-NMR and FTIR spectroscopy. ^{1}H-NMR of PFBN3 is presented in Figure 20. The aromatic protons appeared from 7.5-8.3 ppm while -CH_2 protons near bromine atoms are observed at 3.15 ppm. The –CH_2 protons closest to the aromatic ring resonates at 2.2 ppm. For the aliphatic protons labelled ‘a’, they appear at 0.9 ppm upfield.

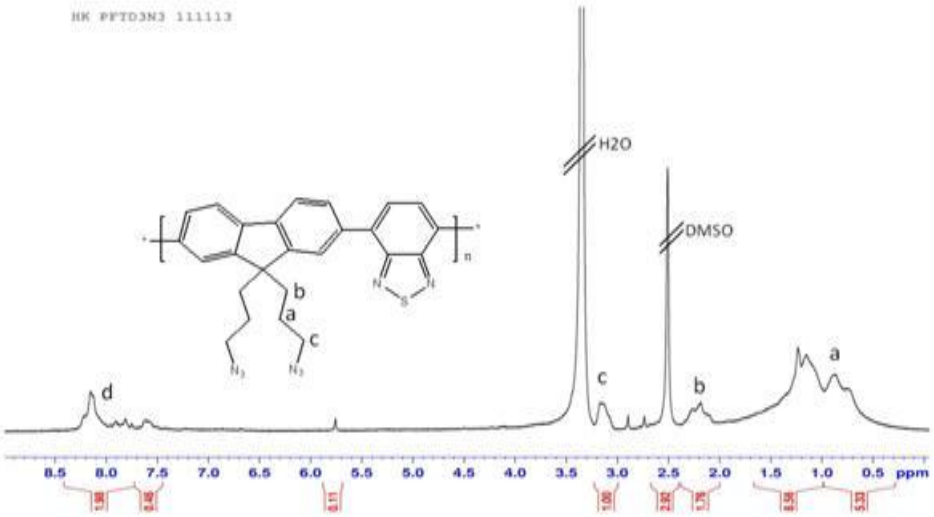

Figure 20:^{1}H-NMR (400 MHz, DMSO-d6, 25^{o}C) spectrum of poly[(9,9-bis(3-azidopropyl)fluorenyl-2,7-diyl)-co-1,4-benzo[2,1,3]thiadiazole (PFBTN3)

The structure of PFBN3 was further confirmed by FTIR spectroscopy. The FTIR spectra in Figure 21 show clear evidence indicating presence of azide functional group in PFBN3 when compare to the precursor which has bromide groups instead. A strong and sharp azide signal at 2095 cm^{-1} is a confirmation of successful PFN3 synthesis.

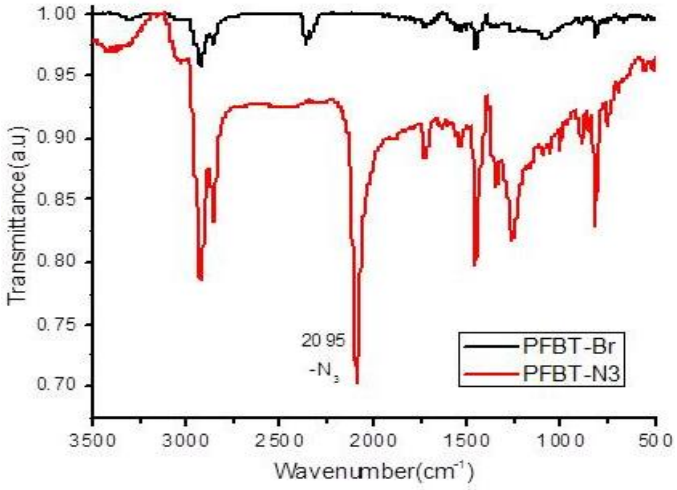

Figure 21: FTIR (Solid state, KBr pellet) spectra of PFBN3

2.1.5. Synthesis and characterization of poly[(2-azidoethyl)-2-(5-(thiophen-2-yl)thiophen-2-yl)thiophene (PTN3)

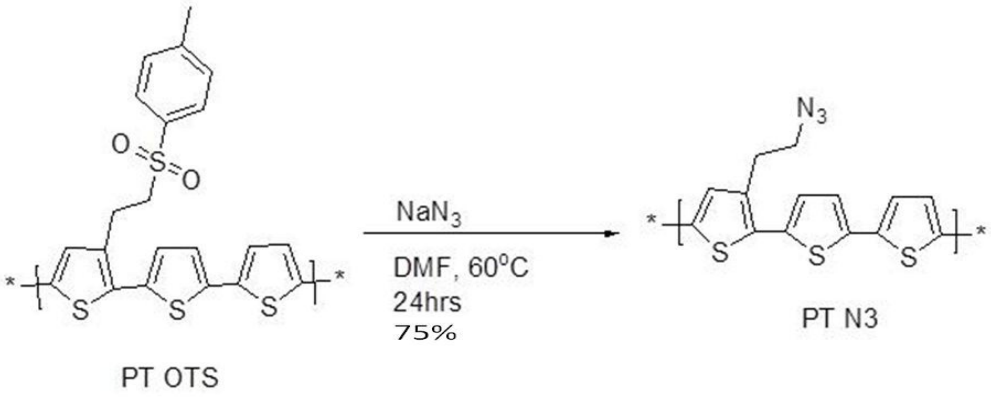

Scheme 16: Synthesis of poly[(2-azidoethyl)-2-(5-(thiophen-2-yl)thiophen-2-yl)thiophene (PTN3)

The synthesis of PTN3 as described in Scheme 16 was accomplished through simple nucleophilic substitution of tosyl group with azide group. Characterization of PTN3 polymer was performed by ^{1}H-NMR and FTIR spectroscopy. From the NMR spectrum in Figure 22, aliphatic protons at position ‘a’ and ‘b’ resonate at 1.95 ppm and 2.91 ppm respectively. Comparing the integrations, an equivalent of five protons resonates in the aromatic region from 7.10-7.58 ppm.

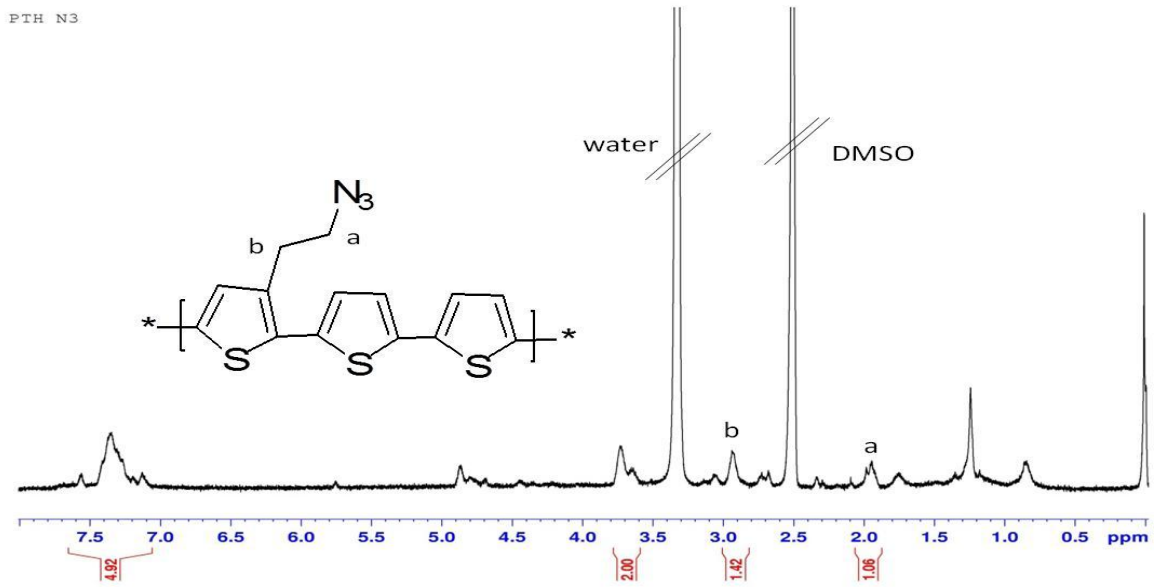

Figure 22: ^{1}H-NMR (400 MHz, DMSO-d6, 25^{o}C) spectrum of poly[(2-azidoethyl)-2-(5-(thiophen-2-yl)thiophen-2-yl)thiophene (PTN3)

In addition to ^{1}H-NMR results, FTIR data also indicate a distinct azide signal at 2095 cm^{-1} which confirmed the successful synthesis of PTN3. Both PT-OTS and PTN3 polymers show Ar-H stretching at 3030 cm^{-1} and C-H stretching at 2927 cm^{-1}.

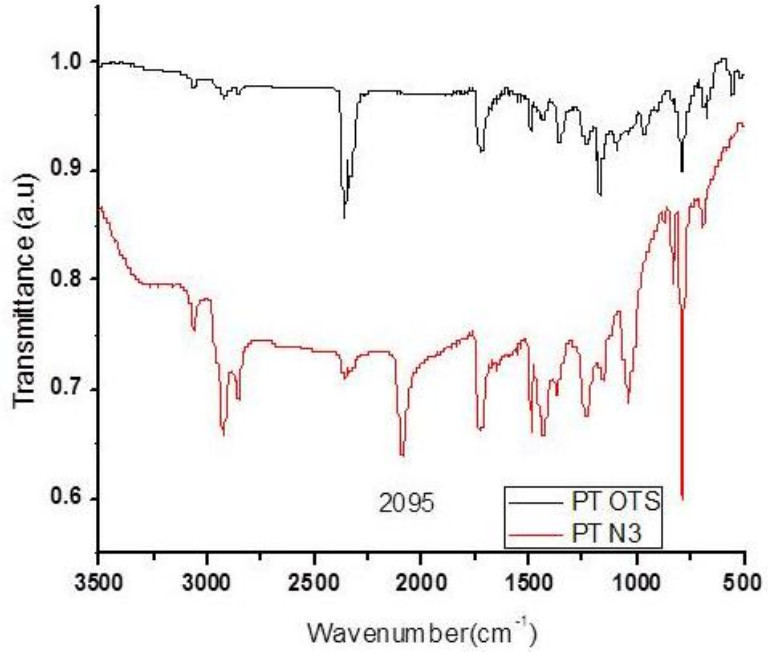

Figure 23: FTIR (Solid state, KBr pellet) spectra of poly[(2-azidoethyl)-2-(5-(thiophen-2-yl)thiophen-2-yl)thiophene (PTN3)

The optical properties determined by UV-Vis and Fluorescence spectroscopy revealed that the red emitting PTN3 polymer has a maximum absorbance at 460 nm and fluorescence maximum at 560 nm with a shoulder at around 630 nm in THF. Emission in the red region makes PTN3 particularly desirable for the design of blue, green and red polymer multishell nanoparticle system.

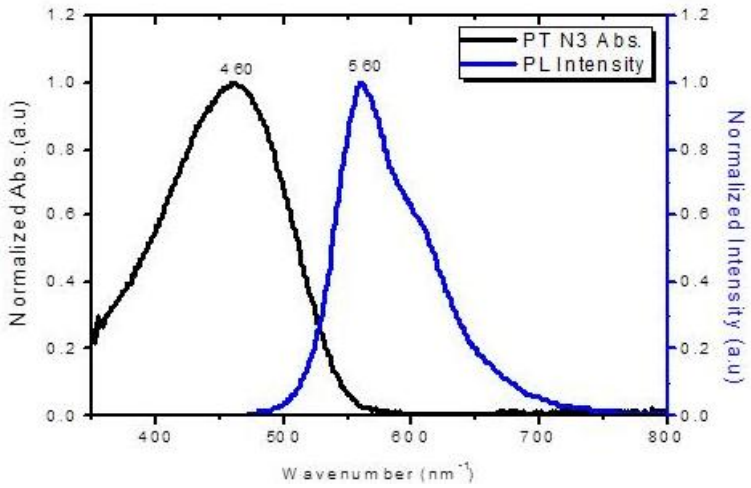

Figure 24: UV-Vis and fluorescence spectra of poly[(2-azidoethyl)-2-(5-(thiophen-2-yl)thiophen-2-yl)thiophene (PTN3) in THF

2.1.6. Synthesis and characterization of Poly[(4-(2-(prop-2-ynyloxy)ethyl)thiophen-2-yl)-co-(1.4-benzo{1,2,5}thiadiazole)] (PBTTH)

The synthesis of PBTTH polymer begins with 'A' in Scheme 17. 'A' was subjected to base hydrolysis using aquous KOH at 50 ^{0}C for 4h. After completion of reaction, solvents were removed and residue washed with water several times to obtain hydroxylated red polymer 'B'. In the second step, 'B' was treated with propargyl bromide using sodium hydride in DMF. After 12h solvents were evaporated under reduced pressure and crude product washed with water and then dissolved in THF before precipitating it in cold methanol. A pure red polymer PBTTH was obtained with alkyne end groups. These polymers were characterized using NMR, FTIR, UV-Vis and fluorescence spectroscopy.

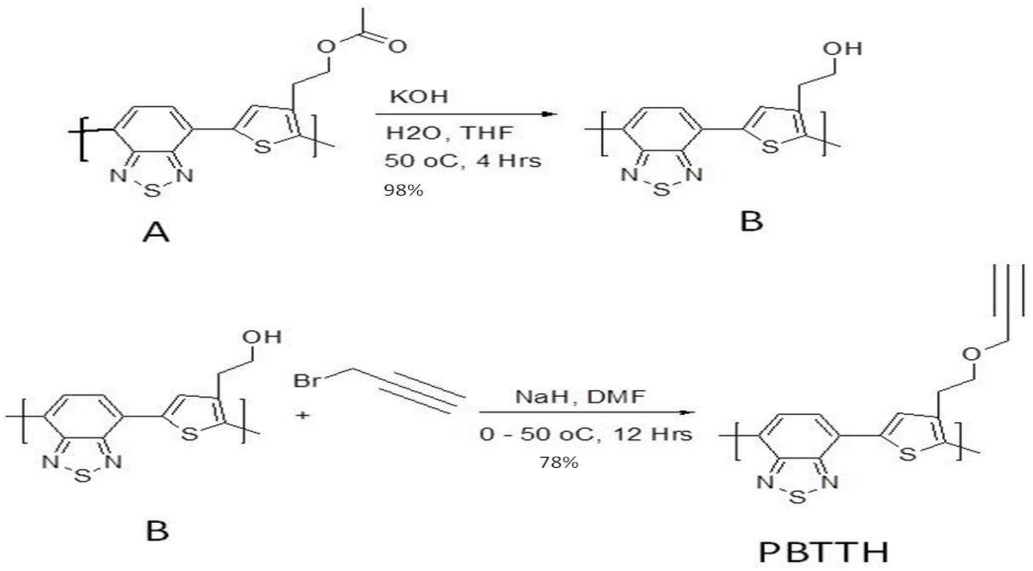

Scheme 17: Synthesis scheme for Poly[(4-(2-(prop-2-ynyloxy)ethyl)thiophen-2-yl)-co-(1.4-benzo{1,2,5}thiadiazole)] (PBTTH)

The ^{1}H-NMR spectrum of hydroxylated polymer in Figure 25 indicates a typical hydroxyl signal at 4.75 ppm. This suggests the complete hydrolysis of the acetylated starting polymer into hydroxylated polymer. Protons in the aliphatic region are represented by ‘a’ and ‘b’. Protons in position ‘b’ are next to electron withdrawing oxygen as a result they are deshielded and downfield shifted to 3.64 ppm, while ‘a’ resonates at 2.85 ppm because they are relatively at a distance from the oxygen atom. An equivalent of three protons appears in the aromatic region agreeing with the expected structure.

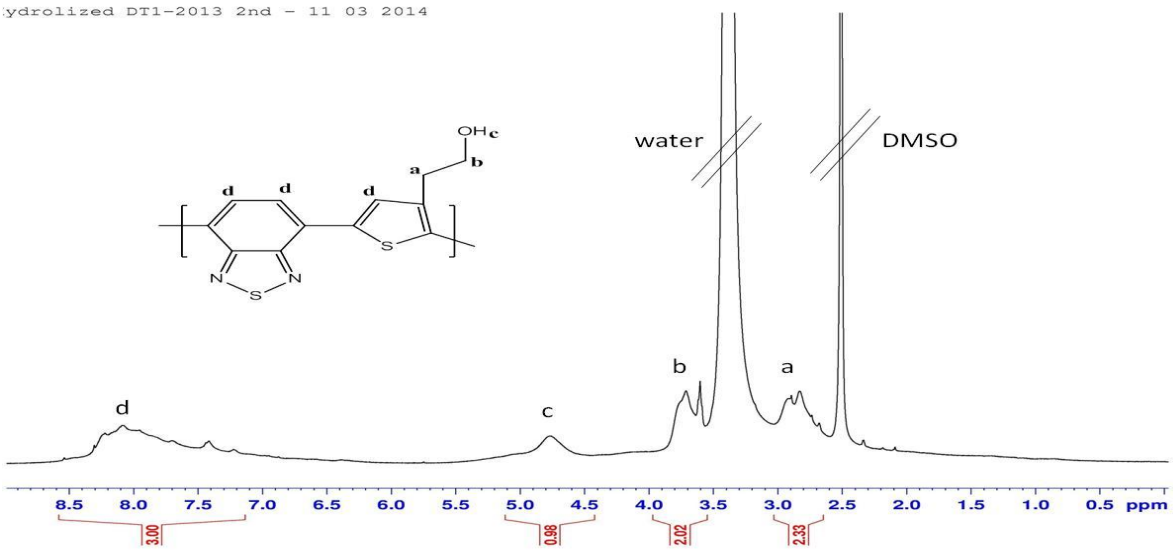

Figure 25: ^{1}H-NMR (400 MHz, DMSO-d6, 25^{o}C) spectrum of hydrolysed red polymer ‘B’.

Furthermore the hydrolysis of acetylated red polymer was confirmed by FTIR spectroscopy as shown in Figure 26. In the acetylated red polymer a sharp carbonyl peak appears at 1745 cm^{-1}. However, after complete hydrolysis the carbonyl peak disappeared while a broad hydroxyl peak appears at 3330 cm^{-1} in hyroxylated red polymer. The complete removal of carbonyl peaks and the appearance of entirely hydroxyl peaks suffice to confirm complete hydrolysis and hence formation of hydroxylated red polymer as the product.

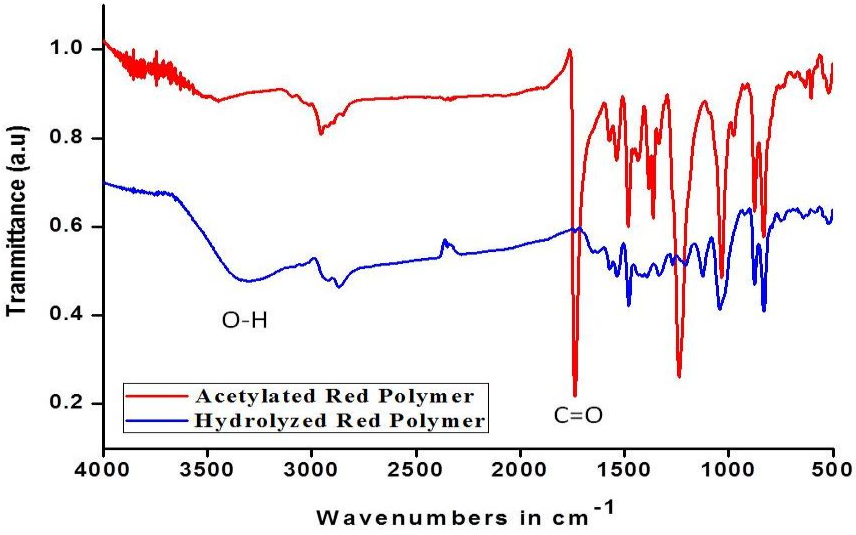

Figure 26: FTIR (Solid state, KBr pellet) spectra of hydrolysed red polymer 'B'

After synthesizing the hydroxylated polymer, it was treated with propargyl bromide to yield PBTTH. According to ^{1}H-NMR spectrum of PBTTH in Figure 27, a signal corresponding to protons of terminal alkyne occurred at 3.45 ppm and a singlet peak of protons labelled 'd' is deshielded by oxygen atom and hence resonates at 4.87 ppm.

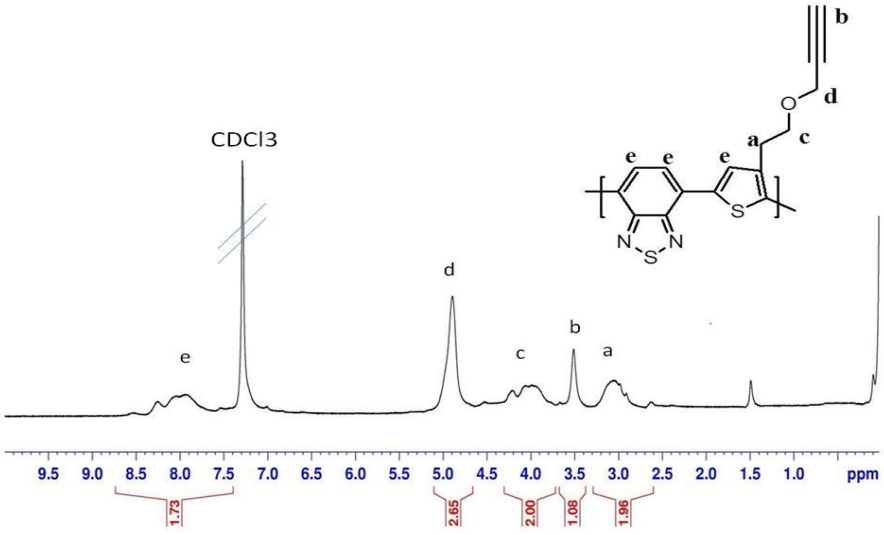

Figure 27: ^{1}H-NMR (400 MHz, CDCl3, 25^{o}C) spectrum of Poly[(4-(2-(prop-2-ynyloxy)ethyl)thiophen-2-yl)-co-(1.4-benzo{1,2,5}thiadiazole)] (PBTTH)

Further characterization of PBTTH by FTIR spectroscopy is shown in Figure 28. From the spectrum, C-H stretching of terminal alkyne at 3330 cm^{-1} and C≡C stretching at 2118 cm^{-1} are distinct peaks of terminal alkyne, indicating the successful synthesis of PBTTH polymer. Furthermore, when this result is compared with the starting hydroxylated red polymer, no corresponding signal for terminal alkyne can be seen. Only a broad hydroxyl signal can be seen which disappeared after functionalization with propargyl bromide to yield PBTTH polymer.

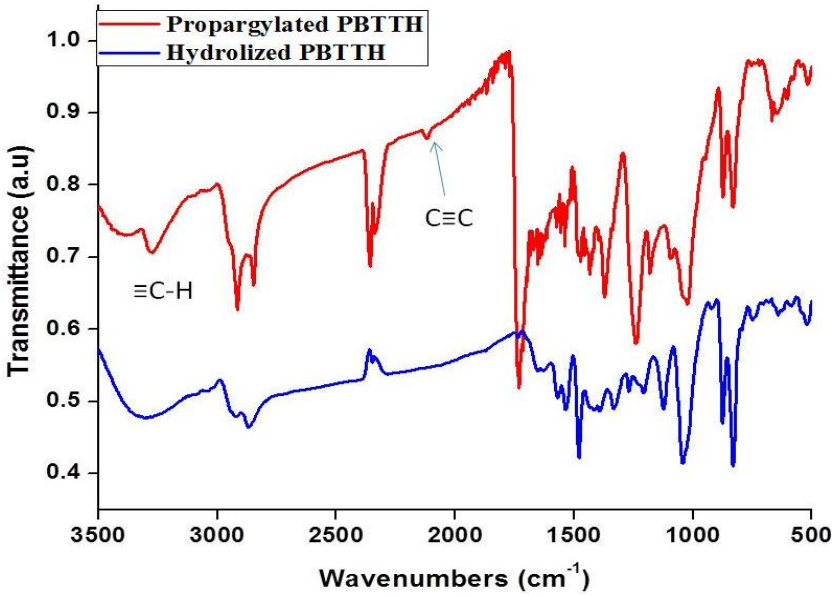

Figure 28: FTIR (Solid state, KBr pellet) spectra of Poly[(4-(2-(prop-2-ynyloxy)ethyl)thiophen-2-yl)-co-(1.4-benzo{1,2,5} thiadiazole)] (PBTTH)

UV-Vis and fluorescence spectra of PBTTH in THF are shown in Figure 29. The red emitting PBTTH polymer has a maximum absorbance at 482 nm and emission maximum at 612 nm.

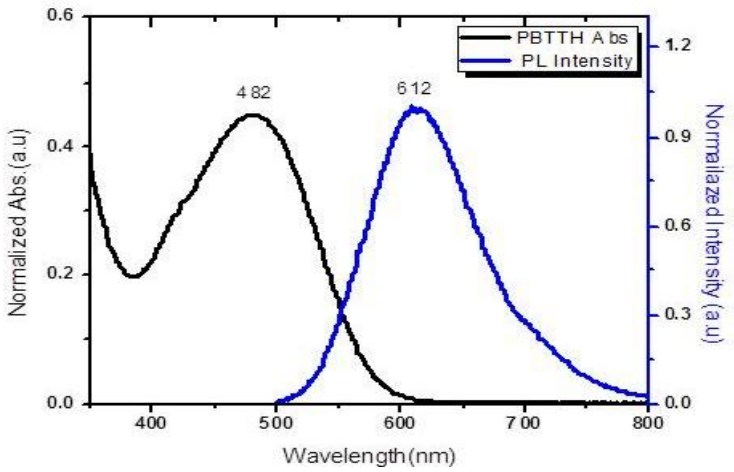

Figure 29: UV-Vis and fluorescence of Poly[(4-(2-(prop-2-ynyloxy)ethyl)thiophen-2-yl)-co-(1.4-benzo{1,2,5} thiadiazole)] (PBTTH) in THF

2.2. Synthesis of water dispersible conjugated polymer nanoparticles

After preparing the necessary polymers with appropriate functional groups, the next step was the preparation of nanoparticles. Nanoparticles were prepared by the reprecipitation method [68] as described in Scheme 18.The formation of nanoparticle is triggered by rapid addition of polymer solution in THF into deionized water while sonicating. The driving force for nanoparticles formation is hydrophobic effect, polymer chains tend to avoid contact with water and by doing so fold into spherical nanoparticles. In this experiment, single polymer nanoparticle dispersions were prepared by taking the same quantity from stock PFBN3 solutions filtered via syringe filter. The concentration of PFBN3 was maintained at 6.0 x 10^{-2} mM while that of PFBT was varied for comparison. To obtain stable nanoparticles rotary evaporator was used to remove THF.

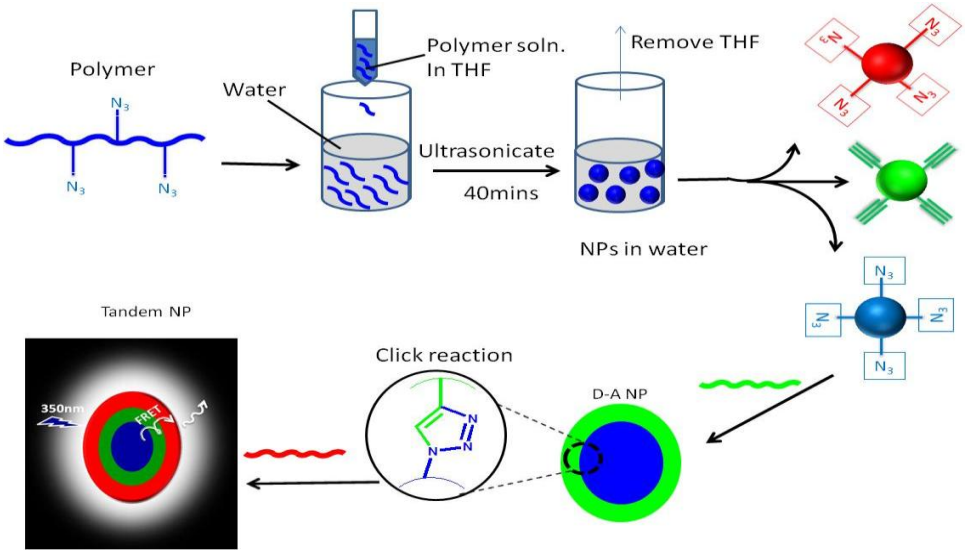

Scheme 18: General Scheme of preparation of white emitting conjugated polymer nanoparticles

For the preparation of bipolymer nanoparticles, catalytic amount of copper sulfate and sodium ascorbate were each dissolved in 250 µL water and injected into the preformed donor nanoparticle while sonicating. The desired amount of acceptor polymer measured from stock solution is diluted in 2 mL THF and ultrasonicated for 10 min before injecting into the preformed donor nanoparticle. Utrasonication was continued for 30 min after which THF was removed. For the control experiment, catalyst was not added.

In the case of tandem nanoparticles, solution of red polymer in THF was injected into rapidly sonicating, preformed biopolymer nanoparticle in deionized water. Polymers with azide or alkyne groups were utilized to form chemical bonds between the polymers as nanoparticles

are form through click reaction. The click reactions lead to the formation of triazole rings that ensure stable and shape-persistent nanoparticles.

Morphological properties of the nanoparticles were determined by dynamic light scattering (DLS), scanning electron microscope (SEM) and transmission electron microscope (TEM). For energy transfer studies in biopolymer and tandem nanoparticles, steady -state and time-resolved fluorescence spectroscopy were performed.

2.2.1. Synthesis and characterization of PFBN3 NPs

PFBN3 NP(donor) was prepared by taking 0.5 mg from stock solution, diluting it in 2mL THF and utrasonicated for 10 min. The solution was then injected into rapidly sonicating 20 mL of deionized water (18.2 MΩ) and ultrasonicated for another 40 min. THF was removed to obtained stable nanoparticles. The size of donor NP was determined by DLS in Figure 30 to be 64 nm.

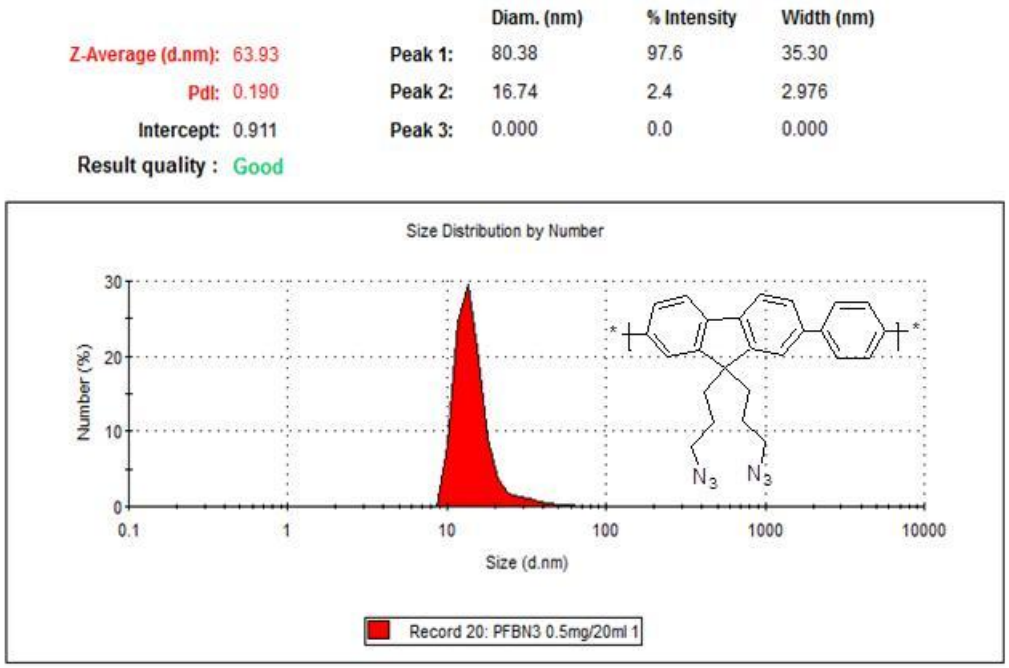

Figure 30: Size distribution by number of PFBN3 (donor)

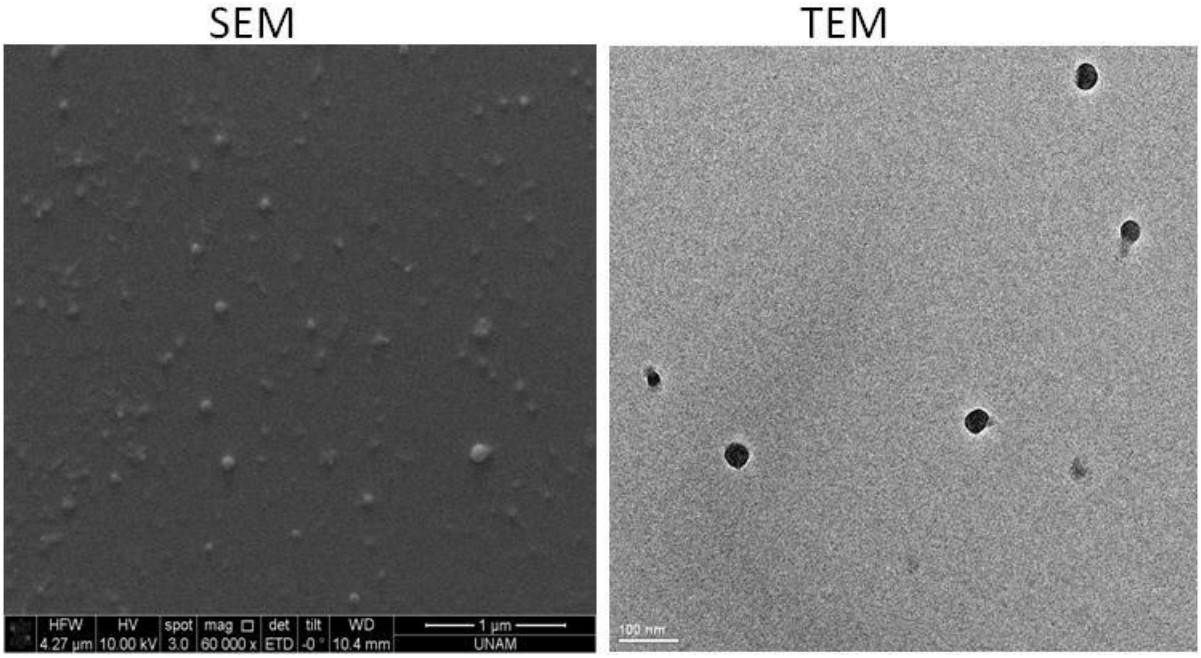

Figure 31: SEM and TEM micrographs of PFBN3 NPs

The morphology of the NPs was determined by both SEM and TEM as presented in Figure 31.The SEM and TEM micrographs show spherical shape nanoparticles with more or less uniform distribution and no sign of aggregation.

In Figure 32, the absorbance and emission of PFBN3 NPs in water was compared with that of PFBN3 in THF. Interesting changes in optical properties were observed upon NP formation. The absorbance shifted from 350 nm in THF to 355 nm in NP dispersion in water. In the same token, a red shift in photoluminescence from 407 nm in THF to 420 nm in NPs dispersion was observed. Moreover, a relatively more pronounced shoulder peak at 446 nm in the case of NPs in water can be seen compare to a small shoulder peak at 426 nm for PFBN3 in THF. Many studies explored the photophysical properties of CPN and the redshift in fluorescence is widely attributed to change in conformation and segmental aggregation of polymer chain within the nanoparticles.[90]

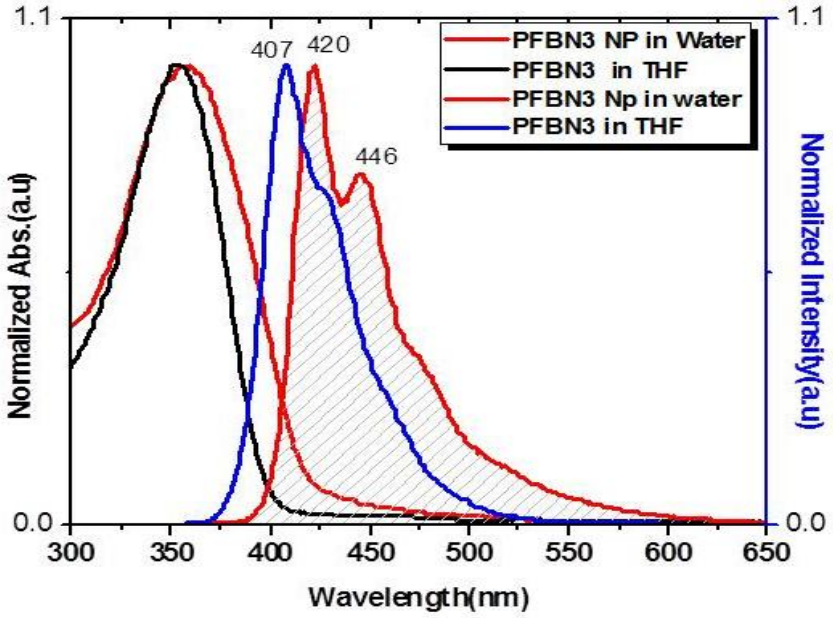

Figure 32: Absorbance and emission spectra of PFBN3 in THF and PFBN3 NPs in water (λ_{ex}=350nm)

2.2.2. Synthesis and characterization of PFBT-Pgy NPs

PFBT NPs (acceptor) were prepared by taking 0.5 mg polymer from stock solution in THF which was filtered using syringe filter. It was then diluted in total of 2 mL THF and sonicated for 10 min. The polymer solution was injected into 20 mL of water and sonicated for another 40 min. After removing THF, the size of the resulting NPs was determined by DLS to be 63 nm as presented in Figure 33.

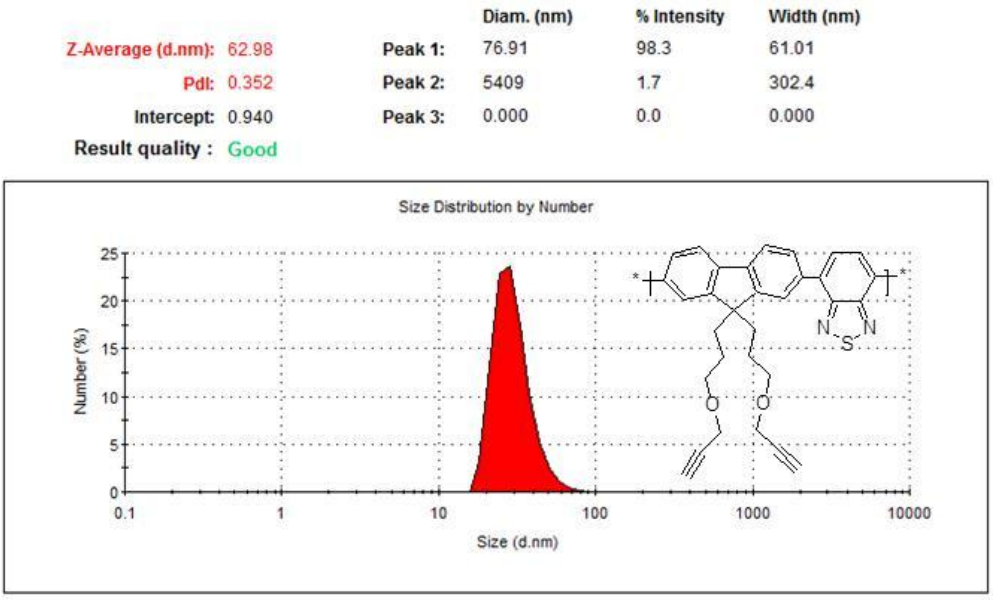

Figure 33: Size distribution by number of PFBT NPs

The morphology of PFBT NPs was studied using SEM and TEM. Details of PFBT NPs micrographs reveal that they assume a spherical shape and are evenly distributed with no sign of aggregation. In Figure 34, SEM and TEM micrographs of PFBT NPs are shown which agreed with DLS results presented earlier.

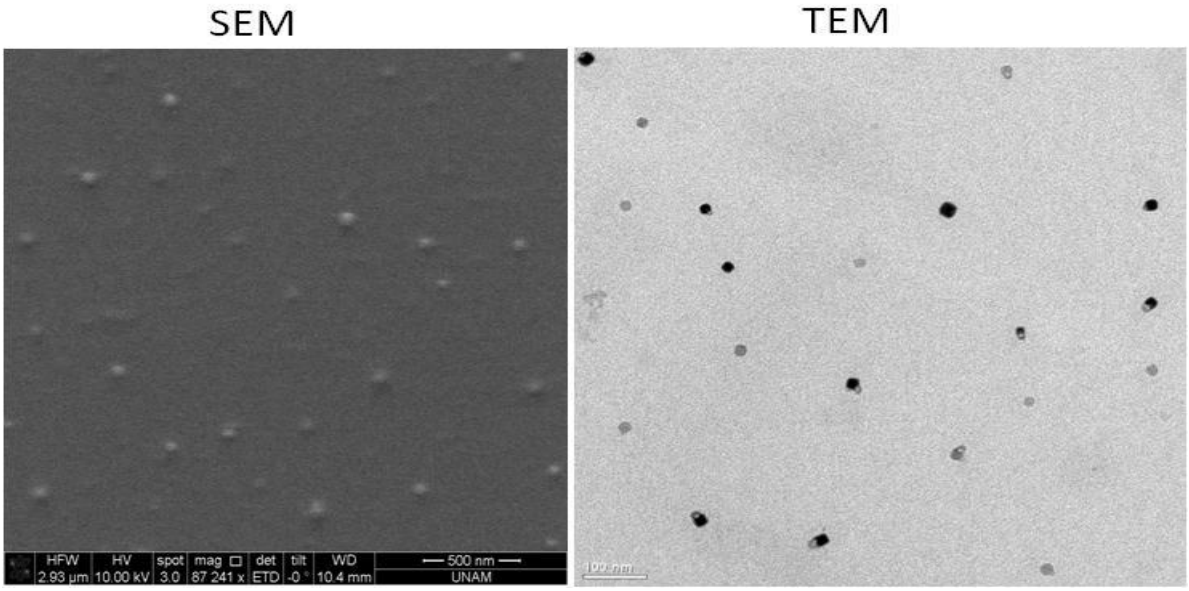

Figure 34: SEM and TEM micrographs of PFBT NPs

Figure 35 draws a comparison between the optical properties of PFBT solution in THF and PFBT NPs dispersion in water. A slight shift in absorbance was observed: 8 nm redshift was observed from 432 nm in THF solution to 440 nm in NPs. For the photoluminescence, 9 nm redshift was observed from 535 nm in polymer solution to 544 nm in NP dispersions.

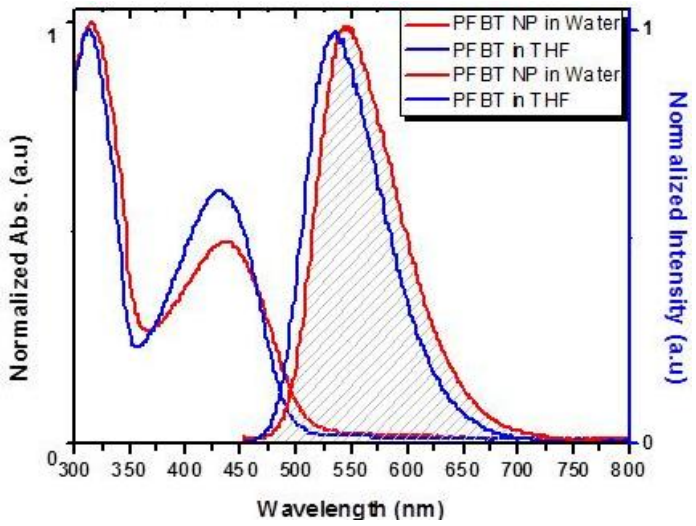

Figure 35: Absorbance and emission spectra of PFBT in THF and PFBT NPs in water (λ_{ex}=435nm)

Spectral overlap between the emission of donor (D) and the absorbance of acceptor (A) fluorophores is an important requirement for fluorescence resonance energy transfer (FRET). FRET is an essential physical phenomenon with potential applications in optoelectronic devices and biomedical sciences.[91]Figure 36 shows a spectral overlap involving donor and acceptor NPs in water. The donor NPs emits both at 420 nm and 446 nm while the acceptor has a broad absorbance band at 444 nm. The strong spectral overlap observed is an indication that FRET is possible between D-A if other conditions are met.

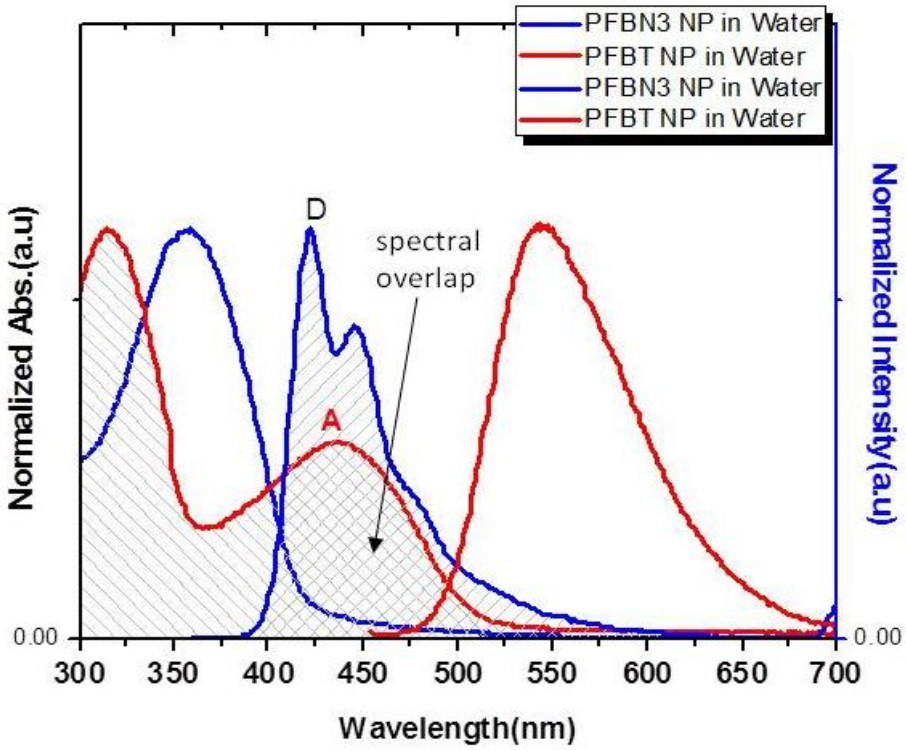

Figure 36: Spectral overlap between donor and acceptor

2.2.3. Synthesis and characterization of PTN3 NPs

PTN3 NPs were prepared from PTN3 polymer solution. PTN3 was dissolved in THF and filtered using syringe filter. The clear solution was sonicated for 10 min followed by injection into large volume of water while sonicating. Ultrasonication was continued for 40 min after which THF was removed under reduced pressure. The size of NPs was determined by DLS be 80 nm (Figure 37).

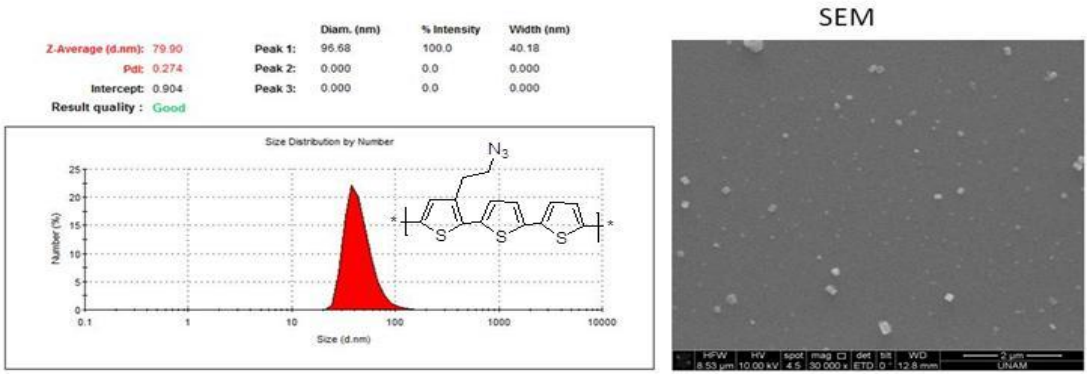

Figure 37: Size distribution by number and SEM micrograph of PTN3 NPs

The optical properties of PTN3 NPs dispersion in water were compared with PTN3 polymer solution in THF for evidence of any changes. It was observed that there is no significant shift in absorbance of both PTN3 polymer solution and its NPs at 460 nm. However, a great change in fluorescence was noticed when PTN3 solution was compared with its NPs as presented in Figure 38. Upon NP formation, a considerable redshift from 560 nm to 621 nm could be seen clearly. The conformations of conjugated polymer are known to change with solvent, as a result a more ordered aggregation in PTN3 chains within the NPs might lead to a synergetic π-π stacking and hence the large redshift observed.[92]

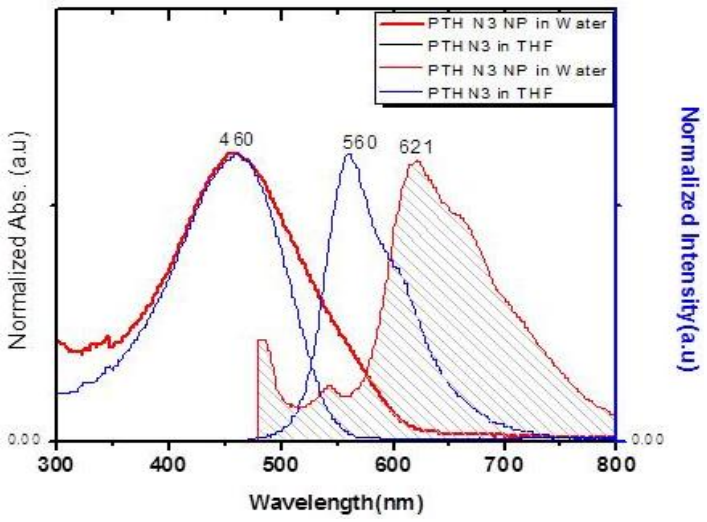

Figure 38: Absorbance and emission spectra of PTN3 in THF and PTN3 NPs dispersion in water. (λ_{ex}=460 nm)

2.2.4. Synthesis and characterization of PBTTH NPs

PBTTH NPs was synthesized through the reprecipitation method. PBTTH polymer was first dissolved in THF and because its solubility wasn't great in THF, it was filtered many times with a 0.45 uM syringe filter until a clear solution was obtained. The polymer solution was injected into 20 mL water and ultrasonicated for 30 min. In order to prevent the NPs from

dissolving again, THF was evaporated with rotary evaporator. Morphological characterization of NPs was performed with DLS and SEM while optical properties were determined by UV-VIS and fluorescence Spectroscopy.

DLS results (Figure 39) suggest that the size of PBTTH NPs is 80 nm. The larger size seen in PBTT NP compare to donor NP explains how solubility is important in forming smaller and more monodispersed NPs.

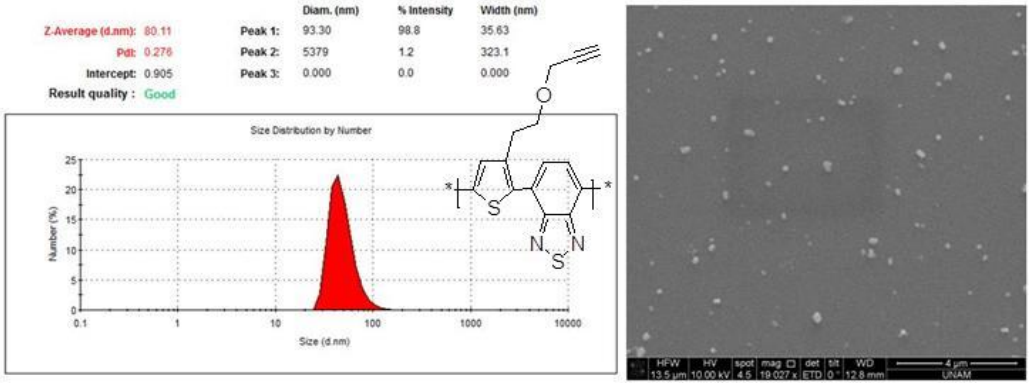

Figure 39: Size distribution by number and SEM micrographs of PBTTH NPs

UV-Visible spectra reveal low absorbance intensity when PBTTH was converted into NPs. However, the absorbance maxima at 483 nm remain the same in both PBTTH solutions in THF and PBTTH NPs dispersion. Interestingly, as oppose to absorbance, a slight red shift in emission of PBTTH NPs from 612 nm to 620 nm was observed. In any case the results confirmed the formation PBTTH NPs as evidence from changes in optical properties. The observation of redshift in emission wavelength of PBTTH just as in donor NPs strongly suggest a conformational change in the polymer chain as they are converted into NPs.

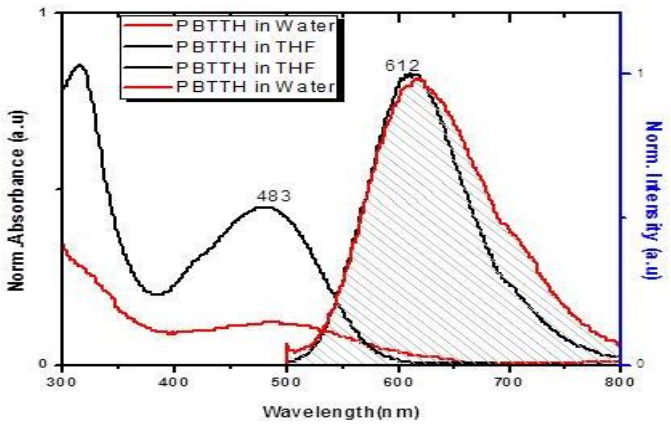

Figure 40: Absorbance and emission spectra of PBTTH in THF and PBTTH NPs dispersion in water. (λ_{ex}=483 nm)

2.3. White-emitting bipolymer nanoparticles

In a bid to synthesize white emitting bipolymer nanoparticles, four nanostructure designs were investigated. PFBN3 and PFBT polymers were utilized as donor and acceptor pair, so as to study energy transfer dependent on nanoparticle morphology and designs. Using FRET, we seek to tune the emission of the hybrid NPs to white which has potential application in solid state lighting.

In the first method, NPs of donor and acceptor were prepared separately from PFBN3 and PFBT-Pgy respectively. The resulting NPs were then mixed and denoted NP mixed (Scheme 19). In the second design, solutions of PFBN3 and PFBT-Pgy polymers were mixed at certain ratios and from this solution of the two polymers, nanoparticles were prepared. The third designs involve sequentially formed NPs; PFBN3 NP was prepared first as the core followed by addition of PFBT solution to the preformed NPs. Here PFBN3 (donor) is core while PFBT (acceptor) is the shell and are designated DA. In the fourth method, which is the reverse of the third method, the acceptor is the core while donor is the shell and are designated AD.

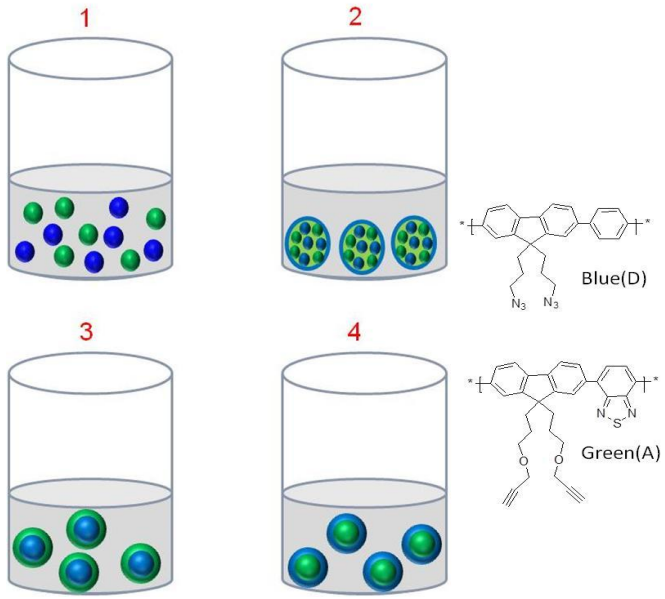

Scheme 19: Representation of nanostructured designs. NP mixed (1), Soln NP (2), DA (3) and AD (4)

2.3.1. Morphological study of bipolymer nanoparticles

The morphology of the bipolymer NPs were determined by DLS, SEM and TEM (Figure 41). The zeta size average of bipolymer NP is 99 nm. Compare to donor or acceptor NPs alone, an increase of 35 nm of size was observed upon bipolymer NP formation. This shows successful coating of one NP with another. Both SEM and TEM results indicate spherical shape nanoparticles with no signs of aggregation.

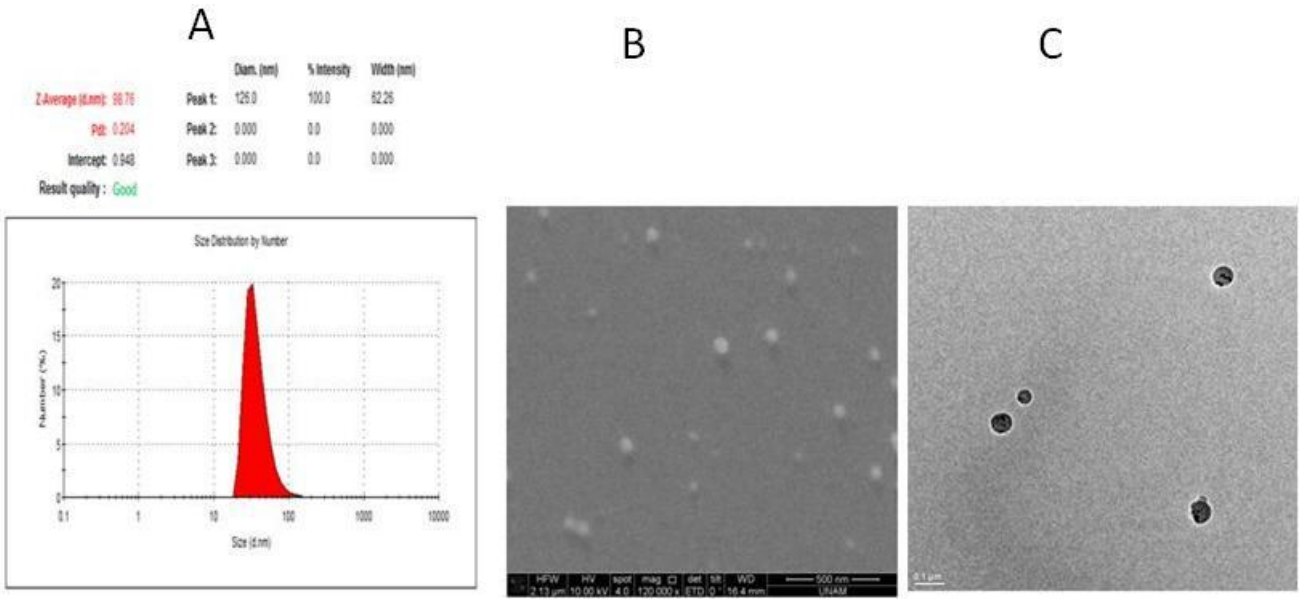

Figure 41: (a)DLS: Zeta-size of DA 45 NP (99nm),(b)SEM micrograph of DA45.(c)TEM micrograph of DA NPs.

2.3.2. Förster Resonance Energy Transfer in bipolymer nanoparticles

In the first bipolymer NP design (Figure 42a) separately formed NP were mixed with 55 mol% donor and 45 mol% acceptor. With respect to donor and acceptor NP alone, there was no significant change in the optical properties of the mixed NPs. The emission spectrum shows two peaks at 420 nm and 544 nm corresponding to the exact emission of donor and acceptor NPs alone respectively. However, the emission at 544 nm in mixed NPs does suggest that there is energy transfer from donor to acceptor. When the emission intensity at 350 nm excitation is compare with the emission intensity at 435 nm excitation, a ratio of 0.81 was calculated. This ratio means that the emission intensity of acceptor was enhanced 0.81 fold through FRET compare to the acceptor alone. The low energy transfer can be explained by the large distance between donor and acceptor in solution.

For the second bipolymer NP design (Figure 42b), where solutions of donor and acceptor were mixed prior to NPs formation, a 5 nm blue shift was observed along with 3.2 fold enhancement of acceptor emission intensity at 350 nm excitation. However, the emission due to the donor component was quenched as a result of energy transfer from donor to acceptor. The complete energy transfer using 45 mol% acceptor is also obvious from the inset photograph of dispersion of NPs under UV lamp (366 nm) showing only green color (Figure 42b).

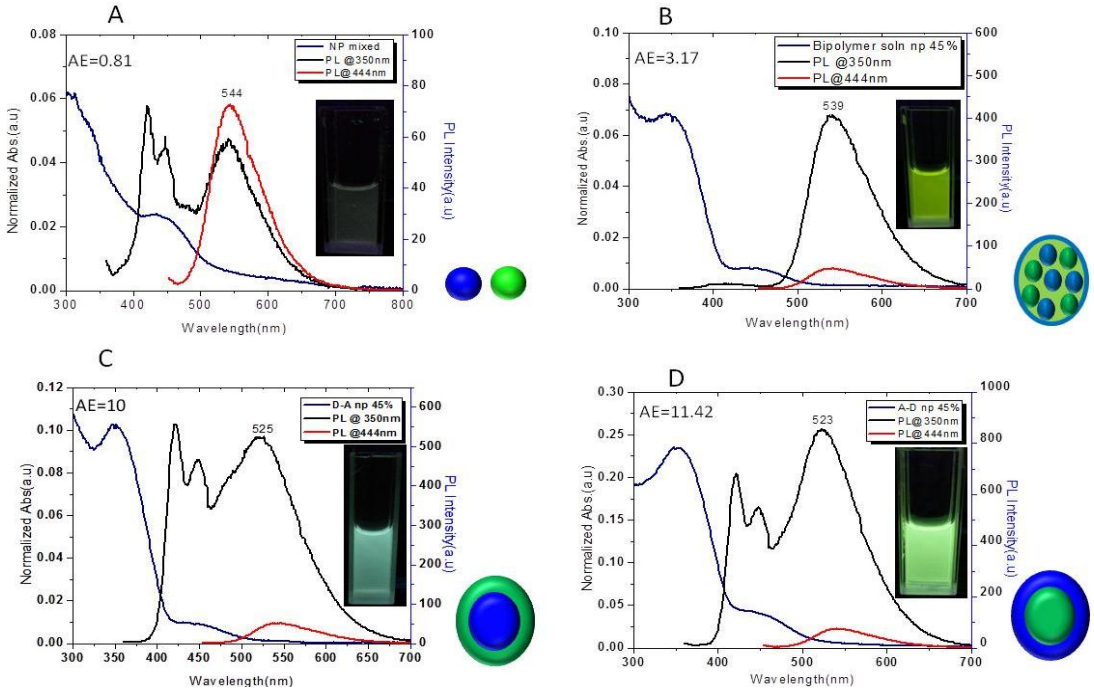

Figure 42: Absorbance and emission spectra of bipolymer NP dispersion in water (a) NP Mixed (PFBN3+PFBT NPs) (b) Soln NP (PFBN3+PFBT solution) NP (c) DA 45 NP (PFBN3/PFBT) (d) AD 45 NP (PFBT/PFBN3) (λ_{ex}=350nm)

The third bipolymer NP design involve a novel NPs prepared sequentially. Here, the donor forms the core which is coated with 45 mol% of acceptor (Figure 42c). Excitation of DA 45 NP at donor excitation resulted in 19 nm blue-shift of the emission of the acceptor. The blue-shift is attributed to an increased D-A interactions. The increased oscillating dipole-dipole interactions upon excitation of donor create a nearby electric field, which does not allow the acceptor molecules to find their minima for relaxation so that PFBT moieties emit at higher energies.[93]Furthermore, an efficient energy transfer leading to 10 fold enhancement of acceptor emission was observed at donor excitation. The incomplete energy transfer maintain a balance between the emission of both donor and acceptor components leading to white emission as can be seen in the inset photograph of DA 45 NP.

Similarly, in the fourth NP design where the acceptor forms the core surrounded by donor polymer (Figure 42d), a 21 nm blue-shift in the acceptor emission was observed as noticed in the opposite design. However, the emission of the acceptor was enhanced by 11 fold with white-green emission color. The slightly higher emission intensity of the acceptor is due to efficient energy transfer. Since the acceptor forms the core of the NP, loss of energy through reflection and other non-rediative means is negligible.

Interestingly, similar bipolymer nanoparticles designs were accomplished with catalyst-free conditions (Figure 43). The emission spectra of catalyst-free NPs in Figure 43 A, B and C

corresponds to the spectra of catalysed bipolymer NPs in Figure 42 B, C and D respectively. Each of the catalyst free NPs showed enhance energy transfer. For comparison, NPs of the same design and ratio of donor and acceptor were prepared; each contains 10 mol% acceptor (Figure 43d). With donor core surrounded by acceptor, one was formed using copper sulfate to catalyse click reaction while the other NPs were formed without any catalyst involved. Catalyst-free 1,3-dipolar cycloaddition, however, is not an unusual reaction, an example of catalyst-free 1,3-dipolar cycloaddition is Huisgen 1,3-dipolar cycloaddition. But what makes catalyst-free azide-alkyne cycloaddition work so successfully in multi-shell nanoparticles is that when forming multishell nanoparticles, the azide and alkyne functional groups of the participating polymers are brought to very close proximity as nanoparticles are formed. The close proximity of the functional groups lead to the formation of 1,2,3-triazole ring. In other words the nanoparticles play the role of catalyst by bringing the azide-alkyne functional groups together and hence lower the activation energy for click reaction. From the emission of the acceptor components, a 3 fold more enhancement was observed for catalyst-free NPs than NPs formed using catalyst. An enhancement of 26 and 23 times was calculated for catalyst-free and catalysed NPs respectively. This discrepancy is partly due to the quenching effect of copper on the emission of catalysed NPs.

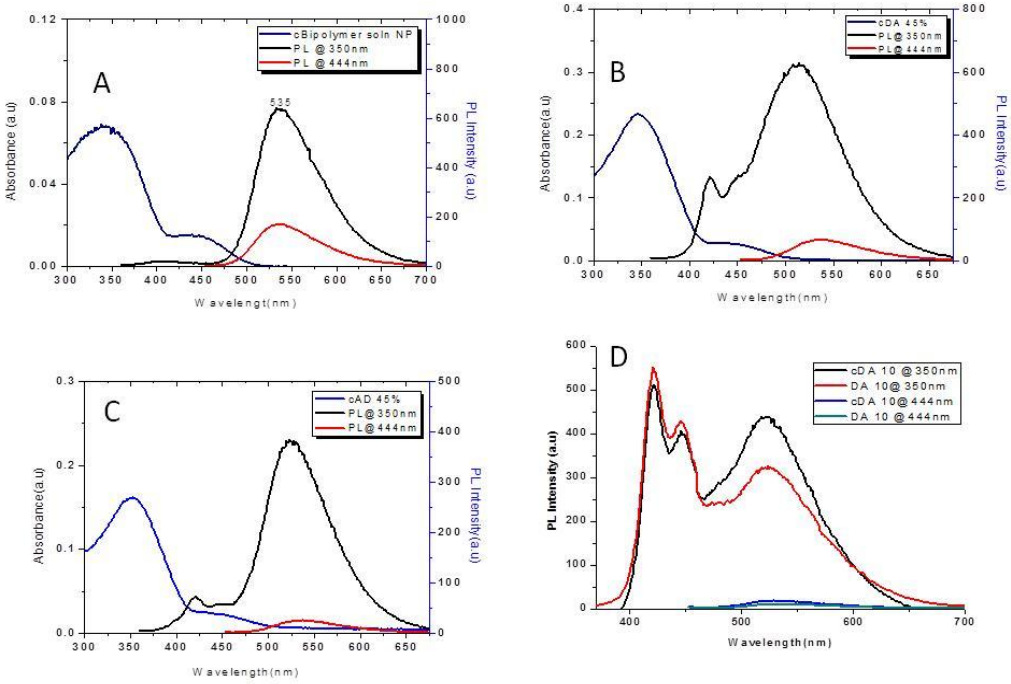

Figure 43: Absorbance and emission of catalyst-free bipolymer nanoparticles (a) c. Soln NP (b) c. DA 45 NP (c) c. AD 45 NPs (d) c.DA 10 and DA 10% NP. (λ_{ex}=350 nm)

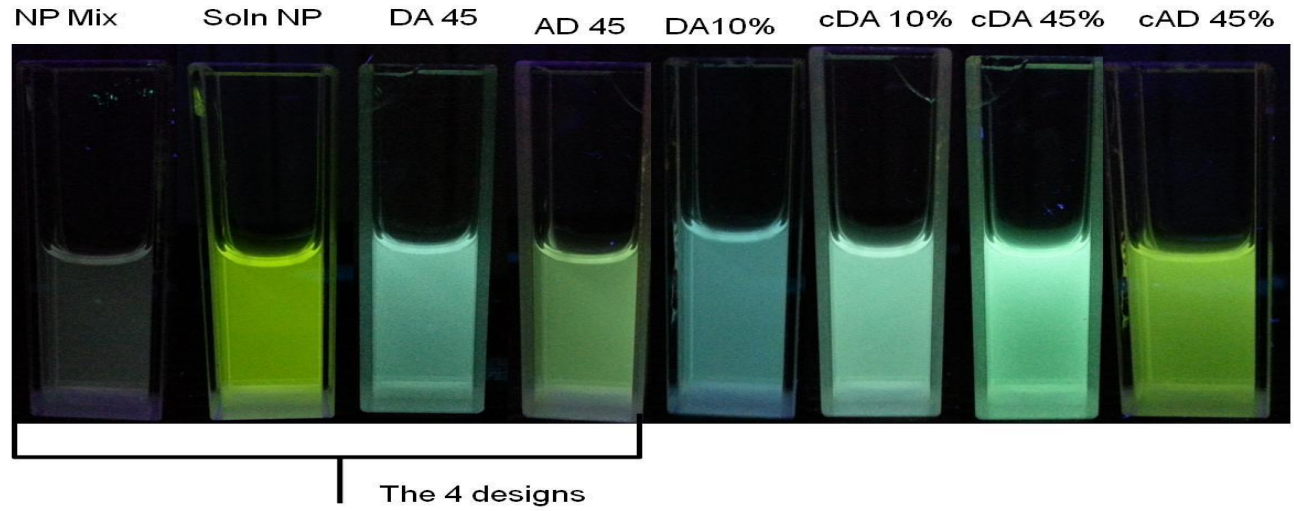

Figure 44: Photographs of bipolymer NPs dispersion in water under UV (366nm)

The photographs of the four NPs design (Figure 44) indicate a dim green emission in the case NP mixed; this is due to the inefficient energy transfer when separate NPs are at a large distance in solution. The bright green emission corresponds to a complete or near complete energy transfer to the acceptor. When AD 45 is compared with c.AD45 NPs (Figure 44), it can be clearly seen that emission of c.AD45 NP is brighter because there are no catalyst to quench its emission.

Time-resolved fluorescence spectroscopy

Time-resolved fluorescence spectroscopy is an extension of steady-state fluorescence spectroscopy. Steady-state measurement of fluorescence emission (intensity vs. wavelength) gives relative and averaged information. In contrast, fluorescence lifetime gives an absolute (independent of concentration) measurement and permits the dynamic picture of fluorescence to be acquired. Apart from the ability to give absolute measurements, fluorescence lifetime measurement is preferable because it's independent of concentration within certain constrain. This means that changing the concentration either by diluting or concentrating the sample, would not affect the lifetime values.

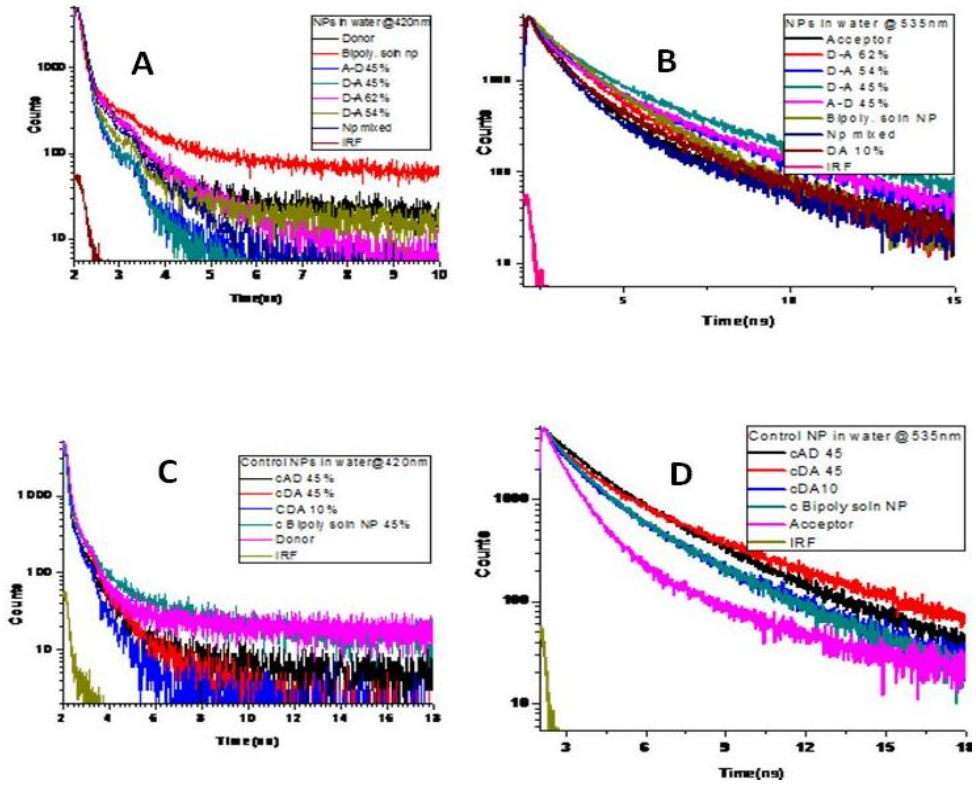

Figure 45: Biexponentially fitted decay curves of bipolymer nanoparticles (a) Fluorescence life-time decay curves of catalysed NPs at 420nm, (b) At 535nm (c) Fluorescence life-time decay curves of catalyst-free NPs at 420 (d) At 535nm

The decay curves of catalysed NPs show shorter decay lifetime than the donor at 420 nm and longer decay lifetime at 535 nm than the acceptor alone (Figure 45a&b). These further illustrate the energy transfer between donor and acceptor. Similar trend of decrease in lifetime at 420 nm and increase in lifetime at 535 nm was observed for catalyst-free NPs (45c&d). In fact the lifetimes at 535 nm for catalyst-free NPs are longer than in the case of catalysed NPs; which is in agreement with steady-state fluorescence results.

Table 1: Fluorescence lifetime of NPs dispersion in water (intensity weighted)

S/N	NPs in Water	τ_{avr}[ns] @420nm	τ_{avr}[ns] @535nm	η[%]
1	DA 45	0.098	1.516	39.51
2	cDA 45	0.061	2.130	62.35
3	AD 45	0.082	1.229	49.38
4	cAD 45	0.073	2.110	54.94
5	Soln NP	0.124	1.300	23.45
6	C . Soln NP	0.057	1.560	64.81
7	NP mixed	0.144	0.826	-
8	DA 10	0.090	1.000	44.44
9	C DA10	0.071	1.590	56.17
10	DA 54	0.100	1.371	38.27
11	DA 62	0.043	1.182	73.45
12	Donor NP	0.162	-	-
13	Acceptor NP	-	1.079	-

The fluorescence lifetime of the NPs reveal quantitative measurement of the energy transfer efficiency. The average lifetime of donor NP dispersion in water was found to be 0.162 ns while acceptor NP was 1.079 ns. Using equation (1), the energy transfer efficiencies were calculated in table 1.

$$\eta = 1 - \frac{\tau_{DA}}{\tau_{D}} \qquad \text{Eq. (1)}$$

Where η denote energy transfer efficiency, τ_{DA} and τ_{D} denotes the averages lifetimes of donor in the presence and absence of acceptor respectively.

However, the energy transfer efficiency of NP mixed was not calculated using equation 1 because the donor-acceptor pairs are randomly moving in solution with no fixed distance. Nonetheless, all the other NPs bound by a fixed distance could be evaluated using Eq. 1. DA 62 which contains 62 mol% acceptor as the shell shows the highest energy transfer efficiency of 73.45%. The high energy transfer efficiency of DA62 is due to high acceptor concentration which leads to complete energy transfer from the low content donor core. As for DA45 and cDA45 representing catalysed bipolymer NP and catalyst-free NP respectively, the difference in energy transfer efficiencies is in agreement with steady-state fluorescence results. The efficiencies of DA45 and cDA45 are 39.51% and 62.35% respectively. Again the lower energy transfer efficiency of DA45 compare to cDA45 was due to the quenching effect of copper sulfate used as a catalyst during NP preparation. Quenching by catalyst was more

pronounced in the NP designs where solutions of donor and acceptor were mixed before NPs were prepared. For example catalyst-free c.Soln NPs has an efficiency of 64.81% while catalysed Soln. NPs is 23.45%. The high quenching in this particular case can be understood from the efficient mixing and distribution of the catalyst throughout the bipolymer nanoparticles.

In order to understand the effect of click reaction on the shape and morphology of bipolymer NPs, sequentially formed NPs were prepared from non-functionalized polymers as a control experiment. When compared with functionalized polymers which undergo click reaction to form stable NPs, an interesting difference in optical properties and morphology were observed

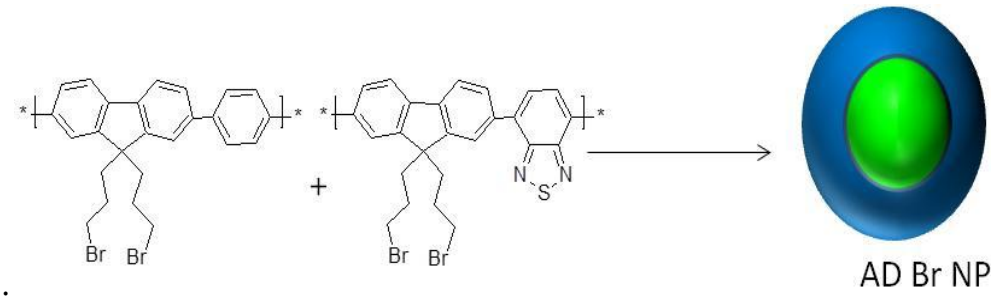

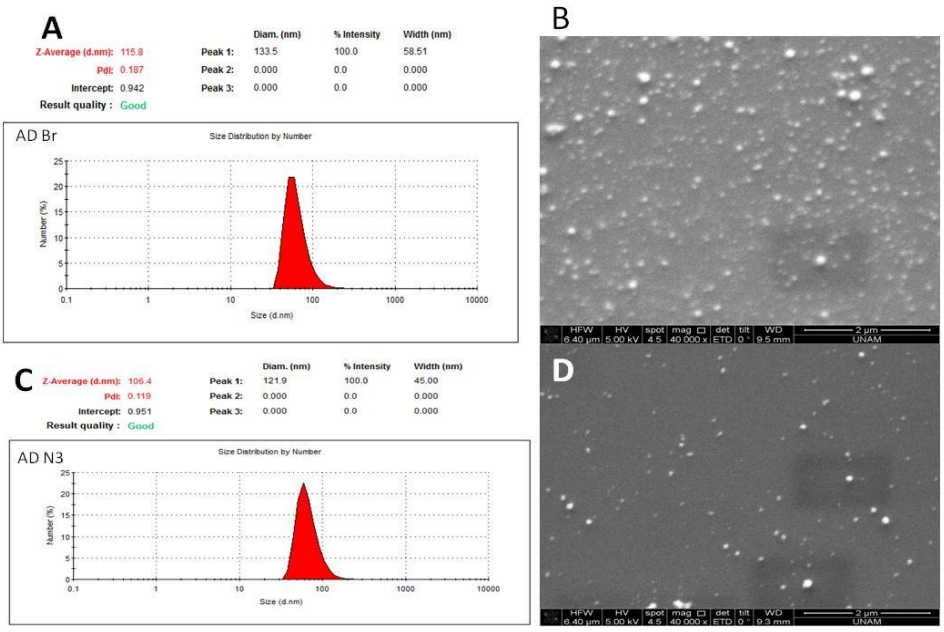

Figure 46: (a) DLS: Zeta size of AD Br NP from non-functionalized polymers (115 nm) (b) SEM micrograph of AD Br (c) DLS: Zeta size of AD N3 formed by click reaction (106 nm) (d) SEM micrograph of AD N3.

According to DLS and SEM data (Figure 46), when bipolymer NPs are prepared by click reaction (ADN3), they tend to exhibit smaller, monodispersed and more compact

nanoparticles than the nanoparticles prepared from non-functionalized polymers (ADBr). Despite the small size differences; ADN3 is 106 nm while ADBr is 115 nm, the SEM micrographs (Figure b&d) showed that ADN3 NPs are more monodispersed.

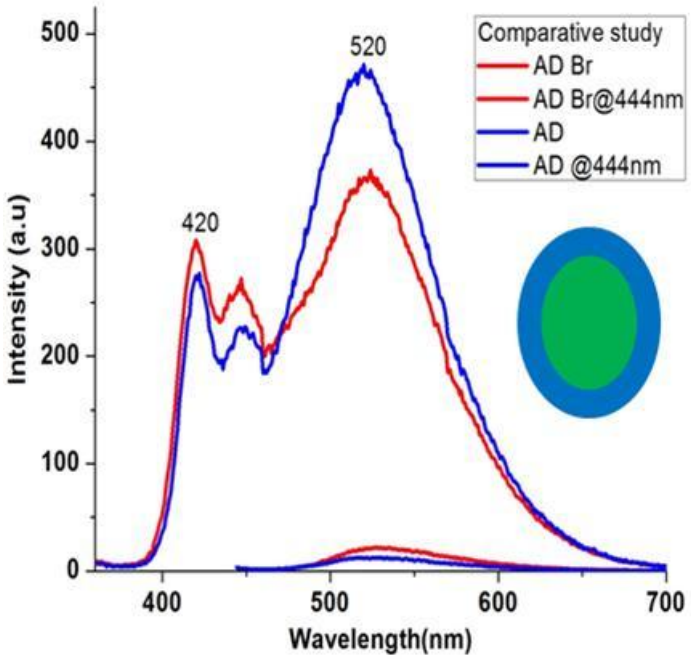

Figure 47: Photoluminescence spectra of bipolymer NPs. (λ_{ex}=350 nm)

The optical properties ADN3 and ADBr were compared in Figure 47. Because of the compact nature of ADN3 NPs which provides a favourable D-A distance for energy transfer, ADN3 demonstrated higher energy transfer than ADBr. Both NPs emits at 420 nm and 520 nm. The emission at 520 nm was 24 nm blue shifted, compare to acceptor alone.

Dissolution of NPs in THF

When solution of PFBN3 polymer (donor) is mix with PFBT polymer (acceptor) in THF, no energy transfer was observed. By adding increasing concentration of acceptor to the donor, the emission of the donor gradually quenched. But the quenching in donor emission does not correspond to an increase in the emission of the acceptor. In other words, there was no energy transfer owing to the fact that the donor and acceptor pair are too far apart for efficient energy transfer (See Figure 48).

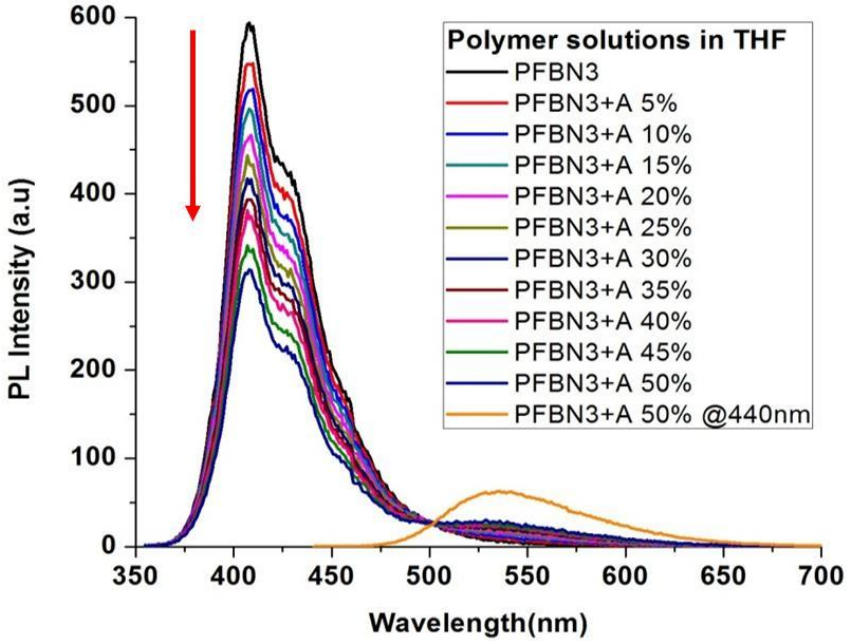

Figure 48: Emission spectra of donor polymer with increasing concentration of acceptor in THF. (λ_{ex}=350 nm)

However, when bipolymer NPs dispersion in water were dissolve in THF by first removing the water and adding THF (Figure 49a), their energy transfer efficiency fall drastically to an unprecedented low level. This can be attributed to the swelling of the NPs in THF which is a good solvent, hence, putting the donor and acceptor at an unfavourable distance for efficient FRET to occur. Interestingly, the low energy transfer observed in solution of bipolymer NPs in THF which does not occur at all in the case of solution of ADBr NPs or bare donor and acceptor polymers in THF suggested that the bipolymer NPs are covalently bound through click reaction. The triazole rings cross-linking donor and acceptor NPs ensure that even when the NPs are in good solvents (i.e. THF), they only swell to certain degree but do not disintegrate into their respective polymer chains. In fact, the SEM micrograph (Figure 50) showed that solutions of bipolymer NPs in THF are in the form of nanoparticles and not in separate polymer chains. Their size, however, enlarged from 99 nm in water to 300 nm in THF. Despite the morphology of the bipolymer NPs in THF are nanoparticle-like, their emission wavelengths shifted to the emission wavelength of the corresponding polymers in THF. The emission of NPs shifted from 420 nm and 544 nm to 407 nm and 535 nm of polymer chain respectively.

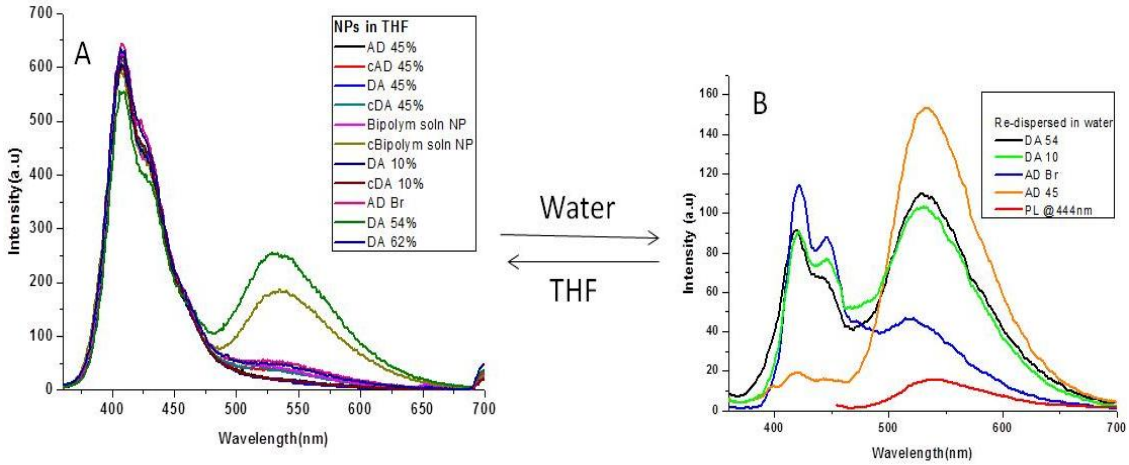

Figure 49: (a) Dissolution of NPs in THF (b) Re-dispersion of NPs in water. (λ_{ex}=350 nm)

To demonstrate further that the NPs are stabilized by cross-linking; the THF was evaporated and re-dispersed the NPs in water once again. The re-dispersed NPs were compared with NPs prepared from non-functionalized polymers (ADBr NP). All the NPs dispersion in water that were cross-linked through click reaction show restoration of energy transfer (Figure 49b). However, the energy transfer in ADBr NPs was not fully restored (Figure 49b).

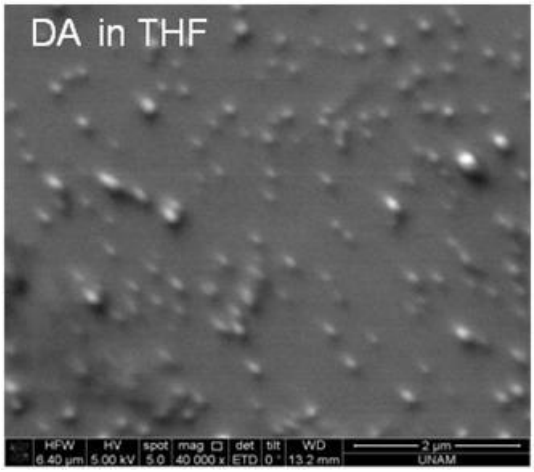

Figure 50: SEM micrograph of bipolymer NPs in THF

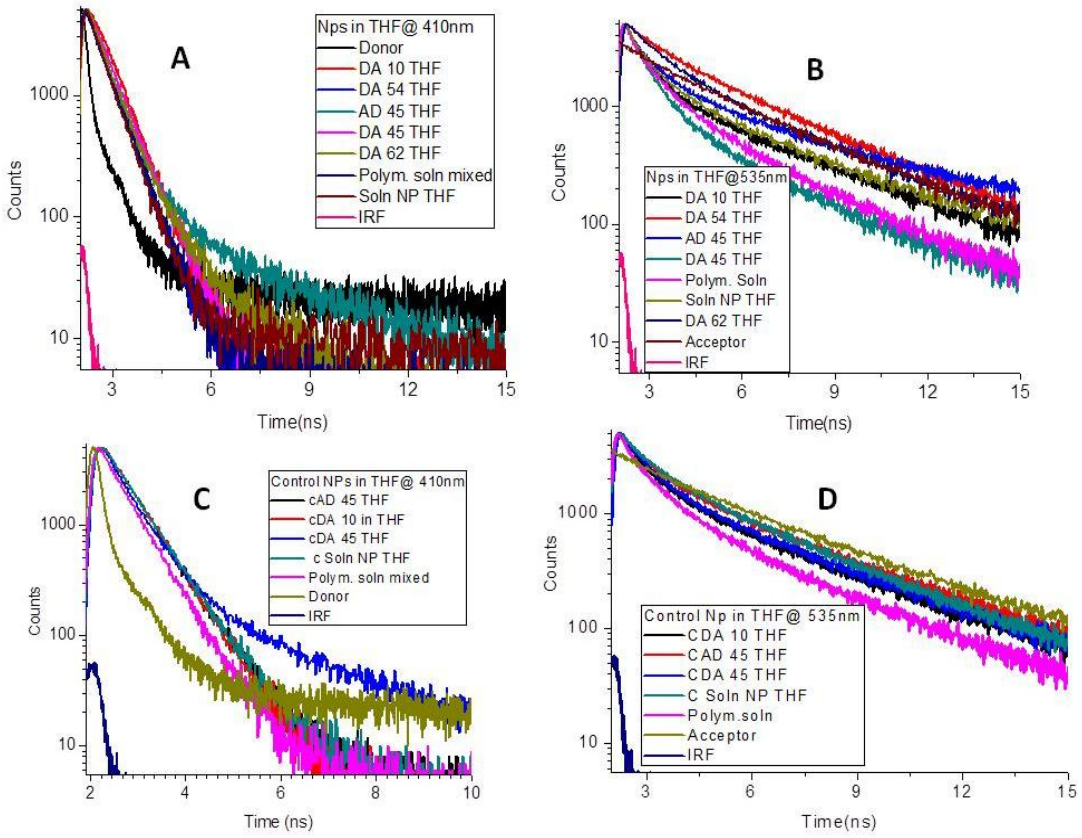

Figure 51: Biexponentially fitted decay curves of bipolymer nanoparticles in THF (a) Fluorescence life-time decay curves of catalysed NPs at 410 nm (b) At 535 nm (c) Fluorescence life-time decay curves of catalyst-free NPs at 410 nm. (d) At 535 nm.

As evidenced in the steady-state fluorescence, time-resolved fluorescence also indicates low energy transfer in solution of bipolymer NPs in THF (Figure 51). For the donor component at 410 nm, bipolymer NPs in THF are decaying slightly faster than the donor alone, which is an indication of energy transfer. Furthermore, the acceptor component at 535 nm shows a better clue of energy transfer. When the bipolymer NPs are compare with acceptor polymer in THF, they show prolonged decay lifetime than polymer solution.

Table 2: Fluorescence lifetime of NPs in THF (intensity weighted)

NPs in THF	τ_{avr}[ns] @410nm	τ_{avr}[ns] @535nm	η[%]
DA 45	0.583	1.04	4.43
cDA 45	0.560	1.57	8.20
AD 45	0.558	1.91	8.52
cAD 45	0.585	1.81	4.10
Soln NP	0.501	1.53	17.87
C . Soln NP	0.608	1.82	0.33
NP mixed	0.530	1.23	-
DA 10	0.593	1.41	2.77
C DA10	0.589	1.50	3.44
DA 54	0.515	2.67	15.57
DA 62	0.512	2.15	16.07
Donor NP	0.610	-	-

Tabulated fluorescence lifetimes and energy transfer efficiencies of solution of bipolymer NPs in THF are shown in Table 2. Three bipolymer NPs: DA54, DA62 and soln NPs showed considerable energy transfer efficiency of 15.57%, 16.07% and 17.87% respectively in THF. The lifetime of donor NPs alone in THF is 0.61 ns which is longer than the lifetime of all the bipolymer NPs in THF. If the lifetime of the bipolymer NPs are shorter than the lifetime of donor alone, then energy transfer has occurred.

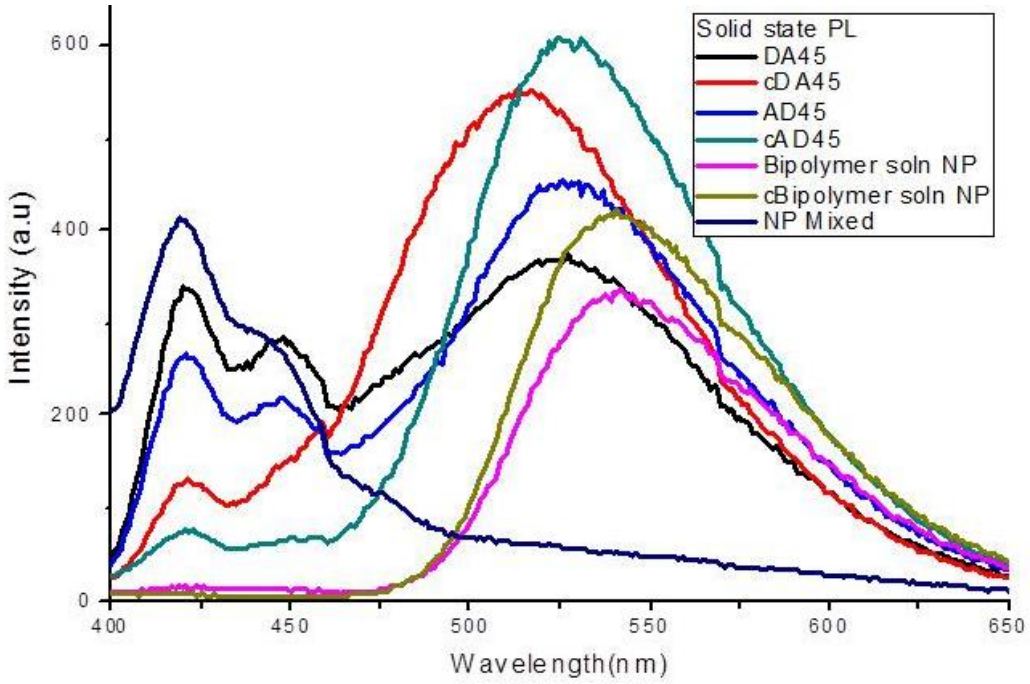

Figure 52: Solid state photoluminescence of bipolymer NPs. (λ_{ex}=350 nm)

For possible application of these bipolymer NPs in solid state lighting, they should show energy transfer in the solid state as well. Thin film of bipolymer NPs were prepared on quartz surface by drop casting. Interestingly, all the bipolymer NPs exhibit high level of energy transfer comparable to those in NPs dispersion in water (Figure 52). For NP mixed, where NPs are prepared separately from donor and acceptor and then mix physically, very low energy transfer was observed. This result confirms that even at high concentration of physical mixture of donor and acceptor, they might not be at a favourable distance or orientation for energy transfer to take place.

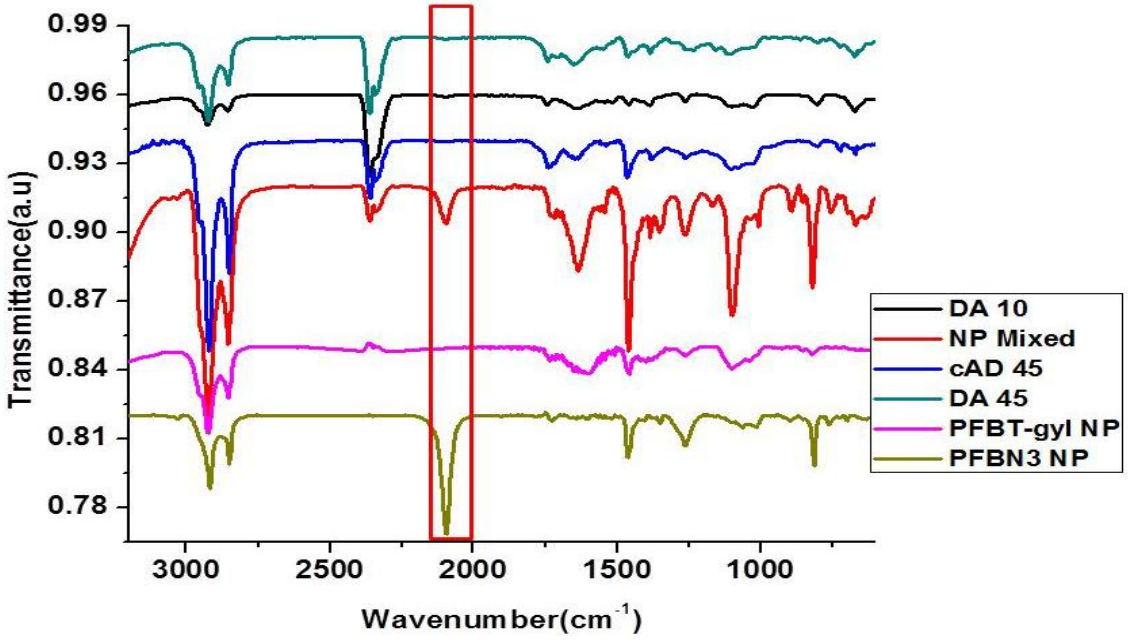

Figure 53: FTIR (solid state, KBr pellet) spectra of bipolymer NPs

The FTIR spectra of some bipolymer NPs are compared with the spectra of PFBN3 NPs (donor) and PFBT NPs (acceptor) in Figure 53. The donor NPs which are functionalized with azide groups show a strong stretching band of azide at 2098 cm^{-1}. When donor and acceptor NPs were physical mixed, a broad stretching of azide was observed as well; this indicates that click reaction does not take place between the functional groups of donor and acceptor NPs when they are mixed physically. Interestingly, in the case of bipolymer NPs prepared by click reaction, the azide stretching band at 2098 cm^{-1} disappeared indicating the formation of triazole ring from azides and alkynes.

2.4. White-emitting Tandem Nanoparticles

Nanoparticles consisting of many polymers are also regard to as tandem nanoparticles. To generate a broad spectrum that can cover the entire visible region, different polymers emitting blue, green and red are combined. Through energy transfer from one polymer to the other, a broad spectrum resembling natural light can be obtained for possible application in solid state lighting.

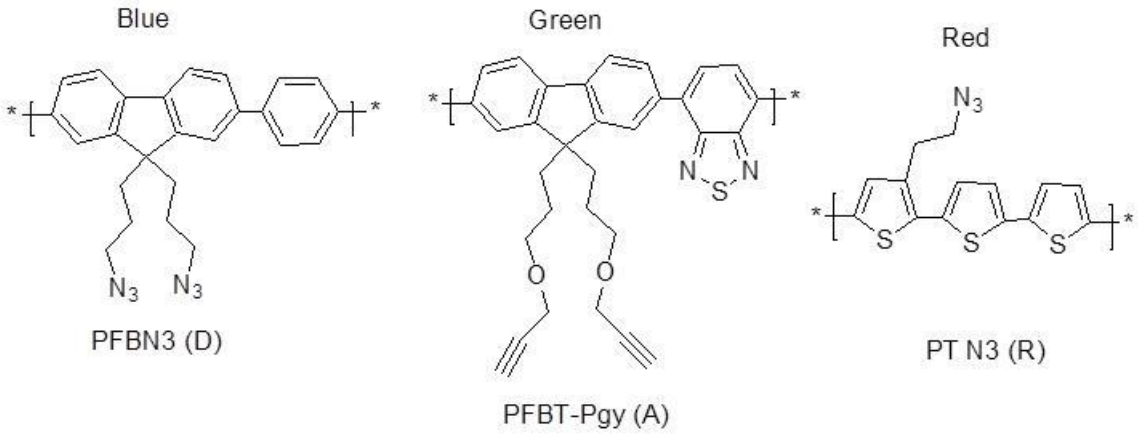

Scheme 20: Structures of polymers used in the preparation of tandem NPs

Tandem NPs were designed from three polymers (Scheme 20) using four nanostructured design methods (Figure 54). In the first method, 'NPs Mixed' was design by preparing NPs from each of the three polymers separately and then mixing them in certain ratio. In the second method, 'T Sol NP' was prepared by mixing solution of the three polymers in THF and then NPs were made from the resulting solution. In the third and fourth methods, sequentially formed NPs were prepared; NPs of one polymer is first prepared, followed by coating with the second polymer. The resulting bipolymer NPs is further coated with the third polymer to obtain sequentially formed tandem NPs.

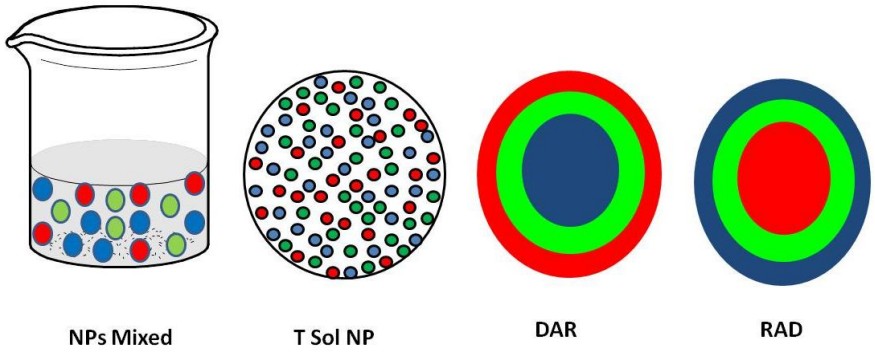

Figure 54: Nanostructured designs for tandem NPs

2.4.1. Morphological study of Tandem NPs

The size and morphology of tandem NPs were determined by DLS and SEM. According to DLS results, average size of the tandem NPs is 118 nm which corresponds to 20 nm increase in size compare to bipolymer NPs. The increase in size from 98 nm in bipolymer NPs to 118 nm in tandem NPs is a clear indication of the successful formation of tri-component NPs. The SEM micrographs of tandem NPs show spherical particles with no formation of aggregates.

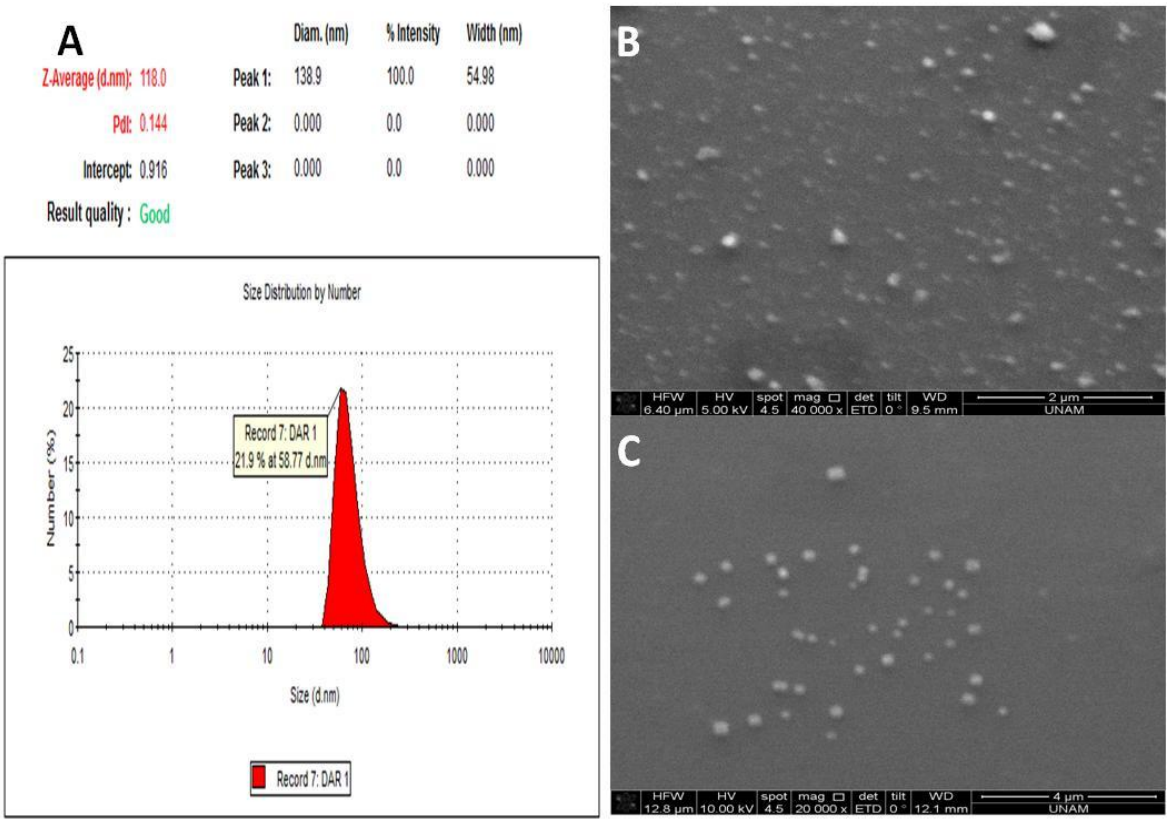

Figure 55: (a)DLS: Zeta-size of DAR NP (118nm),(b)SEM micrograph of DAR.(c)SEM micrograph of DAR 12 NPs.

2.4.2. Förster Resonance Energy Transfer in Tandem Nanoparticles

The energy transfer study of the four tandem NPs designs are presented in Figure 56. Each of the tandem NPs contain equal ratio of blue, green and red polymer for comparison. They all contain 58 mol% blue, 24 mol% green and 18 mol% red polymer.

In the first method, NPs mixed show emission spectrum similar to the individual NPs. Some energy transfer from blue to green and then to red polymer could be observed. However, the energy transfer was inefficient owing to the large distance of the NPs in solution. The dominance of the donor component at 420 nm results in blue color.

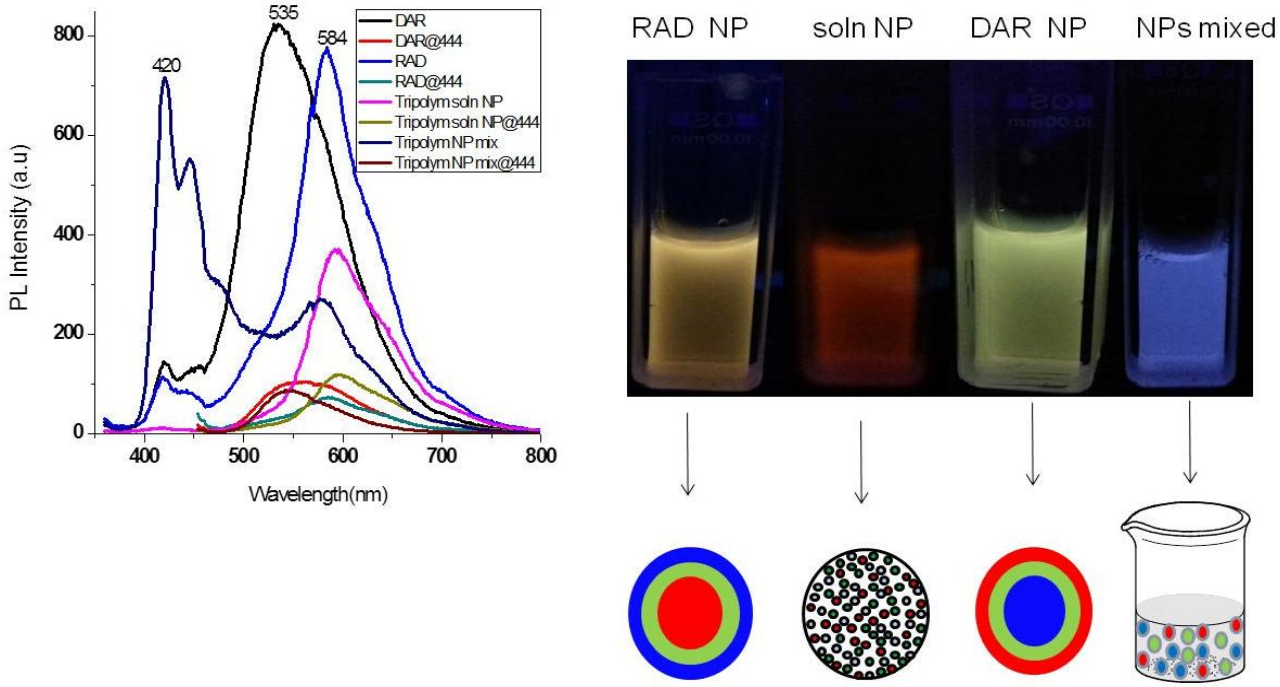

Figure 56: The emission spectra of tandem NPs with their corresponding emission colors. (λ_{ex}=350 nm)

In the second designs, where solutions of three polymers were simultaneously used to prepare 'T Sol NPs', a complete energy transfer from donor to acceptor and finally to the red polymer was observed. This result is similar to those observed in the bipolymer NPs mentioned earlier. All the blue and green polymer components of the spectrum at 420 nm and 535 nm respectively have been transferred to the red polymer component at 595 nm. The emission of the red polymer was enhanced 3 fold through energy transfer compare to the emission of the red polymer at its excitation wavelength.

In the third design denoted DAR NPs, blue polymer NPs was coated with green polymer followed by red polymer. DAR NPs show high energy transfer to the green polymer component with 10 nm blue shift. The emission intensity of the blue polymer component at 420 nm was very low due to the efficient energy transfer to acceptors. The emission intensity of the green polymer was 8 times higher at 350 nm excitation than its own excitation at 444 nm.

Finally, for the fourth design denoted by RAD NP, red polymer NPs was coated with green polymer followed by blue polymer. Formation of sequentially formed tandem NPs was evidenced from the spectral changes. The distinct emission of the three polymers can be seen at the 350 nm excitation wavelength. However, the emission intensities of blue and green polymers are very low compare to the red polymer due to energy transfer. Furthermore, the

emission of the red polymer was 35 nm blue-shifted compare to polythiophene NPs alone. In addition, the emission intensity of the red polymer component of RAD NPs is 6.6 times higher than the emission intensity of red polymer NPs at its own excitation wavelength. Such amplified emission is attributed to high energy transfer and prevention of aggregated quenching of the red polymer when doped with other polymers. This strategy of enhancing emission can be used to obtain brighter NIR chromophores for imaging applications.

When the emission colors of the four designs under study are compared in terms of purity of white emission, DAR NPs turns out to be better. Hence further tuning of DAR NPs emission to get white emission was done by manipulating the ratios of the three polymers involved. A new white emitting tandem NPs denoted DAR12% was prepared with 88 mol% blue, 9 mol% green and 3 mol% red polymers. The green and red polymers in DAR12% add up to 12% while in DAR NPs mentioned previously they were 42%. Reduction of the blue and green polymer components from 42% to 12% is expected to induce incomplete energy transfer and hence generation of white emission. In Figure 57, the emission spectrum of DAR 12% showed the distinct emissions of the three polymers. Due to incomplete energy transfer and wide coverage of the visible region, white emission was achieved.

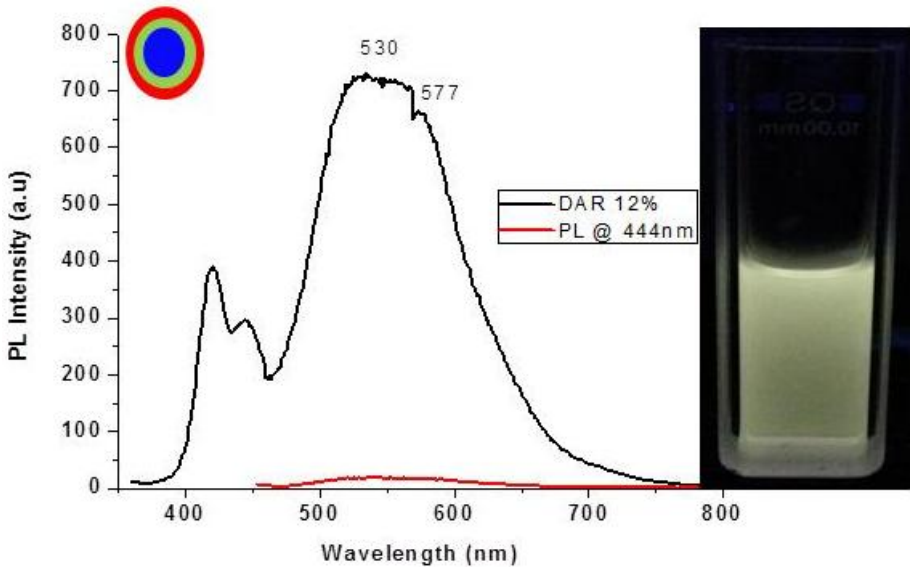

Figure 57: Emission spectrum of DAR 12% NPs (λ_{ex}=350 nm)

Moreover, the emission of DAR 12% NP was tuned by further limiting the green and red polymer components to give DAR 6% and DAR 4% NPs. In DAR 6%, the compositions of polymers are 94 mol% blue, 4.5 mol% green and 1.5 mol% red polymers. The purity of white emission from DAR 6% was the best achieved (Figure 58). For DAR 4% where the

compositions are 96 mol% blue, 3 mol% green and 1 mol% red polymer, the white emission is comparable to that of DAR 6% NPs.

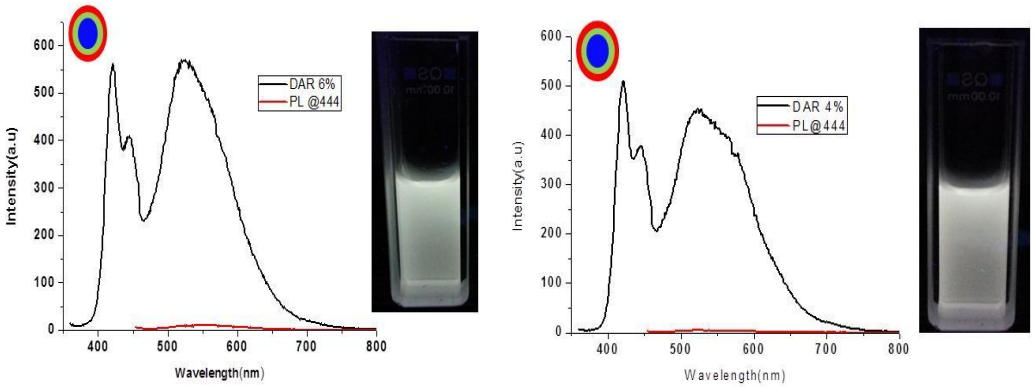

Figure 58: Emission spectra of DAR 6% NPs (left) and DAR 4% (right) (λ_{ex}=350 nm)

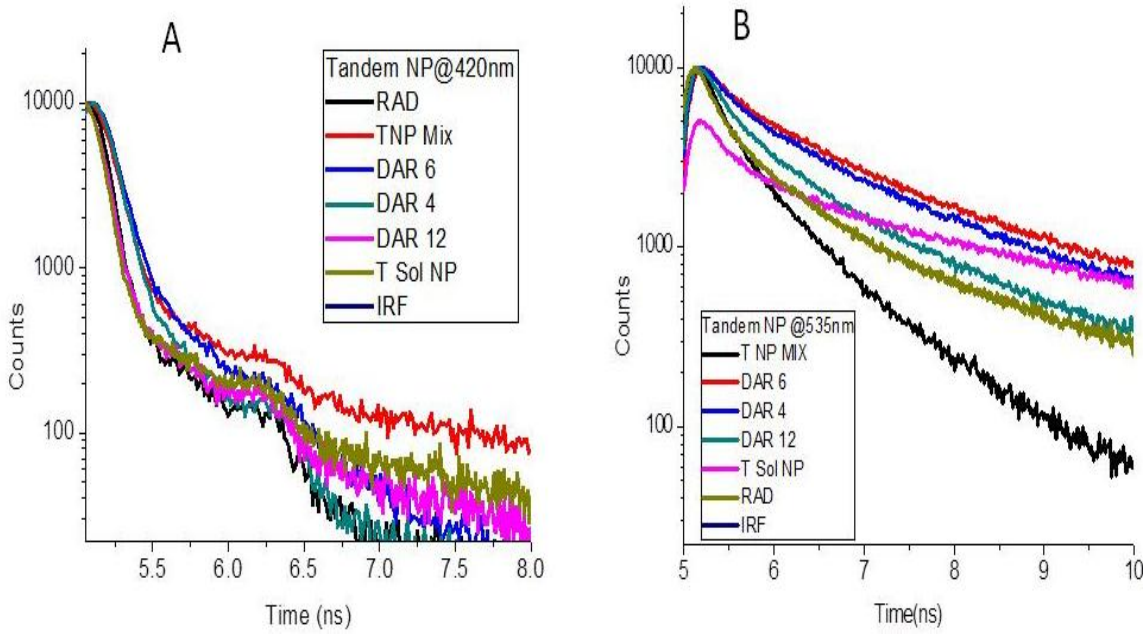

Figure 59: Biexponentially fitted decay curves of tandem nanoparticles (a)Fluorescence life-time decay curves of tandem NPs at 420 nm, (b)At 535 nm

The fluorescence decay curves of tandem NPs at 420 nm (Figure 59b) show that NPs mixed has longer lifetime compare to sequentially formed NPs. This indicates an inefficient energy transfer in NPs mixed. Furthermore, the fluorescence decay curves at 535 nm (Figure 59b) illustrate energy transfer in the tandem NPs except for NPs mixed which has the shortest lifetime at 535 nm.

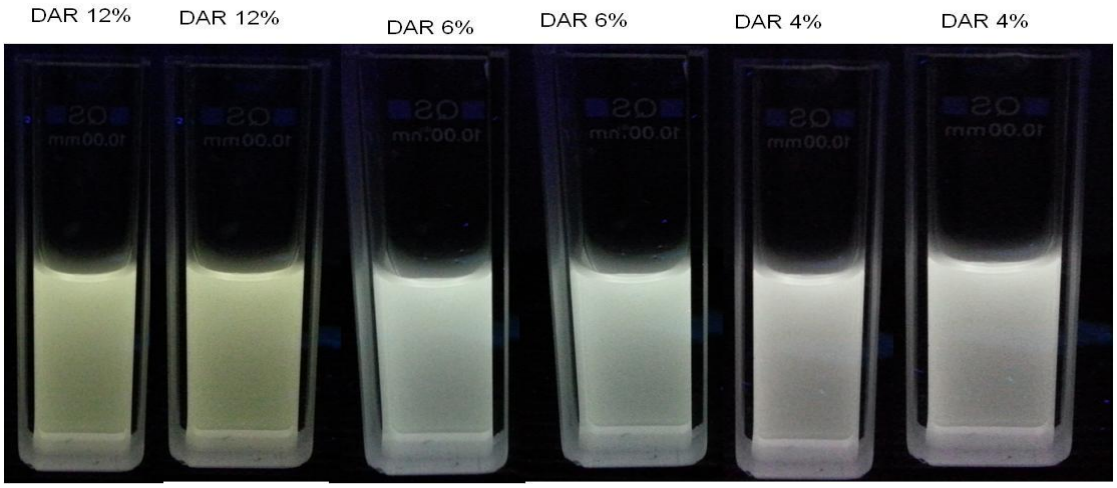

Figure 60: Tandem NPs under UV-366 nm

2.4.3. White emitting tandem nanoparticles

Another white emitting tandem NPs were designed from three polymers consisting of red emitting poly(thiophene-co-benzothiadiazole) derivatives (PBTTH-Pgy) instead of polythiophene (PTN3) in the previous example.

The energy transfer study of the four tandem NPs designs are presented in Figure 62. The ratio of the composition of each polymer in the NPs was kept constant, while merely changing the nanostructure designs. They all contain 81 mol% blue, 2 mol% green and 17 mol% red polymer.

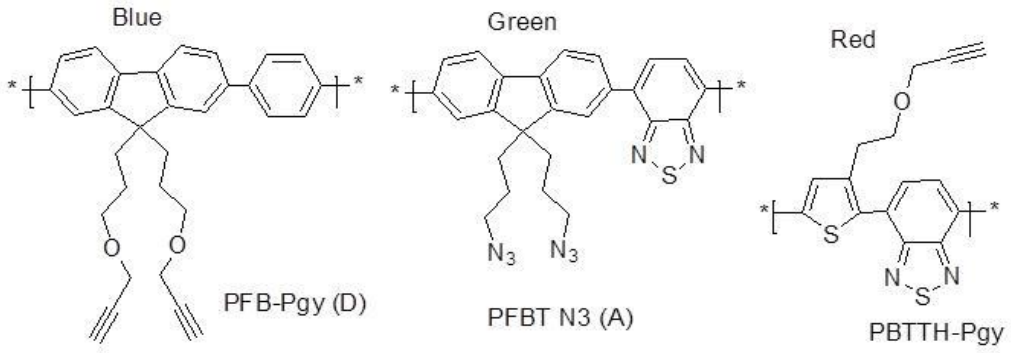

Scheme 21: Structure of polymers used in the preparation of tandem NPs

Tandem NPs were designed from blue, green and red emitting polymers (Scheme 21) using four nanostructured design methods (Figure 61). In the first method, X10 was design by preparing NPs from each of the three polymers separately and then mixing them. In the second method, 'X9' was prepared by mixing solution of the three polymers in THF and then NPs were made from the resulting solution. In the third and fourth methods (i.e. X8 and X5),

sequentially formed NPs were prepared; NPs of one polymer is first prepared, followed by coating with the second polymer. The resulting bipolymer NPs was further coated with the third polymer to obtain sequentially formed tandem NPs (Figure 61).

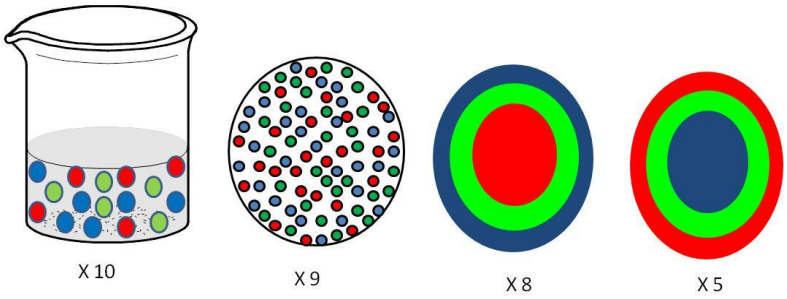

Figure 61: Representation of tandem NP designs

The emission spectra of tandem NPs are shown in Figure 62. X10 being prepared from physically mixing NPs of the three polymers, showed an intense peak at 420 nm corresponding to the donor component. However, the acceptor emission at 535 nm was quenched due to inefficient energy transfer. Again, this can be understood from the fact that the X10 NPs are moving freely in solution with large distance between them which can hinder energy transfer.

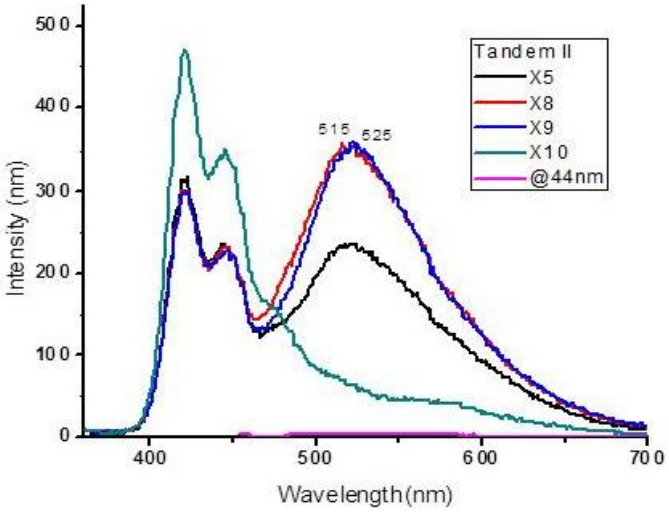

Figure 62: Emission spectrum of tandem NPs

For X9 where solution of the three polymers were first prepared and made NPs from the resulting solution, we observed decrease in the intensity of donor emission and increase in acceptor emission. Similarly, in X8 where NPs are formed sequentially with the red polymer as core, energy transfer leads to enhanced emission at 525 nm. The emission of tandem NPs were 19 nm blue-shifted from 544 nm to 525 nm. This effect was already observed in other NPs designs.

Finally, X5 was designed sequentially so that blue emitting polymer forms the core and the green emitting polymer forms a sandwich between the blue emitting core and red emitting polymer shell. The SEM micrograph of X5 is shown in Figure 63. X5 shows incomplete energy transfer with emissions at 420 nm, 525 nm and 585 nm which lead to white emission (Figure 65).

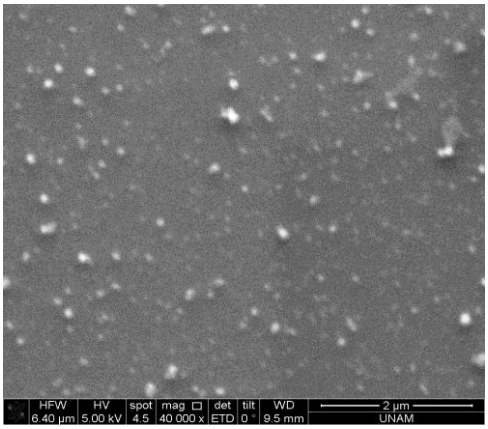

Figure 63: SEM micrographs of X5 NPs (130 nm)

Further insight into to the mechanism of energy transfer in the tandem NPs in question were provided by time-resolved fluorescence lifetime measurements. When X10, which is a physical mixture of three NPs, is compared with X5, X8 and X9, it has longer lifetime at 420 nm (see Table 3). This trend can also be observed in Figure 64a. At 535 nm, X10 shows the shortest lifetime of all. The short lifetime of X10 is due to low energy transfer in mixture of NPs.

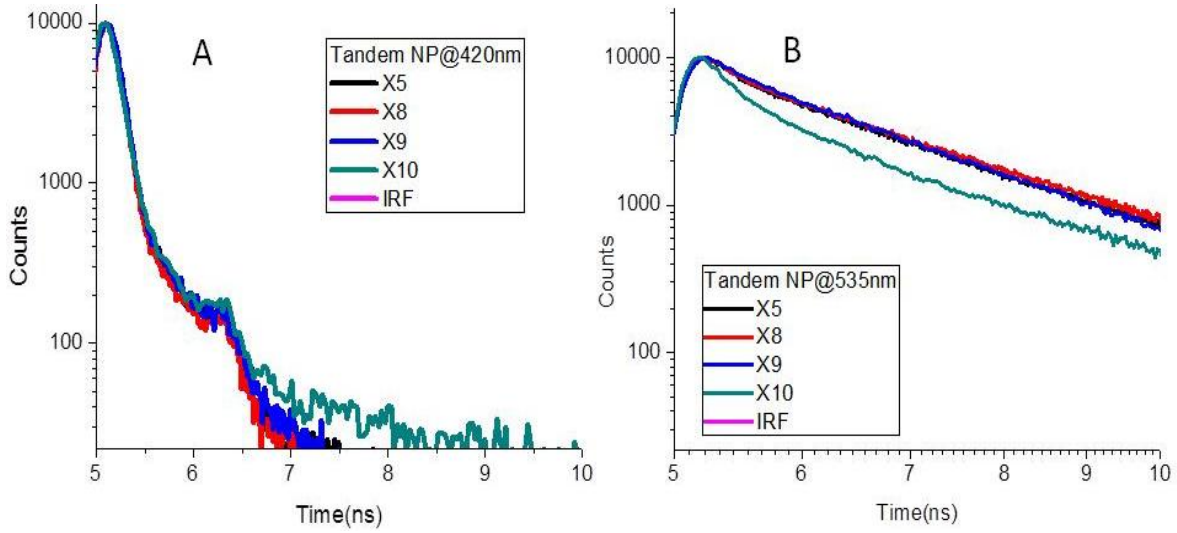

Figure 64: Biexponentially fitted decay curves of tandem nanoparticles (a)Fluorescence life-time decay curves of tandem NPs at 420 nm, (b)At 535 nm

Table 3: Fluorescence lifetime of tandem NPs in water

S/N	NPs in water	τ_{avr}[ns] @420nm	τ_{avr}[ns] @535nm	η[%]
1.	RAD	0.055	1.692	66
2.	T Sol	0.048	1.287	70
3.	T.NPs mixed	0.158	0.091	-
4.	DAR 12	0.101	1.908	38
5.	DAR 6	0.108	2.461	33
6.	DAR 4	0.126	2.282	22
7.	X 5	0.107	2.424	33
8.	X 8	0.062	2.455	61
9.	X 9	0.088	2.237	46
10.	X10	0.181	0.667	-
11.	Donor	0.162	-	

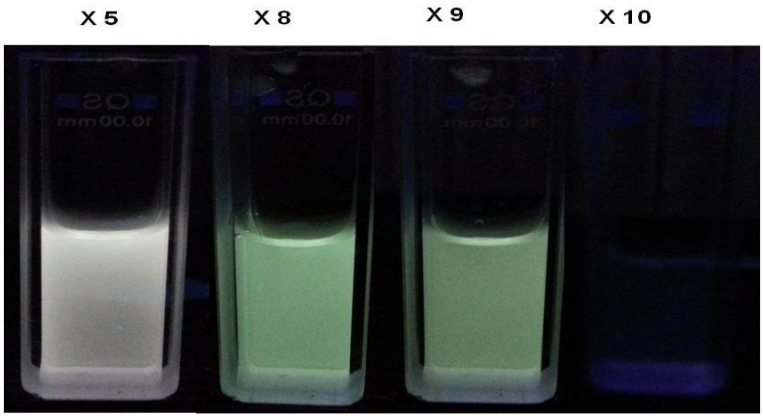

Figure 65: Photographs of tandem NPs under UV-366 nm

Enhancing red emitting polymer for bioimaging applications

Recently, there are growing research interest towards the development of in vivo fluorescence imaging probes with emission in the far-red/near-infrared region (> 650 nm), as it offers a unique window for bioimaging with low biological autofluorescence and high tissue penetration.Despite the high optical properties of conjugated polymers, their fluorescence quantum yield, particularly in the red or NIR region drops drastically when converted into nanoparticles. The common approach to obtain brighter NPs for imaging is to use FRET to shift fluorescence emission to the NIR for improved tissue penetration depth and reduce autofluorescence background.

Brighter red polymers can be achieved by dopping them with other chromophores that can enhance their emission through FRET. In Scheme 22, 20 mol% green emitting polymer was used to coat 80 mol% red emitting polymer. The red emitting forms the core of the NPs surrounded by green emitting polymer. In this way, red polymer being inside, there is efficient energy transfer and the lost of energy to the environment is minimized.

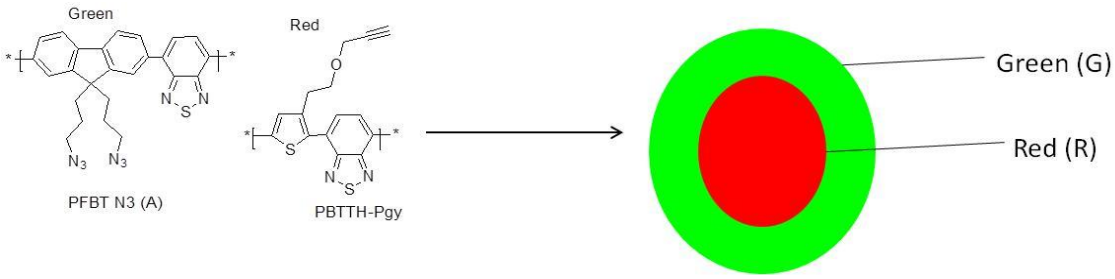

Scheme 22: Preparation of brighter red polymer NPs (RG)

The emission of RG NPs is shown in Figure 66. Because of blue-shifting, the emission maximum appears at 630 nm. A broad and less intense shoulder peak can also be seen at 701 nm which corresponds to the emission of red polymer NPs alone. However, the low emission intensity at 701 nm was thought to be due to poor solubility of the red polymer in THF which was used in the preparation of the NP. When the emission intensity of RG NPs at 444 nm excitation is compare to the emission intensity of red polymer alone at 502 nm excitation wavelength, RG NPs show significantly enhanced emission of up to 3 times higher than red polymer NPs alone.These RG NPs can have potential imaging appplications.

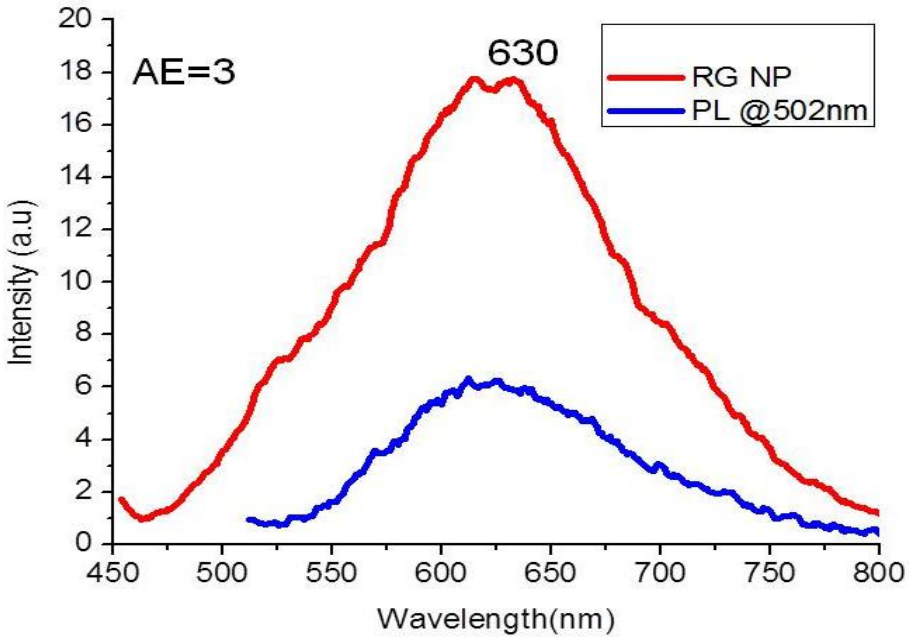

Figure 66: Emission spectrum of RG NPs

3. CONCLUSION

In summary, series of blue, green and red emitting conjugated polymers carrying azide or alkyne functional groups have been synthesized and characterized. These polymers were successfully converted into shape-persistent and water dispersible nanoparticles using different nanostructured designs via 1, 3-dipolar cycloaddition (click reaction). The emission of the nanoparticles can be tuned by manipulating polymer concentration, energy transfer and nanostructure designs, hence the conjugated polymer nanoparticles promise potential applications in the areas of optoelectronic such as white polymer light emitting diodes and cellular imaging.

In this project, poly[(9,9-bis{3-azidopropyl}fluorenyl-2,7-diyl)-*co*-benzene] (**PFBN3**) which is a blue emitter serves as a donor, while poly[(9,9-bis(3-(prop-2 ynyloxy)propyl)fluorenyl-2,7-diyl)-*co*-(1,4-benzo-{2,1,3}-thiadiazole)] (**PFBT-Pgy**) a green emitting polymer with strong spectral overlap with the emission of the donor serves as the acceptor. The blue and green emitting polymers were design to form bipolymer nanoparticles .In addition, red emitting polymers such as poly[(2-azidoethyl)-2-(5-(thiophen-2-yl)thiophen-2-yl)thiophene (**PTN3**) and Poly[(4-(2-(prop-2-ynyloxy)ethyl)thiophen-2-yl)-co-(1.4-benzo{1,2,5}thiadiazole)] (**PBTTH-Pgy**) were each incorporated into multi-shell nanoparticle design to form tandem white emitting nanoparticles.

It turns out that among the bipolymer nanoparticles, DA45% and DA10% exhibit an impressive white emission. The emissions of these nanoparticles could be changed completely by merely changing the nanostructrure designs. Furthermore, tandem nanoparticles prepared using blue, green and red emitting polymers show greater flexibility in emission color tunability. Their emissions span all across the visible region, making them an ideal design for white emission. Tandem white emitting nanoparticles such as DAR12%, DAR 6%, DAR 4% and X5, show white emission with limited amount of dopants. DAR 6% nanoparticles consist of 6% dopants which ensure incomplete energy transfer, leading to broad white emission spectrum. The nanostructure design and ratio of polymers in DAR6% was considered as the optimum design for tandem white emitting nanoparticles. In addition, it was proven that the emission of NIR polymers can be enhanced by doping with other polymers for imaging applications. Together, this work represents a foundation for synthesis and design of multicomponent conjugated polymer nanoparticles for their potential applications in next generation solid state lighting.

4. EXPERIMENTAL SECTION

General

All the reagents utilized in the experiments were purchased from Sigma-Aldrich Chemical Co. and were used as received. The purification of monomers were done using column chromatography loaded with silica gel (Kieselgel 60, 0.063-0.200 mm) and thin layer chromatography (TLC) coated with silica gel (Kieselgel F254, 1 mm) to monitor separation of products. For structural characterization of the polymers, ^{1}HNMR- Nuclear Magnetic Resonance (NMR Bruker Avance III 400MHz spectrometer) and FTIR (BRUKER OPTIK GmbH, TENSOR) were utilized. To obtain water dispersible polymers, the polymers were converted into nanoparticles in deionized Milli-Q (18.2 MΩ) water. For optical properties both polymers and their corresponding nanoparticles were characterized by UV-vis spectrophotometer (CARY UV-VIS) and Fluorescence spectrophotometer (CARY Eclipse Fluorescent spectrophotometer) equipped with xenon lamp excitation source. The size of the nanoparticles was measured using Dynamic light scattering (DLS, Zetasizer Nano-ZS) with laser light source (wavelength 633nm). The morphology of the nanoparticles was determined by Environmental scanning electron microscope (ESEM, Quanta 200 FEG SEM) and Transmission electron microscope (TEM, FEI Tecnai G2 F30). The photophysical properties of nanoparticles including bipolymer and tandem nanoparticles were investigated using Time-resolved fluorescence spectroscopy (PicoQuant, FluroTime200) equipped with Time-correlated single photon counting(TCSPC) electronics which is capable of detecting picoseconds and slower lifetime values.

4.1.1. Synthesis and characterization of poly[(9,9-bis{3-azidopropyl}fluorenyl-2,7-diyl)-*co*-benzene] (PFBN3)

Synthesis of 2,7-dibromo-9,9-bis(3-bromopropyl)-9H-fluorene[95]

2,7-dibromoflourene (2.00 g, 6.17 mmol), 1,3-dibromo propane(13.46 g, 6.67 mL, 61.67 mmol,) and TBAB (0.53 g, 1.63 mmol) were placed in a 2-necked RB and dried under vacuum for 30 min. Then aqueous solution of NaOH (50 wt%, 10 g NaOH in 10 mL H_2O) was added to the reaction mixture and heated up to 80 ^{o}C for 3h while stirring. After the completion of reaction, solvent and the excess amount of 1,3- bromopropane were removed by rotary evaporator under reduced pressure. Then the crude product was extracted by chloroform and water. The chloroform part was washed with 2N HCl (25 mL), brine solution (25 mL) and water (25 mL). Then chloroform was evaporated and the crude product was

purified by column chromatography using cyclohexane as an eluent. Yield: 1.01 g, 47%. ^{1}H NMR (400 MHz, $CDCl_3$, 25 ^{0}C) δ ppm: 1.14-1.17 (m, 4H), 2.15-2.17 (t, 4H, *J* = 7.2 Hz), 3.14-3.18 (t, 4H, *J* = 6.6 Hz), 7.51-7.59 (m, 6H aromatic). ^{13}C NMR (400 MHz, $CDCl_3$, 25 ^{0}C) δ ppm: 27.05, 33.91, 38.51, 54.25, 120.09, 121.44, 122.87, 126.12, 127.71, 128.03, 130.99, 138.98, 139.97, 140.07, 148.47, 151.23.

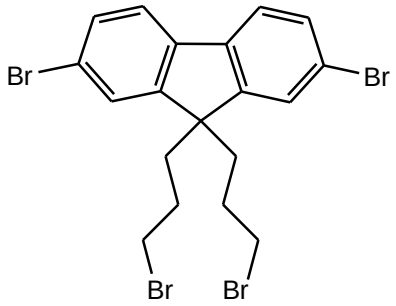

Scheme 23: 2,7-dibromo-9,9-bis(3-bromopropyl)-9H-fluorene

Synthesis of poly[9,9-bis(3-bromopropyl)-9*H*-fluorene-*co*-benzene], PFB

2,7-dibromo-9,9-bis(3-bromopropyl)-9H-fluorene (500 mg; 0.882 mmol) and benzene 1,4-diboronic acid (293 mg; 1.76 mmol) were dissolved in 10 mL of degassed THF in a 2-neeked RB. 10 mL of degassed toluene was added to this reaction mixture and stirred for 10 min. Then an aqueous solution of K_2CO_3 (852 mg, 6.17 mmol, in 10 mL of degassed water) was added to the reaction mixture followed by the addition of TBAB. Then the reaction mixture was subjected to 3 free-thaw-pump cycle to remove oxygen. Then a catalytic amount of $Pd(PPh_3)_4$ was added and the reaction mixture was heated up to 90 ^{o}C for 12h while stirring. After the completion of reaction, the solvent was completely evaporated by rotary evaporator. The crude product was washed thoroughly with water to remove the impurities and the precipitate was dissolved in minimum amount of THF. Then it was poured to cold methanol and the precipitated pure polymer was filtered and dried under vacuum. Yield: 325 mg, 64%
IR (Solid state, KBr): ν (cm^{-1}): 3030, 1598, 2919, 1458, 1262.^{1}H NMR: (400 MHz, $CDCl_3$, 25^{0}C) δ ppm: 1.23-1.38 (m, 4H), 2.24–1.42 (m, 4H), 3.12-3.27 (m, 4H), 7.41-7.48 (m, 1H), 7.51–7.58 (m, 2H), 7.64-7.78 (m, 6H), 7.84-7.96 (m, 5H). ^{13}C NMR (400 MHz, $CDCl_3$, 25 ^{0}C) δ ppm: 26.93, 34.36, 38.76, 54.24, 120.33, 121.51, 126.69, 126.83, 127.36, 128.87, 139.93, 140.29, 149.97.

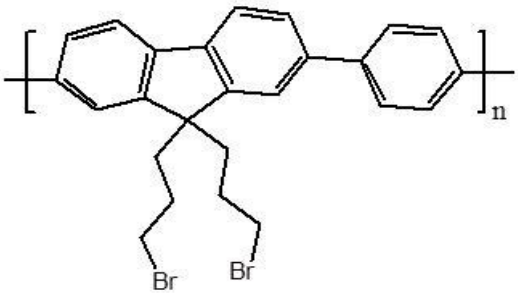

Scheme 24: Poly [9,9-bis(3-bromopropyl)-9H-fluorene-co-benzene]

Synthesis of poly [9,9-bis(3-azidopropyl)-9*H*-fluorene-*co*-benzene], PFBN3

Poly [9,9-bis(3-bromopropyl)-9*H*-fluorene-*co*-benzene] (200 mg, 0.357 mmol) and NaN_3(70 mg, 1.07 mmol) was dissolved in degassed DMF (15 mL) and then the reaction mixture was heated up to 50-60 ^oC for 24 h while stirring. After the completion of reaction, the solvent was completely evaporated by rotary evaporator. The crude product was washed with water thoroughly. The precipitate was dissolved in minimum amount of THF and precipitated to cold methanol, the precipitated pure polymer was filtered and dried. Yield: 105 mg, 60%. IR (Solid state, KBr): ν (cm^{-1}): 3030, 1598, 2919, 1458, 1262, 2098. ^1H NMR (400 MHz, $CDCl_3$, 25 ^0C) δ (ppm): 0.98-1.78 (m, 4H), 2.18-2.36 (m, 4H), 3.02-3.17 (m, 4H), 7.40-7.95 (m, aromatic, 10H). ^{13}C NMR (400 MHz, $CDCl_3$, 25 ^0C) δ ppm: 23.41, 29.69, 37.10, 54.51, 120.12, 122.02, 126.03, 130.98, 139.06, 140.16, 148. 49, 150.74

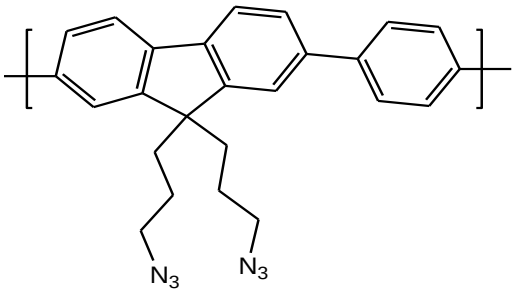

Scheme 25: Poly [9,9-bis(3-azidopropyl)-9H-fluorene-co-benzene]

4.1.2. Synthesis and characterization of poly[(9,9-bis(3-(prop-2-ynyloxy)propyl)fluorenyl-2,7-diyl)-*co*-benzene (PFB-Pgy)

Poly [9, 9-bis(3-bromopropyl)-9*H*-fluorene-*co*-benzene],PFB (21 mg, 0.0438 mmol) and K_2CO_3 (30 mg, 0.217 mmol,) were dissolved in DMF (4 mL) in a 2 necked RB. Then propargyl alcohol (1.93 g, 0.034 mol, 2 mL) was added to it. The temperature of the reaction mixture was then maintained at RT and stirred for 48h. After the completion of reaction, the solvent and the excess of propargyl alcohol were evaporated under reduced pressure. The crude product was thoroughly washed with water and dissolved in

minimum amount of THF. Then it was poured into cold methanol to precipitate the pure product as dark-grey solid. Yield: 15 mg, 78%. IR (Solid state, KBr pellet) ν(cm^{-1}) ,3300 (≡C-H stretch), 2119 (C≡C stretch), 2926 (-C-H stretch). ^{1}H NMR (400 MHz, $CDCl_3$, 25^0C) δ in ppm: 1.31 (m, 4H, -CH_2), 1.87(m, 4H, -CH_2), 2.32 (s, 1H, ≡C*H*), 3.41 (m, 4H, -CH_2), 4.00 (m, 4H, -CH_2), 8.15 (m, 9H, aromatic). ^{13}C NMR (400 MHz, $CDCl_3$, 25 ^{0}C) δ ppm: 24.45, 29.86, 57.89, 70.12, 70.22, 75.46, 120.34, 127.67.

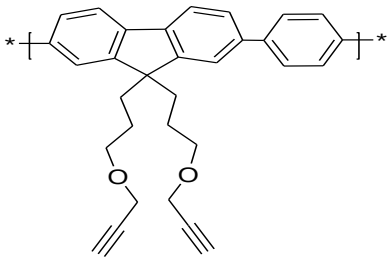

Scheme 26: Poly[(9,9-bis(3-(prop-2-ynyloxy)propyl)fluorenyl-2,7-diyl)-co-benzene]

4.1.3. Synthesis and characterization of poly[(9,9-bis(3-(prop-2 ynyloxy)propyl)fluorenyl-2,7-diyl)-*co*-(1,4-benzo-{2,1,3}-thiadiazole)] (PFBT-Pgy)

The precursor, PFBT-Br was obtained through Suzuki cross-coupling reaction as described in the literature.[96] Poly [4-(9,9-bis(3-bromopropyl)-9*H*-fluoren-7-yl)-*co*-(1,4-benzo-{2,1,3}-thiadiazole] PFBT-Br (250 mg, 0.461 mmol) was dissolved in DMF(8 mL). K_2CO_3 (318 mg, 2.31 mmol) was added to excess propargyl alcohol(2.89g, 0.05mol, 3 mL) in a two-neck flask and stirred for 30 min. PFBT-Br solution was then injected into the reaction flask and stir at room temperature for 48h. After the completion of reaction, the solvent and the excess of propargyl alcohol were evaporated under reduced pressure. The crude product was thoroughly washed with water and dissolved in minimum amount of THF. Then it was poured into cold methanol to precipitate the pure product as yellow solid. Yield: 77%. IR (Solid state, KBr): ν (cm^{-1}): 3300, (≡C-H stretch), 2119 (C≡C stretch), 2926 (-C-H stretch) 1727 (-C-N stretch. ^{1}NMR (400 MHz, $CDCl_3$, RT). δ in ppm: 1.31 (m, 4H, -CH_2), 1.87(m, 4H, -CH_2), 2.32 (s, 1H, ≡C*H*), 3.41 (m, 2H, -CH_2), 4.00 (m, 2H, -CH_2), 7.40-8.00 (m, 8H, aromatic).

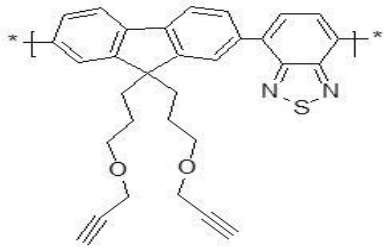

Scheme 27: Poly[(9,9-bis(3-(prop-2 ynyloxy)propyl)fluorenyl-2,7-diyl)-co-(1,4-benzo-{2,1,3}-thiadiazole)]

4.1.4. Synthesis and characterization of poly[(9,9-bis(3-azidopropyl)fluorenyl-2,7-diyl)-co-1,4-benzo[2,1,3]thiadiazole (PFBTN3)[97]

Poly[(9,9-bis(3-bromopropyl)-9H-fluoren-7-yl)benzo[c][1,2,5]thiadiazole] (250 mg, 0.461 mmol) and NaN_3 (90 mg, 1.383 mmol) was dissolved in degassed DMF (15 mL) and then the reaction mixture was heated up to 50-60 ^oC for 24h while stirring. After the completion of reaction, the solvent was completely evaporated by rotary evaporator. The crude product was washed with water thoroughly. The precipitate was dissolved in minimum amount of THF and precipitated with cold methanol; the precipitated pure polymer was filtered and dried. Yield: 160 mg, 75%. IR (Solid state, KBr): ν (cm^{-1}): 3030, 1598, 2919, 1458, 1262, 2095 (azide stretching). ^1H NMR (400 MHz, $CDCl_3$, 25^0C) δ ppm: 0.98-1.78 (m, 4H), 2.18-2.36 (m, 4H), 3.02-3.17 (m, 4H), 7.40-7.95 (m, aromatic, 8H).

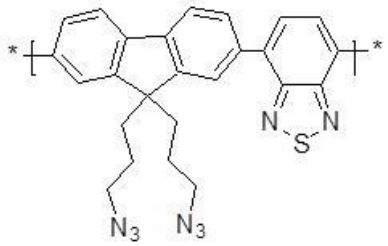

Scheme 28: Poly[(9,9-bis(3-azidopropyl)fluorenyl-2,7-diyl)-co-1,4-benzo[2,1,3]thiadiazole

4.1.5. Synthesis and characterization of poly[(2-azidoethyl)-2-(5-(thiophen-2-yl)thiophen-2-yl)thiophene (PTN3)

Synthesis of 2-(2,5-dibromothiophen-3-yl)ethanol

To a two neck round- bottom flask was added 100 mL degassed ethyl acetate (EtOAc). To this flask NBS (10.412 g, 49.14 mmol) was subsequently added and stirred for 20 min while the flask was opened to N2 inlet. The flask was then covered with aluminıum foil and added 2-(thiophen-3-yl)ethanol (3.00 g, 23.40 mmol, 2.62 mL,). After addition of 3-Thiophene-ethanol the reaction mixture was sonicated for 10 min and allowed to stir at room temperature

for 24h. The reaction mixture was first extracted with EtOAc/Water, brine and then again with water and dried over Na2SO4. The solvent was evaporated under reduced pressure from the reaction mixture which provided yellow liquid. Product was purified by column chromatography using cyclohexane as an eluent. Yield: 1.43 g, 22%. ^{1}H NMR (400 MHz, $CDCl_3$, 25^{0}C) δ ppm: 1.61 (s, 1H), 2.09 (t, 2H), 4.18 (t, 2H), 7.56 (s, aromatic)

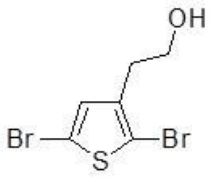

Scheme 29: 2-(2,5-dibromothiophen-3-yl)ethanol

Synthesis of 2-(2,5-dibromothiophen-3-yl)ethyl 4-methylbenzenesulfonate

2-(2,5-dibromothiophen-3-yl)ethanol (1.00 g, 3.49 mmol) was dissolved in DCM (20 mL) and stirred at 0 ^{0}C. To this flask, p-toulene sulphonyl chloride (0.99 g, 5.24 mmol) and pyridine (0.58 g, 7.34 mmol, 0.59 mL) were subsequently added. The reaction mixture was allowed to stir at 0 ^{0}C for 3h. After completion of reaction, the mixture was diluted with DMC and washed with water, 1N HCl, $NaHCO_{3\,(aq)}$, and brine. The crude product was dried over Na_2SO_4 and purified by column chromatography using cyclohexane as eluent. Yield: 1.32 g, 87 %. ^{1}H NMR (400 MHz, $CDCl_3$, 25^{0}C) δ ppm: 2.47 (s, 3H), 2.88 (t, 2H), 4.18 (t, 2H), 6.69 (s, 1H), 7.32-7.73 (m, aromatic).

Scheme 30: 2-(2,5-dibromothiophen-3-yl)ethyl 4-methylbenzenesulfonate

Synthesis of Poly[(thiophen-2-yl)thiophen-2-yl)-3-(2-tosylethyl)thiophene], PTOTS

Stannyl-bithiophene (1.69 g, 2.27 mmol, 1.24 mL) and 2-(2,5-dibromothiophen-3-yl)ethyl 4-methylbenzenesulfonate (1 .00 g, 2.28 mmol) were placed in two necked flask and dried under vacuum. 50 mL of degassed THF/DMF (1:1) was added into the reaction flask followed by three freeze-thaw cycles and addition of catalytic amount of $Pd(PPh_3)_4$. The reaction mixture was allowed to stir at 80^{0}C for 12h. After the completion of reaction, the reaction mixture was quenched in cold methanol which leads to the formation of precipitate. The solid residue was purified by soxhlet extraction using methanol, n-hexane and

chloroform. Yield: 0.63 g, 62%. IR (Solid state, KBr): ν (cm^{-1}): 3050, 785, 2921, 2848.^{1}H NMR (400 MHz, $CDCl_3$, 25^{0}C) δ ppm: 2.68 (s, 3H), 2.88 (t, 2H), 3.71 (t, 2H), 6.67-7.22 (m, 5H)

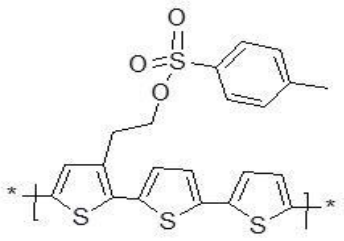

Scheme 31: Poly[(thiophen-2-yl)thiophen-2-yl)-3-(2-tosylethyl)thiophene], PTOTS

Synthesis of Poly[(2-azidoethyl)-2-(5-(thiophen-2-yl)thiophen-2-yl)thiophene

Poly[(thiophen-2-yl)thiophen-2-yl)-3-(2-tosylethyl)thiophene], PTOTS (100 mg, 0.232 mmol) and NaN_3(23 mg, 0.347 mmol,) was dissolved in degassed DMF (15 mL) and then the reaction mixture was sonicated for a while and allowed to stir at RT for 72h. After the completion of reaction, the solvent was completely evaporated by rotary evaporator. The crude product was washed with water thoroughly. The precipitate was dissolved in minimum amount of THF and precipitated in water; the precipitated pure polymer was filtered and dried. Yield: 53 mg, 75%. IR (Solid state, KBr): ν (cm^{-1}): 3030, 2919, 2848, 2098 (azide stretching). ^{1}H NMR (400 MHz, $CDCl_3$, 25^{0}C) δ ppm: 1.78-2.00 (m, 2H), 2.98 (m, 2H), 7.40-7.95 (m, aromatic, 6H).

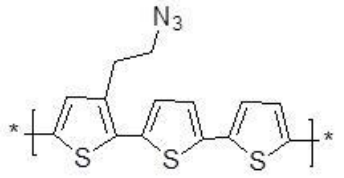

Scheme 32: Poly[(2-azidoethyl)-2-(5-(thiophen-2-yl)thiophen-2-yl)thiophene

4.1.6. Synthesis and characterization of Poly[(4-(2-(prop-2-ynyloxy)ethyl)thiophen-2-yl)-co-(1.4-benzo{1,2,5}thiadiazole)] (PBTTH-Pgy)

Synthesis of poly(2-(5-(benzo[c][1,2,5]thiadiazol-4-yl)-*co*-thiophen-3-yl) ethanol

Hydrolized Red Polymer**:** poly(2-(5-(benzo[c][1,2,5]thiadiazol-4-yl)-*co*-thiophen-3-yl) ethyl acetate (200 mg, 0.661 mmol) was dissolved in 10 mL THF in a round bottom flask.[98]Aqueous solution of KOH (2 eq; 1.32 mmol, 76 mg in 10 mL H_2O) was added to it and stirred the reaction mixture for 4 h at 50 ^{o}C. After the completion of reaction, the solvents were removed by rotary evaporator under reduced pressure. The crude product was

thoroughly washed with water to obtain the pure polymer as a red powder. Yield: 158 mg, 92%. 1NMR (400 MHz, $CDCl_3$, RT) δ in ppm: 2.84 (m, 2H, -C*H*$_2$), 3.77 (m, 2H, -C*H*$_2$), 4.53 (br, 1H, -O*H*), 8.12 (m, 3H, aromatic). IR (Solid state, KBr pellet) ν(cm^{-1}) 3310 (br, -OH), 3040, 1478 (weak, aromatic), 2942 (-C-H stretch).

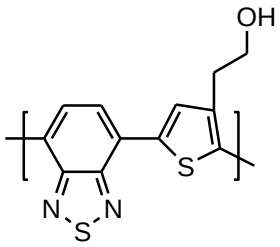

Scheme 33: Poly[(4-(2-(prop-2-ynyloxy)ethyl)thiophen-2-yl)-co-(1.4-benzo{1,2,5}thiadiazole)]

Synthesis of poly(2-(5-(benzo[c][1,2,5]thiadiazol-4-yl)- *co*- 3-(2-(prop-2-yn-1-yloxy)ethyl)thiophene), Propargylated Red Polymer (PBTTH-Pgy):

Hydrolyzed red polymer (150 mg, 0.058 mmol) and NaH (9.60 mg, 0.288 mmol,) were dissolved in DMF in a 2 necked RB. Then the reaction mixture was cooled down to 0 ^oC and propargyl bromide (141 mg, 0.12 mmol, 90 µL) was added to it drop wise. After the addition, the temperature of reaction mixture was heated up to 60 ^oC and stirred overnight. After the completion of reaction, the solvent and the excess of propargyl bromide were evaporated under vacuum. The crude product was thoroughly washed with water and dissolved in minimum amount of THF. Then it was poured to cold methanol to precipitate the pure product as red solid. Yield: 169 mg, 78%. IR (Solid state, KBr pellet) ν(cm^{-1}), 3272 (≡C-H stretch), 2117 (C≡C stretch), 2926 (-C-H stretch), 1727 (-C-N stretch). ^1H NMR (400 MHz, $CDCl_3$, 25^0C) δ in ppm: 3.05 (m, 2H, -C*H*$_2$), 3.5 (s, 1H, ≡C*H*), 4.00 (m, 2H, -C*H*$_2$), 4.93 (m, 2H, -C*H*$_2$), 8.15 (m, 3H, aromatic).

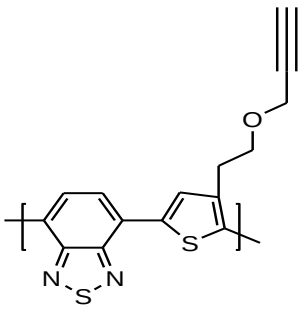

Scheme 34: poly(2-(5-(benzo[c][1,2,5]thiadiazol-4-yl)- co- 3-(2-(prop-2-yn-1-yloxy)ethyl)thiophene), Propargylated Red Polymer

4.2.1 Synthesis and characterization of PFBN3 NPs

PFBB3 NPs were prepared by reprecipitation method. 0.5 mg of PFBN3 was measured from stock solution and diluted to 2 mL in THF and ultrasonicated for 10 min. The solution was then filtered through 0.45 μM syringe filter and injected into 20 mL of Milli-Q water (18.2 MΩ) and ultrasonicated for 40 min. THF was removed under reduced pressure at 40 ^{o}C to obtain stable NPs. Characterization of NPs was done by UV-VIS spectroscopy, Fluorescence spectroscopy, DLS(Zeta sizer), SEM and TEM. All the results confirmed formation of stable NPs

4.2.2 Synthesis and characterization of PFBT-Pgy NPs

0.5 mg of PFBT-Pgy was dissolved in 2 mL THF and ultrasonicated for 10 min. The solution was then filtered through 0.45 μM syringe filter and injected into 20 mL of Milli-Q water (18.2 MΩ) and ultrasonicated for 40 min. THF was removed under reduced pressure at 40 ^{o}C to obtain stable NPs. Characterization of NPs was done by UV-VIS spectroscopy, Fluorescence spectroscopy, DLS(Zeta sizer), SEM and TEM.

4.2.3 Synthesis and characterization of PTN3 NPs

First, 0.25 mg of PTN3 was measured from the stock solution and diluted to 2 mL in THF and ultrasonicated for 10min. The solution was then filtered through 0.45 μM syringe filter and injected into 20 mL of Milli-Q water (18.2 MΩ) and ultrasonicated for 40 min. THF was removed under reduced pressure at 40 ^{o}C to obtain stable NPs. Characterization of NPs was done by UV-VIS spectroscopy, Fluorescence spectroscopy, DLS(Zeta sizer), SEM and TEM.

4.2.4 Synthesis and characterization of PBTTH-Pgy NPs

First, 0.25 mg of PBTTH-Pgy was measured from the stock solution and diluted into 2 mL THF and ultrasonicated for 10 min. The solution was then filtered through 0.45 μM syringe filter several times until clear solution was obtained. The clear solution was injected into 20 mL of Milli-Q water (18.2 MΩ) and ultrasonicated for 40 min. THF was removed under reduced pressure at 40 ^{o}C to obtain stable NPs. Characterization of NPs was done by UV-VIS spectroscopy, Fluorescence spectroscopy, DLS(Zeta sizer), SEM and TEM. All the results confirmed formation of stable NPs.

White-emitting bipolymer nanoparticles

Four methods were used to design bipolymer NP dispersion in water. PFBN3 and PFBT-Pgy were chosen because of the strong spectral overlap. The amount of donor in each sample was kept constant.

Method 1

0.5 mg of PFBN3 polymer was dissolved in 2 mL THF and ultrasonicated for 10 min. The solution was then filtered through 0.45 μM syringe filter and injected into 20 mL of Milli-Q water (18.2 MΩ) and ultrasonicated for 40 min. THF was removed under reduced pressure at 40 ^{o}C to obtain stable NPs. Similarly, 0.5 mg (45 mol%, by weight) PFBT-Pgy polymer was used to prepare acceptor NPs. The two NPs were then mixed and denoted NP mixed.

Method 2

0.5 mg PFBN3 and 0.5 mg (45mol%, by weight) PFBT-Pgy were dissolved in 2 mL THF and ultrasonicated for 10 min. The solution was then filtered through 0.45 μM syringe filter and injected into 20 mL of Milli-Q water (18.2 MΩ) and ultrasonicated for 1hr. THF was removed under reduced pressure at 40^{o}C to obtain stable NPs. The resulting NPs was denoted Soln NPs.

Method 3

In this design, bipolymer NPs were formed sequentially. First, 0.5 mg of PFBN3 (D) polymer was dissolved in 2 mL THF and ultrasonicated for 10 min. The solution was then filtered through 0.45 μM syringe filter and injected into 20 mL of Milli-Q water (18.2 MΩ) and ultrasonicated for 40 min. After 40 min of ultrasonication, a filtered solution of 0.5mg (45 mol%, by weight) PFBT-Pgy (A) in 2 mL THF was added into the preformed PFBN3 NPs while ultrasonicating. Ultasonication was continued for another 40 min. THF was removed under reduced pressure at 40 ^{o}C to obtain stable NPs. The resulting bipolymer NPs was denoted DA45%, donor being core and surrounded with 45 mol% acceptor. Also DA10% and DA62% were prepared similarly with the same donor concentration (0.5 mg) but 10 mol% and 62 mol% of acceptor respectively.

Method 4

In this design, bipolymer NPs were formed sequentially. First, 0.5 mg (45 mol%, by weight) of PFBT-Pgy (A) polymer was dissolved in 2 mL THF and ultrasonicated for 10 min. The solution was then filtered through 0.45 μM syringe filter and injected into 20 mL of Milli-Q

water (18.2 MΩ) and ultrasonicated for 40 min. After 40 min of ultrasonication, a filtered solution of 0.5 mg PFBN3 (D) in 2mL THF was added into the preformed PFBT-Pgy NPs while ultrasonicating. Ultasonication was continued for another 40 min. THF was removed under reduced pressure at 40 ^{o}C to obtain stable NPs. The resulting bipolymer NPs was denoted AD45%, acceptor being core and surrounded with donor.

White-emitting tandem nanoparticles

White emitting tandem NPs were obtained using three polymers: PFBN3, PFBT-Pgy and PTN3 polymers. Four methods of nanostructured designs were prepared and investigated.

Method 1

0.5 mg PFBN3, 0.25 mg PFBT-Pgy and 0.12 mg PTN3 polymers were converted separately into their respective NP form by reprecipitation method as described earlier. The resulting NPs of the three polymers were mixed physically and denoted NP Mixed.

Method 2

0.5 mg PFBN3, 0.25 mg PFBT-Pgy and 0.12 mg PTN3 polymers were dissolved in 2mL THF and ultrasonicated for 10 min. The solution was then filtered through 0.45 μM syringe filter and injected into 20 mL of Milli-Q water (18.2 MΩ) and ultrasonicated for 1hr. THF was removed reduced pressure at 40 ^{o}C to obtain stable NPs. The resulting NPs was donated T.soln NPs.

Method 3

In this design, tandem NPs was formed sequentially. First, 0.5 mg of PFBN3 (D) polymer was dissolved in 2 mL THF and ultrasonicated for 10 min. The solution was then filtered through 0.45 μM syringe filter and injected into 20 mL of Milli-Q water (18.2 MΩ) and ultrasonicated for 40 min. After 40 min of ultrasonication, a filtered solution of 0.25 mg (24 mol%, by weight) PFBT-Pgy(A) in 2 mL THF was added into the preformed PFBN3 NPs while ultrasonicating. Ultasonication was continued for 30 min. Finally, 0.12 mg (18 mol %, by weight) PTN3 solution in 2mL THF was also added to the preformed bipolymer NPs and ultasonated for another 30min. THF was removed under reduced pressure at 40 ^{o}C to obtain stable NPs. The resulting tandem NPs was denoted DAR. For DAR 12%, DAR 6% and DAR 4%, the amount of PFBN3 (0.5 mg) was constant while PFBT-Pgy was 0.06 mg (9 mol %), 0.03 mg (4.5 mol %) and 0,02 mg (3 mol %) and PTN3 was 0.01 mg (2 mol %), 0.006 mg (1.5 mol %) and 0.0033 mg (1 mol %) respectively.

Method 4

This design is the reverse of the third method; here tandem NPs was also formed sequentially. First, 0.12 mg (18 mol %, by weight) PTN3 polymer measured from the stock solution and diluted in 2 mL THF and ultrasonicated for 10 min. The solution was then filtered through 0.45μM syringe filter and injected into 20 mL of Milli-Q water (18.2 MΩ) and ultrasonicated for 40 min. After 40 min of ultrasonication, a filtered solution of 0.25 mg (24 mol %, by weight) PFBT-Pgy(A) in 2 mL THF was added into the preformed PTN3 NPs while ultrasonicating. Ultasonication was continued for 30min. Finally, 0.5 mg PFBN3 solution in 2 mL THF was also added to the preformed bipolymer NPs and ultasonated for another 30 min. THF was removed under reduced pressure at 40 ^{o}C to obtain stable NPs. The resulting tandem NPs was denoted RAD.

References

1. Hangarter, C. M.; Bangar, M.; Mulchandani, A.; Myung, N. V. *J. Mater. Chem.*, **2010**, 20, 3131–3140 | 3131
2. Rahman, M. A.; Kumar, P.; Park, D. and Shim, Y. Sensors **2008**, 8, 118-141
3. Werkmeister, F.; & Nickel, B. *J. Mater. Chem.* B**, 2013**, 1,3830
4. Shirakawa, H.; Louis, E. J.; MacDiarmid, A. G.; Chiang, C. K.; Heeger, A. J., *J. Chem. Soc. Chem. Comm.* **1977**, 16, 578-580.
5. http://www.nobelprize.org/nobel_prizes/chemistry/laureates/2000/advanced-chemistryprize2000.pdf
6. Thompson B.C.; Fréchet J. M. J, Angew. Chem. Int. Ed. **2008**, 47, 58
7. Fichou, D. ed, Handbook of Oligo- and Polythiophenes, Wiley-VCH, Weinheim, Germany, **1999**.
8. Bell, V. L. *J. Polym. Sci. Polym. Chem. Ed.*, **1976**,14, 225–235
9. (a) Wu, C. W.; Tsai, C. M.; Lin, H. C. Macromolecules **2006**,39, 4298–4305; (b) Wang, R.; Wang, W. Z.; Yang, G. Z.; Liu, T.; Yu, J.; Jiang, Y. *J Polym Sci Part A: Polym Chem*. **2008**, 46,790–802
10. (a) Setayesh, S.; Grimsdale, A. C.; Weil, T.; Enkelmann, V.; Mullen, K.; Meghdadi, F.; List, E. J. W.; Leising, G. *J Am Chem Soc*. **2001**, 123, 946–953; (b) Sung, H. H.; Lin, H. C. *J. Polym Sci Part A: Polym Chem* **2005**, 43, 2700–2711; (c) Tsai, L. R.; Chen,Y. *J. Polym Sci Part A: Polym Chem*. **2007**, 45, 4465–4476
11. Pei, Q.; Yang, Y. *J. Am. Chem. Soc*. **1996**, 118, 7416-7417
12. Wang, H.; Xu, Y.; Tsuboi, T.; Xu, H.; Wu, Y.; Zhang, Z.; Miao, Y.; Hao, Y.; Liu, X.; Xu, B.; Huang, W. *Organic Electronics* **2013**,14 827–838
13. Ahn, T.; Shim, H. *Macromol. Chem. Phys.* **2001**, 202, 3180-3188
14. Lee, B.R.; Lee, W.; Nguyen, T.L.; Park, J.S.; Kim, J.; Kim, J. Y.; Woo, H. Y. and Song, M. H. *Appl. Mater. Interfaces* **2013**, 5, 5690−5695
15. Bundgaard, E.; Krebs, F.C.*Solar Energy Materials & Solar Cells* **2007** 91,954–985
16. Sirringhaus, H.; Wilson , R. J., Friend R. H.; Inbasekaran M.; Wu W.; Woo, E. P.; Grell M.; Bradley D. D. C. *Applied Physics Letters* **2000**, 77, 406; doi: 10.1063/1.126991
17. Yan,M.; Gao, W.; Ge, S.; Ge, L.; Chu, C.; Yu, J.; Song, X.; Hou, S. *J. Mater. Chem*. **2012**, 22, 5568
18. Ribeiro, C.; Brogueirab, P.; Lavareda, G.; Carvalho, C. N.; Amaral, A.; Santos, L.; Morgado, J.; Scherf, U.; Bonifácio, V.D.B. *Biosensors and Bioelectronics* **2010** 26, 1662–1665
19. Gao, W.; Yan, M.; Ge, S.; Liu, X.; Yu, J. Spectrochimica Acta Part A: *Molecular and Biomolecular Spectroscopy* **2012**, 95, 218–223
20. Liu, J.; Min, C.; Zhou, Q.; Cheng, Y.; Wang, L.; Ma, D.; Jing, X.; Wang, F.; *Applied Physics Letters* **2006**, 88, 083505; doi: 10.1063/1.2178408
21. Gurunathan, K.; Murugan, A.V.; Marimuthu, R.; Mulik, U.P.; Amalnerkar, D.P. *Materials Chemistry and Physics* **1999**, 61, 173-191
22. Diaz A.F.; Kanazawa K.K. J.S. Miller (Ed.), Extended Linear Chain Compounds, vol. 3, Plenum Press, New York, **1982**, p. 417.
23. http://www.nobelprize.org/nobel_prizes/chemistry/laureates/2010/advanced-chemistryprize2010.pdf

24. Miyaura N.; Yamada K.; Suzuki A. *Tetrahedron Lett*. **1979**, 20, 3437.
25. Miyaura, N. and Suzuki A. *J. Chem. Soc. Chem. Commun*. **1979**, 866
26. Negishi, E.-I.; King, A. O. and Okukado, N. *J. Org. Chem.* **1977**, 42, 1821.
27. King, A. O.; Okukado, N.; and Negishi E.-I. *Chem. Commun.* **1977**, 683.
28. Negishi, E.-I. Ed. J. H. Brewster, Plenum Press, New York, **1978**, pp. 285-317.
29. Heck, R. F.; Nolley, J. P. *J. Org. Chem.* **1972**, 37, 2320
30. Milstein, D.; and Stille, J. K. *J. Am. Chem. Soc*. **1978**, 100, 3636. (b) Milstein, D.; and Stille, J. K. *J. Am. Chem. Soc.* **1979**, 101, 4992.
31. **http://www.organic-chemistry.org/namedreactions/stille-coupling.shtm**
32. Uchino, M.; Yamamoto, A.; Ikeda, S. *J. Organometal. Chem*. **1970**, 24, C63.
33. Tamao, K.; Sumitani, K.; Kumada, M. *J. Am. Chem. Soc*. **1972**, 94, 4374
34. Sonogashira, K.; Yatake, T.; Tohda, Y.; Takahashi, S.; and Hagihara, N. *J. Chem. Soc., Chem. Commun*. **1977**, 291-292
35. Liang, B.; Dai, M.; Chen, J. and Yang, Z. *J. Org.Chem*. **2005**, *70*, pp 391–393
36. Komáromi, A.; Novák, Z. *Chem. Commun*. **2008**, 4968-4970
37. Gu, Z.; Li, Z.; Liu, Z.; Wang, Y.; Liu, C.; Xiang, J. *Catalysis Communications* **2008**, 9, 2154–2157
38. Kolb, H.C.; Finn, M.G.; Sharpless, K.B.; *Angew. Chem., Int. Ed*. **2001**, 40, 2004
39. Iha, R.K.; Wooley, K.L.; Nystrom, A.M.; Burke, D.J.; Kade, M.J.; Hawker, C.J.; *Chem. Rev*. **2009**, 109, 5620.
40. Zhang, L.; Chen, X.; Xue, P.; Sun, H.H.Y.; Williams, I.D.; Sharpless, K.B.; Fokin, V.V.; Jia, G. *J. Am. Chem. Soc*. **2005**, 127,15998
41. Liang, L.; Astruc, D. *Coordination Chemistry* Reviews **2011**,255,2933– 2945
42. Sun, S.; Wu, P. *J. Phys. Chem*. A **2010**, Vol. 114, No. 32
43. Steenis, D. J. V. C.; David, O. R. P.; Strijdonck, G. P. F.; Maarseveen, J.H.; Reek, J.N.H. *Chem. Commun*. **2005**, 4333–4335 | 4333
44. Lutz, J.F. *Angew. Chem. Int. Ed.* **2007**,46, 1018–1025
45. Ossipov, D.A.; Hilborn, *J. Macromolecules* **2006**, 39, 1709–1718.
46. Burroughes, J. H. et al. *Nature* **1990**, 347, 539–541
47. Friend, R. H. et al. *Nature***1999**, 397, 121–128
48. Hoven, C. V.; Garcia, A.; Bazan, G. C.; Nguyen, T. Q. *Adv. Mater*. **2007**, 20, 3793–3810
49. Guenes, S.; Neugebauer, H.; & Sariciftci, N. S. *Chem. Rev*.**2000**, 107, 1324–1338
50. McQuade, D. T.; Pullen, A. E.; Swager, T. M. *Chem. Rev*. **2000**, 100, 2537–2574
51. Thomas, III S. W.; Joly, G. D.; Swager, T. M. *Chem. Rev*. **2007**, 107, 1339–1386
52. Huitema, H. E. A. et al. *Nature* **2001**, 414, 599
53. Dimitrakopoulos, C. D. & Malenfant, P. R. L. *Adv. Mater*.**2002**, 14, 99–117
54. Yen, H.; Tsai, H.; Kuo, C.; Nie, W.; Mohite, A, D.; Gupt, G.; Wang, J.; Wu, J.; Liou, G. S.; Wang, H.; J. *Mater. Chem*. C **2014**, 2, 4374–4378 | 4377
55. Taur, Y.; Ning, T. H.; Fundamentals of Modern VLSI Devices, Cambridge University Press, New York, **1998**,p. 11
56. Uemura, T.; Mamada, M.; Teraoka, R.; Kumaki, D.; Tokito, S. *Chem. Lett*. **2014**, 43, 402–404 | doi:10.1246/cl.131025
57. Burroughes, J. H.; Bradley, D. D. C.; Brown, A. R.; Marks, R. N.; MacKay, K.; Friend, R. H.; Burn, P. L.; Holmes, A. B. *Nature* **1990**, 347,539 -541.
58. Reineke, S.; Lindner, F.; Schwartz, G.; Seidler, N.; Walzer, K.; Lussem, B.; Leo, K. *Nature* **2009**, Vol 459, doi:10.1038/nature08003

59. Nakamura, T.; Tsutsumi, N.; Juni, N.; Fujii, H. *Appl. Phys. Lett*. **2005**, 97, 054505
60. Kido, J.; Hongawa, K.; Okuyama, K.; Nagai, K. *Appl. Phys. Lett.* **1994** , *64* , 815
61. So, F.; Kido, J.; Burrows, P. *MRS BULLETIN* **2008**, 33. 663-669
62. Broadbent, A. D. Color *Research & Applications* **2004**, 29, 4 267–272. doi:10.1002/col.20020
63. D'Andrade, B. W.; Forrest, S. R. *Adv. Mater*. **2004**, 16, 1585.
64. Sharma, V.K; Guzelturk, B; Erdem, T.; Kelestemur, Y.; Demir, H.V. *ACS Appl. Mater. Interfaces* **2014**, 6, 3654-3660
65. Granstrom. M.; Inganas, O. *Appl. Phys. Lett.* **1996**, 68, 147.
66. (a) Shao, Y.; Yang, Y. *Appl. Phys. Lett*. **2005**, 86, 073510; (b) Shih, P. I.; Tseng, Y. H.; Wu, F. I.; Dixit, A. K.; Shu, C. F. *Adv. Funct. Mater*.**2006**, 16, 1582;
67. Liu, J.; Zhou, Q.; Cheng, Y.; Geng, Y.; Wang, L.; Ma, D.; Jing X.; Wang, F. *Adv. Funct. Mater*. **2006,** 16, 957.
68. Tuncel, D. and Demir, H.V. *Nanoscale* **2010**, 2 (4), 484–494.
69. Kaeser, A.; Schenning, A.P.H.J. *Adv. Mater*. **2010**, 22, 2985–2997.
70. Tian, Z.; Yu, J.; Wu, C.; Szymanski, C.; McNeill, J. *Nanoscale* **2010**. 2 (10), 1999–2011.
71. Sarrazin, P.; Chaussy, D.; Vurth, L.; Stephan, O.; Beneventi, D. *Langmuir* **2009**, 25(12), 6745
72. Howes, P.; Thorogate, R..; Green, M.; Jickells, S.; Daniel, B. *Chem. Commun*. **2009**, 2490-2492.
73. Wu, C.; Szymanski, C.; Cain, Z.; McNeill, J. *J. Am. Chem. Soc*. **2007**, 129, 12904–12905
74. Feng, L., Liu, L., Lv, F., Bazan, G. C. and Wang, S. *Adv. Mater*. **2014** doi: 10.1002/adma.201305206.
75. Lakowicz, J.R. Principles of Fluorescence spectroscopy, 3rd edition (New York: Springer, **2006**)
76. Ozel, I. O.; Ozel, T.; Demir, H. V.; Tuncel, D. *Opt. Express* **2010**, 18, 670–684.
77. Grigalevicius, S.; Forster, M.; Ellinger, S.; Landfester, K.; Scherf, U. *Macromol. Rapid Commun*. **2006**, 27, 200–202.
78. Wu, C.; Bull, B.; Christensen, K.; McNeill, J. *Angew. Chem. Int. Ed*. **2009**, 48, 2741–2745.
79. Ye, F.; Wu, C.; Jin, Y.; Chan, Y.-H.; Zhang, X.; Chiu, D. T. J. *Am. Chem. Soc*. **2011**,133, 8146–8149.
80. Wang, X.; Groff, L.C.; McNeill, J. D. *Langmuir* **2013** *29* (45), 13925-13931
81. Nguyen, T. Q.; Doan, V.; Schwartz, B. J. *J. Chem. Phys*. **1999**, 110, 4068−4078.
82. Schwartz, B. J. *Annu. Rev. Phys. Chem.* **2003**, 54,141−172
83. Huebner, C. F.; Roeder, R. D.; Foulger, S. H. *Adv. Funct. Mater*. 2009, 19, 3604–3609.
84. Ozel, I.O.; Ozel, T.; Demir, H.V.; Tuncel, D. *Opt. Express* **2010**, 18 (2), 670–684.
85. Bu, J. et al. Nat. Commun. **2014**, 5, 3799.
86. Wu, C.; Bull, B.; Szymanski, C.; Christensen, K.; McNeill,J.; *ACS Nano*. **2008**, 2, 2415.
87. Kim, S.; Lim, C.; Na, J.; Lee, Y.; Kim, K.; Choi, K.; Leary, J.F.; Kwon, I. C. C*hem. Commun.* **2010**, 46, 1617–1619
88. Ding, D.; Liu, J.; Feng, G. X.; Li, K.; Hu, Y.; Liu, B. *Small* **2013**, 9,3093-3102

89. Li, J.; Liu, J.; Wei, C.; Liu, B.; O'Donnell, M.; Gao, V. *Phys. Chem. Chem. Phys.* **2013**, 15, 17006-17015
90. Potai, R.; Traiphol, R. *Journal of Colloid and Interface Science* **2013,** 403,58–66
91. Kozlov, V. G.; Bulovic, V.; Burrows, P. E.; Forrest, S. R. *Nature* **1997**,389, 362
92. Adam J.; Moule, S. A.; Kronenberg, N. M.; Tsami, A.; Scherf, U.; Meerholz, K. *J. Phys. Chem. C* **2008**,Vol. 112, No. 33
93. Murphy, C. J. *Nat. Mater.* **2007**,6 (4), 259–260
94. Frangioni, J. V. *Curr. Opin. Chem. Biol.* **2003,** 7, 626
95. Park, E-J.; Erdem, T.; Ibrahimova, V.; Nizamoglu, S.; Demir, H.V.; Tuncel, D. *ACS NANO* **2011**, 5, 2483–2492
96. Erdem, T.; Ibrahimova, V.; Jeon, D-W.; Lee, I-H.; Tuncel, D.; Demir, H. V. *J. Phys. Chem. C* **2013**, 117, 18613−18619
97. Ibrahimova, V.; Kocak, M. E.; Onal, A. M.; Tuncel, D. *J. of Polym. Sci., Part A: Polymer Chemistry* **2013**, 51, 815–823
98. Pennakalathil, J.; Ozgun, A.; Tuncel, D. *RSC Advances* **2014**, submitted paper